SEASONAL AND INTRA-SEASONAL DYNAMICS AND PRECURSORS OF RAINFALL OVER NORTHERN TANZANIA

Tibangayuka Abbas Kabanda

A thesis submitted in fulfilment of the

degree of Master of Science

Department of Oceanography,

University of Cape Town

September 1995

CONTENTS:

CHAPTER 5: **The background climate and Vuli wet spells**

List of Figures

List of Tables

ABSTRACT

The structure and variability of inter-annual and intra-seasonal circulation anomalies and their precursors are investigated over northern Tanzania. Area rainfall departures are computed in the period 1960-1990 and wet and dry years are identified. Northern Tanzania experiences bimodal rains centered on the seasons: March to May (Masika) and October to December (Vuli). Station inter-correlations in Masika are of order +0.4, whereas in Vuli correlations are of order +0.7. Using composite sequences of gridded sea surface temperatures (SST), outgoing longwave radiation (OLR) and winds in the lower- and upper-troposphere, the precursors of flood and drought are assessed. Composites are averaged for the specific season and for periods 2, 4 and 6 months prior; and the historical mean is subtracted to produce anomalies. In this way, evolution of extreme rainfall scenarios is tracked for predictive purposes. The patterns analysed show that when positive SST anomalies persist in the Indian Ocean, sympathetic negative OLR values and local rainfall enhancement are observed.

Using pentad (5 day mean) rainfall time series for the area, wet spells are analysed for structure and evolution. ECMWF data for the peak in Vuli rainfall each year from 1986 to 1991 are averaged to form a single composite. The historical mean is subtracted from the composite to produce anomalies for the wet spell and the preceeding pentads.

The composite results show that a NW-SE line of convergent moisture shifts southward from the NW Indian Ocean 10-15 days before the wet spells, while uplift occurs over the highlands to the north. A high pressure drifts northward from the SW Indian Ocean 5-10 days before the Vuli wet spell. During this time a low-level vorticity dipole is maintained in the west Indian Ocean, being negative (cyclonic) off Tanzania and positive off Somalia. The main flux of moisture is from the southern Indian Ocean at the peak of the wet spell. Upper westerly flow increases over the equatorial band from the onset phase. A nearly opposing situation prevails during dry spells where air from the Sahara desert enhances drought.

The results offer statistical guidance in medium-range weather forecasts that may assist agricultural management. Dynamical insights are also gained to improve knowledge of climate-weather teleconnections and tropical-subtropical interactions.

Chapter 1: Introduction

1.1 Motivation

In recent years Tanzania (figure 1.1) has experienced recurring droughts with devastating effects, most notably in 1983-1984. After that drought, rainfall improved significantly until 1993-1994 when below normal rainfall was received in most parts of the country. The most hard hit sector was hydro-electricity which resulted in energy rationing and consequent negative economic growth, which continued to 1995.

This work will contribute to the understanding of climate variations in the northern part of Tanzania and improve the reliability of medium- and long-range forecasts. This will be achieved through analyses of climate variations on inter-annual and intra-seasonal time scales, important to the social-economic benefit of farmers, water managers, energy suppliers and public policy makers in Tanzania.

Knowledge of climate variability will make an essential contribution to such pressing environmentally related issues as desertification, wetlands deterioration, preservation of biological diversity, and limitation of food production. In Tanzania there is a campaign to attract investors to invest in commercial agricultural farming. In order to achieve more sustainable production, it is important for policy makers and economists to understand and accept the variability of climate both inter-annually and intra-seasonally in order to efficiently utilise natural resources. Water requirements for crops differ at various phenological phases and impact

farm management techniques and crop yield. Hence the need to address the seasonal distribution of rainfall, in additional to cumulative totals.

Many earlier studies of Tanzania rainfall have concentrated on inter-annual variability, teleconnections to other parts of Africa and its adjacent oceans, mechanisms of rainfall variability, extreme rainfall conditions etc. However, only a few have directly examined in-season convective variability. In this research, precursors of wet and dry spells in bimodal rains in northern Tanzania will be assessed.

1.2 Climatic Background and Literature Review

The northern Tanzania study region comprises the latitudes 2-5°S and longitudes 32-40°E and has a NW-SE mountain range, which includes Kilimanjaro, and extends from the western Indian Ocean to Lake Victoria. The area experiences two main rainy seasons, namely the long rains (Masika, March-May) and the short rains (Vuli, October-December), which are associated with the northward and southward movement of the ITCZ respectively. Onset and end of rainfall seasons over Tanzania has received considerable attention in recent years, with work by Alusa and Gwange (1978) and Alusa (1978), Mhita and Nasib (1987) among others. The onset, duration and cessation of rains in East Africa were investigated by Mushi and Alusa (1974) and by Kinuthia and Asnani (1979). The long rains start in the first half of March and cease towards the end of May (Nyenzi, 1984).

These rains are associated with the northward passage and enventual disintegration of the near-equatorial trough and embedded confluence zone. The short rains start in the middle of October and continue to early-January (Mhita, Venäläinen, 1992). They are associated with the re-establishment and southward passage of the near-equatorial trough and accompanying wind confluence over the western Indian Ocean. Masika rains are more abundant, and Vuli rains are more variable.

The weather and climate over northern Tanzania is mainly influenced by monsoons, the Intertropical Convergence Zone (ITCZ), the subtropical anticyclones, tropical cyclones, the African jet streams, easterly/westerly wave perturbations, and extra tropical weather systems. Teleconnections with global scale systems like the El Niño/Southern Oscillation and regional systems play an important role. The two major anticyclones which significantly influence northern Tanzania climate are the Arabian and Mascarene high pressure cells (Ogallo, 1989, 1994).

Insight on climate variability has been provided through analysis of the Comprehensive Ocean-Atmosphere Data Set (COADS) sea surface temperatures (SSTs), outgoing longwave radiation (OLR) and surface wind in the Indian and Atlantic Oceans. Teleconnections with rainfall over East Africa have been revealed (Nyenzi 1988, Nicholson and Nyenzi 1990, Nigam and Shen 1993,). Ogallo (1989) noted that some East African rainfall principal component patterns

could be associated with warm and cold episodes over the eastern Pacific. He further observed that such links were highly seasonal with a maximum conditional probability of about 0.7 during Vuli (October-December) season.

Kapala et al (1994), on investigating the catastrophic floods of 1961/62, noted the occurrence of large-scale SST and wind anomalies over the equatorial Indian Ocean. The most striking feature being the development of an anomalously warm pool in the western equatorial Indian Ocean and above normal SST and cloudiness in the Arabian Sea.

Global scale signals in the tropics such as the Quasi-Biennual Oscillation (QBO) and Southern Oscillation (SO) are investigated in this thesis to identify distinctive patterns and relationships with northern Tanzania rainfall. This avenue of research has been covered earlier by Cadet (1985); Ogallo (1987); Ogallo (1988); Ogallo et.al (1988); Nyenzi (1988); and Hutchison (1992). Ogallo and Suleiman, (1987) observed that the chance of receiving below normal rainfall in East Africa associated with El-Nino events, is low for most parts of the region during both seasons. Similar results were observed by Njau (1987) from 300 mb temperatures and Southern Oscillation Index. During 1987-1993 period, most of northern Tanzania regions experienced rainfall below normal. Over the coast, annual rainfall recorded was below normal during March-May (Masika) season while the OND (Vuli) season was interrupted by two years of above normal rainfall for the

same period (Kavishe, 1993). This could be partly attributed to changes in SST and ENSO phase.

The study by Nicholson and Entekhabi (1987) gave evidence of a relationship between east Atlantic SST and East African rainfall, and a fragile connection with the Southern Oscillation Index (SOI) and the Quasi-Biennial Oscillation (QBO). Accordingly, increased rainfall was associated with a warm central Indian Ocean. Hastenrath et.al (1993) found that East African Vuli season rainfall is related to the SO through zonal pressure gradients produced by SST anomalies in the Indian Ocean. In high-phase SO events, SSTs are cool in the western Indian Ocean and surface westerly wind anomalies result in lower tropospheric divergence over equatorial East Africa. A global La Nina thus acts to suppress convection from October to December.

1.3 Intra-Seasonal research

Intra-seasonal oscillations in the atmosphere are generally defined as convective fluctuations with frequencies shorter than the seasonal cycle, of order 10-60 days (Makarau, 1994). At the intra-seasonal time scale, not much work has been covered in respect of Tanzanian climate and this thesis will serve to fill the gap. However, in other parts of Africa there have been efforts to understand climatic variabilities within the season where pentad (5 day) or dekad (10 day) data were analysed.

A recent study by Makarau (1994) observed intra-seasonal oscillations with two cycles: 10 to 25 and 40 to 50 days, when studying wet and dry spells in Zimbabwe summer rainfall. Similarly Levey (1993) found 20-35 day oscillations in precipitation and evaporation pentad time series for central south Africa during austral summer.

Other intra-seasonal oscillation studies which link tropical Africa and the adjacent oceans, include the study by Zhu and Wang (1993) who observed two prominent action centers in the central Indian and western Pacific Oceans for tropical 30-60-day convective variability. Rui and Wang (1990), documented the development and dynamic structure of tropical intra-seasonal convection anomalies using 5-day mean anomalous OLR and ECMWF analysed 200 and 850 hPa wind data. Matarira and Jury (1992), Anyamba (1992) and Murakami (1988) also have discussed intra-seasonal variability in the African sector.

Little work on intra-seasonal variability over tropical East Africa has been documented during Vuli season (October-December). In this thesis, chapters five, six and seven are dedicated to this.

The Vuli October to December season contributes > 30-50% of annual rainfall in northern Tanzania (Nyenzi, 1988). Ogallo (1989) using principal component analysis, found that over the coast of East Africa the first eigen vector could explain over 70 % of the total seasonal rainfall variance. The Vuli season in Tanzania is when rains affect the northern part of the country, assisting in

agricultural production and the replenishing of water resources. These rains are often associated with the retreat of the summer monsoon over India (Asnani 1993).

1.4 Hypothesis

Vuli wet spells are hypothesised to be related to:

i) moisture advection from the western Indian Ocean and Congo Basin.

ii) enhanced southeasterly flow across the Mozambique Channel converging with northeasterlies from the Arabian sea over East Africa.

iii) in-situ convection due to localised instability and heating.

To diagnose the mechanisms underlying intra-seasonal variability, ECMWF data on wind, vertical motion, divergence, atmospheric moisture, and derivatives therefrom, are used. Here ECMWF data for the period 1986- 1991 in the months October to December provide insight to processes responsible for the formation, development, and maturity or persistence of Vuli wet spells.

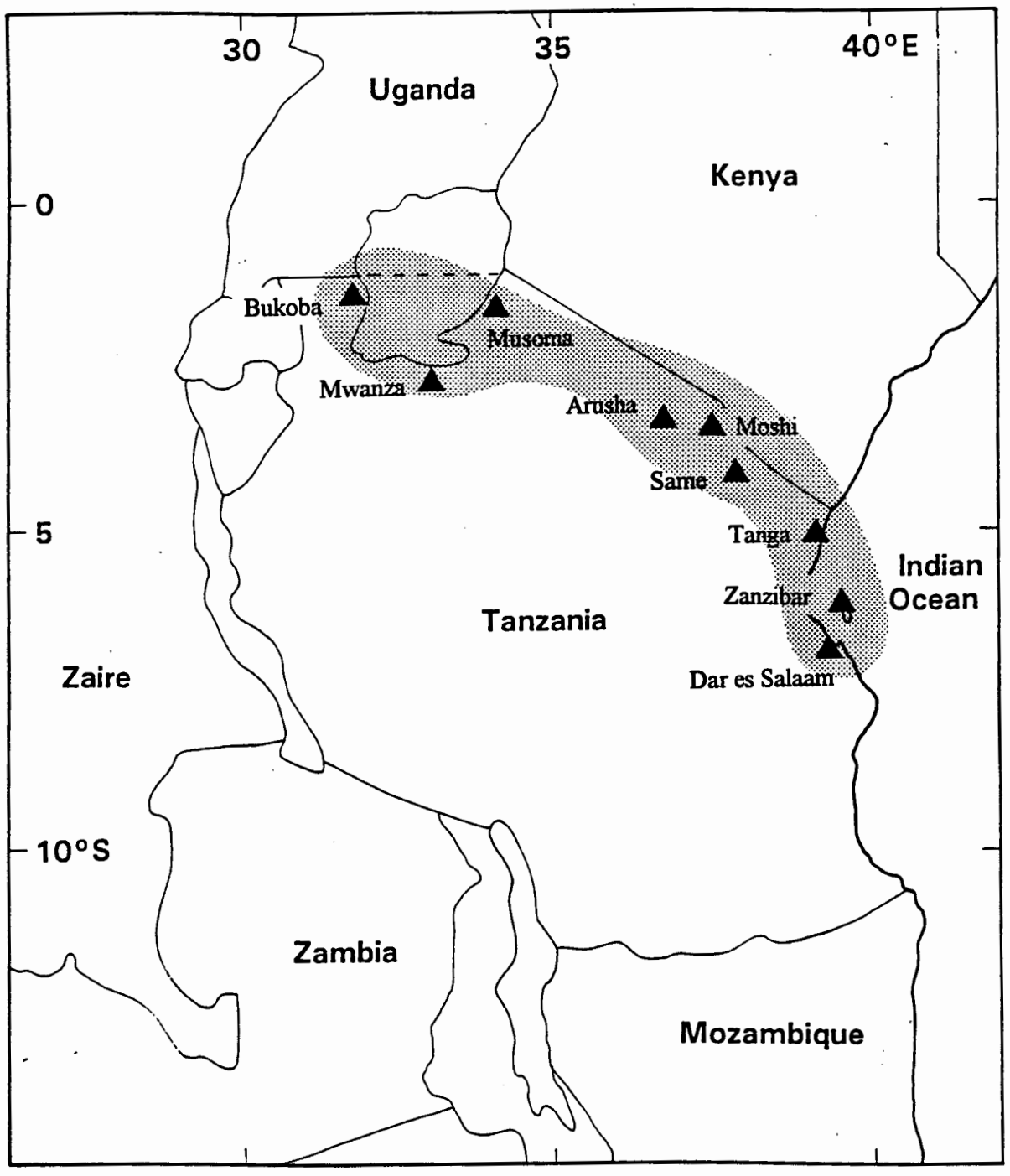

Figure 1.1: Tanzania map showing the study area (shaded); referred as Northern Tanzania in this study.

▲ = Station location

Chapter 2: Data and Methodology

2.1 Data and sources

The data required to undertake this study of predictability and dynamics of Vuli and Masika rainfall over northern Tanzania, include daily, pentads and monthly rainfall data. Monthly data are used for seasonal compositing and analysis of precursor patterns for sea surface temperature (SST), outgoing longwave radiation (OLR), wind, quasi-biennial oscillation (QBO) and southern oscillation index (SOI). ECMWF pentad data are used in intra-seasonal analysis, covered in chapters 5, 6 and 7. The basic parameters obtained are geopotential height, zonal wind component (u), meridional wind component (v), vertical motion (ω), specific humidity (q), temperature (T), and derivatives therefrom as described below.

2.1.1 Rainfall data

The rainfall data used in this study consists of daily, pentad, and monthly totals for 9 stations representing a BI-modal rainfall region in northern Tanzania as illustrated in figure 1.1. All rainfall data were obtained from the Climate section of the Directorate of Meteorology in Tanzania.

The period 1960-1990 was selected since all stations had continuous quality records. At least two stations from each geographic sector (i.e. coast, highlands and Lake Victoria basin) were chosen. Few missing data were filled in using the

long-term monthly mean. The rain-gauge used in Tanzania since 1921 is the standard 12.9 cm and rainfall is measured at a height of 25 cm above the surface.

2.1.2 Sea- surface temperature (SST)

The sea surface temperature used in this study is derived from the Comprehensive Ocean-Atmosphere Data Set (COADS) produced by the National Oceanic and Atmospheric Administration (NOAA). The data were obtained as monthly means on a 2° x 2° grid for the domain extending from 20° N to 40° S and 70° W to 110° E for the period 1950-1988. The preparation and quality control makes COADS data as representative as possible (Rocha 1992). SST affects the generation and intensification of tropical disturbances and variations of the inter-tropical convergence zone (ITCZ), (Gadgil et al., 1984). Here the data are combined into seasonal means for composite analysis.

2.1.3 SOI, Wind, OLR and QBO

Differences between standardised monthly mean atmospheric sea level pressures at Tahiti (17.5° S, 149.6° W) and Darwin (12.4° S, 130.9° E), are known as the Southern Oscillation Index (SOI). A High-SO phase is defined by anomalously high/low pressure at Tahiti/Darwin (Hastenrath et al., 1993). Monthly bulletins issued by Climatic Analysis Center (CAC 1983-), carry tables of SO indices. These indices have been used in a number of studies (e.g. Lindesay,1988; Jury

and Levey 1993: Jury and McQueen, 1993). In this study seasonal values are used in regression analysis to reduce noise associated with large-amplitude equatorial wave disturbances.

Wind, OLR, and QBO data are also provided by the Climate Analysis Center (Washington DC, USA). The horizontal wind data used in this study were available as zonal (u) and meridional (v) components at 700 and 200 hPa levels for the period 1968-1987. The data are at 5° resolution as monthly means. The 700 hPa level is where boundary layer noise is minimised and is close to the level of maximum water vapour transport.

OLR is also available in the same format as wind, and is a product of NOAA satellites from its Advanced Very High Resolution Radiometer (AVHRR). Low (high) values of OLR indicate greater (less) cloudiness and convective activity (Makarau, 1994). The OLR data period is 1975-1988.

The QBO data, available as 30 the hPa zonal wind departure over Singapore, yields a quasi-periodicity of the order of 2.1-2.4 years (Mason, 1992). Rainfall seasonal periodicity over northern Tanzania will be analysed to establish a relationship with QBO.

2.1.4 European Centre for Medium Range Weather Forecasts (ECMWF) data

ECMWF data sets are used in intra-seasonal analysis covered in chapters 5, 6 and 7. The basic parameters obtained are geopotential height, zonal wind component (u) , meridional wind component (v) and vertical movement (ω), specific humidity (q), temperature (T), etc. ECMWF pentad fields were used for analysis of kinematic and thermodynamic structure. The data were extracted for the season October-December (Vuli) in the period October 1986 to December 1991. The domain of analysis incorporates a region extending from 20° N to 40° S and 30° W to 100°E at a resolution of 2.5° by 2.5°.

The ECMWF analysis system undergoes continual revision and operational development so that better forecasts will be realised. Changes made prior 1989 have been discussed by Bengtson and Shukla (1988), Hoskins et al. (1989) and Klinker (1993). The revisions include:

- Improved humidity analysis, including the use of satellite precipitable water data;
- Introduction of improved spatial resolution and vertical model levels and refined structure functions; and
- Improved analysis of divergent wind.

2.2 Methodology

This section highlights the various methods which were used in this study. Different analysis techniques have been employed to understand the evolution of inter-annual variability and intra-seasonal oscillations. A detailed account of each is discussed:

2.2.1 Inter-annual variability analysis

2.2.1.1 Rainfall Time Series and Criteria for Selection :

Rainfall data from the 9 selected stations were all normalised appropriately with respect to the means and standard deviation as follows:

$$Z = (x_i - x) / \sigma$$

Where Z is the normalised standardised departure in values, x_i is individual data points (total rainfall for the month), x is historical mean rainfall and σ is the historical standard deviation. The values of Z provide immediate information about the significance of a particular deviation from the mean (Nyenzi, 1988). An area rainfall index was computed by averaging time series of standardised departures for each month and then combining into seasonal values. This type of normalisation has been used by Nyenzi (1988), Levey (1993) and Makarau (1994) amongst others. Figure 2.1 illustrates the seasonal cycle of area rains centered on April and November.

The seasonal values for 9 individual stations were inter-correlated. Long rain (Masika) inter-correlations are of order + 0.4 (with 30 degrees of freedom),

whereas short rains (Vuli) inter-correlations are of order + 0.7 (significance at the 99% confidence limit). Time series of seasonal area rainfall departures were used to identify wettest and driest years in the period of overlapping OLR data 1975-1987 (figures 2.2a and 2.2b). The criteria used in choosing the wet and dry years were ≥ 0.4 and ≤ -0.2 respectively. Wet years identified for the Vuli (October-December) season include: 1977, 1978, 1982, and 1986. Dry years are 1979, 1980, 1983 and 1987. Wet years in the Masika (March- May) period are 1978, 1979, 1981 and 1986 and dry years are 1980, 1983 and 1984.

2.2.1.2 Spectral analysis

Spectral analysis was performed for the Vuli (October-December) and Masika (March- May) rainfall seasons, to determine statistically significant inter-annual periods and amplitudes corresponding to each season. Relationships with global signals (e.g. ENSO, QBO), may be inferred.

2.2.1.3 Composite analyses

Instead of studying each wet season or pentad case separately, a group of cases assumed to have similar characteristics are averaged together. The seasonal composite analysis utilises SST, OLR, and wind data at 700 and 200 hPa during Vuli and Masika of 1975-87. The compositing procedure consists of adding each

parameter value at the same level at each grid point in the domain for all cases and dividing by the sample size to get the mean value.

This technique has been used before in climatological work such as Cadet (1985), Murakami (1988), Matarira and Jury (1992), Park and Schubert (1993), Levey (1993), Nassor (1994) and Makarau (1994). The advantage of using composites is that common features and patterns are better indicated than in individual cases. This method also reduces the total number of maps and figures. Individual cases were selected according to prescribed criteria and sequences of gridded SST, OLR, and winds were averaged for the specified wet and dry season and for periods 2, 4 and 6 months prior. The historic mean was then subtracted to produce anomalies, thus inter-annual differences and underlying signals could be determined.

2.2.2 Intra-seasonal variability analysis

Sub-seasonal convective variability for the Vuli (October- December) rainfall season is explored in chapters 5, 6 and 7 using pentad data. Daily rainfall and ECMWF data are averaged to pentad (5-day means) in accordance to World Meteorological Organisation (WMO) devised format. The Vuli season comprises 18 pentads starting from pentad 1: 3-7 October, to pentad 18: 27-31 December. Pentad area-averaged rainfall (figures 2.3a-h) were inspected and the following criteria was used to select major wet spells:

>25 mm/pentad occurring in the middle (pentads 8-11) of the Vuli season.

Following identification of the wet spell (P0), the preceding pentads establish the precursor patterns in terms of dry (P2) and onset (P1) phase. These were usually one and two pentads before the wet spell, respectively. Composites based on 5 individual cases were formed, one for each year available except for 1987. Seasonal (October-December) means were determined and anomalies were computed by:

5 case composite - mean = anomaly.

Mean circulation patterns offer little guidance for weather prediction, and as pointed out by Jones (1985), skill in forecasting is measured by how well anomalies can be forecast. Hence, chapters 6, 7 and 8 give much attention to anomaly analysis.

Intra-seasonal composite selection is based on Vuli rainfall data between 1986 and 1991 when overlapping ECMWF weather data is of sufficient quality. More details on pentad formation methodology, is provided in chapter 6. The same procedure was also used for dry spells which is covered in chapter 7.

The basic parameters obtained from the ECMWF center were geopotential height, zonal wind component (u), meridional wind component (v), vertical wind (ω), temperature (T) and humidity (RH). Derived variables such as divergence, vorticity, precipitable water, water vapour flux, horizontal wind velocity, and divergent water vapour flux were then computed.

Table 2.1

List of primary ECMWF parameters used in this thesis.

PARAMETER	PRESSURE SURFACE (hPa)			UNITS
Geopotential height	850	—	200	gpm
Temperature	850	—		°C
Zonal wind	850	—	200	$m\ s^{-1}$
Meridional wind	850	—	200	$m\ s^{-1}$
Vertical motion	—	500	—	$Pa\ s^{-1}$
Relative humidity	850	—		%

Table 2.2

Table of derived parameters calculated and used in this thesis.

PARAMETER	PRESSURE SURFACE (hPa)			UNITS
Divergence	850	—	200	s^{-1}
Vorticity	850	—	200	s^{-1}
Velocity potential	850	—	200	$m^2\ s^{-1}$
Precipitable water	between	1000 - 300	levels	mm
Water vapor flux	between	1000 - 500	levels	$kg\ m^{-1}\ s^{-1}$
Divergent wind comp	—	—	200	$m\ s^{-1}$

2.2.3 Dynamic computations: Derived parameters

The reason for producing secondary derived parameters, is that such values when used in combination with primary parameters yield results which describe meteorological kinematic and thermodynamic structure (Parker 1994).

2.2.3.1 Divergence and Velocity potential

There is a useful decomposition of the horizontal wind field into distinct contributions: uniform translation, horizontal divergence, vorticity and deformation. Bluestein (1992, pp87-113) describes these and provides ways of computing their magnitude. The physical properties of the horizontal two-dimensional wind fields (V), can be described by considering the rotational and irrotational terms, also known as nondivergent and divergent respectively.

That is : $V = V\psi + V\chi$ .....Eq 2.1

where ψ is the stream function (rotational) part of the wind, while χ is the velocity potential (irrotational). In this thesis only the irrotational part of the wind will be analysed as in Levey (1993). A particular contribution, divergence, is of importance because it controls the evolution of the wind field and resultant dynamics through the vorticity equation. Only in the presence of horizontal divergence (Bluestein, 1992, pp. 87-113) will there be vertical motion and the possibility of the release of latent heat from the water vapour.

The contribution to the velocity field from pure divergence can be singled out for further description. Divergence is defined (Bluestein, 1992) as

$\partial u/\partial x + \partial v/\partial y = \delta = \nabla_h . V$.....Eq 2.2

u = zonal wind component

v = meridional wind component

x = longitudinal distance

y = latitudinal distance

The subscript ($_h$) means that derivatives are computed on a horizontal surface. Velocity potential of pure divergence field, is defined as follows: $V = -\nabla_h \chi$ while $\nabla_h . V = -\nabla_h^2 \chi = \delta$ which is the divergent contribution to the total wind field. The isolines of this pure divergence field have vector rates of change which are the divergent contribution of the wind field.

2.2.3.2 Vorticity

Vorticity (ζ) is the rate of spin experienced by the air in the local vertical. Vorticity can be calculated as;

$\zeta = \partial v/\partial x - \partial u/\partial y$ .....Eq 2.3

2.2.3.3 Precipitable Water Precipitable water (PW) is the measure of the atmospheric vertically integrated water content. Theoretically it is the depth of

water that would be obtained if all the water in the column were condensed onto a lower surface of unit area. In mathematical terms, PW is defined between two specific atmospheric levels as:

$$PW = \frac{1}{g} \int_{p_2}^{p_1} q \, d \, p \quad \text{.....Eq 2.5}$$

where: q is the specific humidity between pressure levels.

p_1 and p_2 are 1000 hPa and 300 hPa respectively

$g = 9.80665 \text{ m s}^{-2}$

Measurements are in kg m^{-2} or in millimeters (mm), taking into account that density is 10^3 kg m^{-3} 1 kg m^{-2} of precipitated water is equivalent to 1 mm. For purposes of this study PW is in mm and integration is between the surface (1000 hPa) and 300 hPa. Most of the continental data points are near the 850 hPa level, so the integration starts at that level there.

2.2.3.4 Water vapour flux (Q)

Q is defined as the advection of moisture through a deep tropospheric layer by the horizontal wind. Thus, like precipitable water, **Q** is also obtained through vertical integration.

In this thesis, integration is between the 1000 hPa and 500 hPa levels (except for the plateau). The bulk of horizontal transfer of water vapour in the tropics is near 700 hPa.

$$Q = \frac{1}{g}\int_{p_2}^{p_1} qVdp \quad \text{.....Eq 2.6}$$

where q = specific humidity

V = velocity at a particular level

p_1 and p_2 are 1000 hPa and 500 hPa respectively, however over the plateau the high pressure limit takes the value of 850 hPa.

2.2.3.5 Divergent water vapour flux

The water vapour flux divergence is the velocity potential of water vapour flux. The velocity potential function is solved once the water vapour flux components are known. Water vapour flux divergence is a vertically integrated resultant meteorological variable and gives the sense of the divergent (non-rotational) nature of moisture in the atmosphere. It is a more useful forecasting tool than velocity potential alone, since water vapour is included.

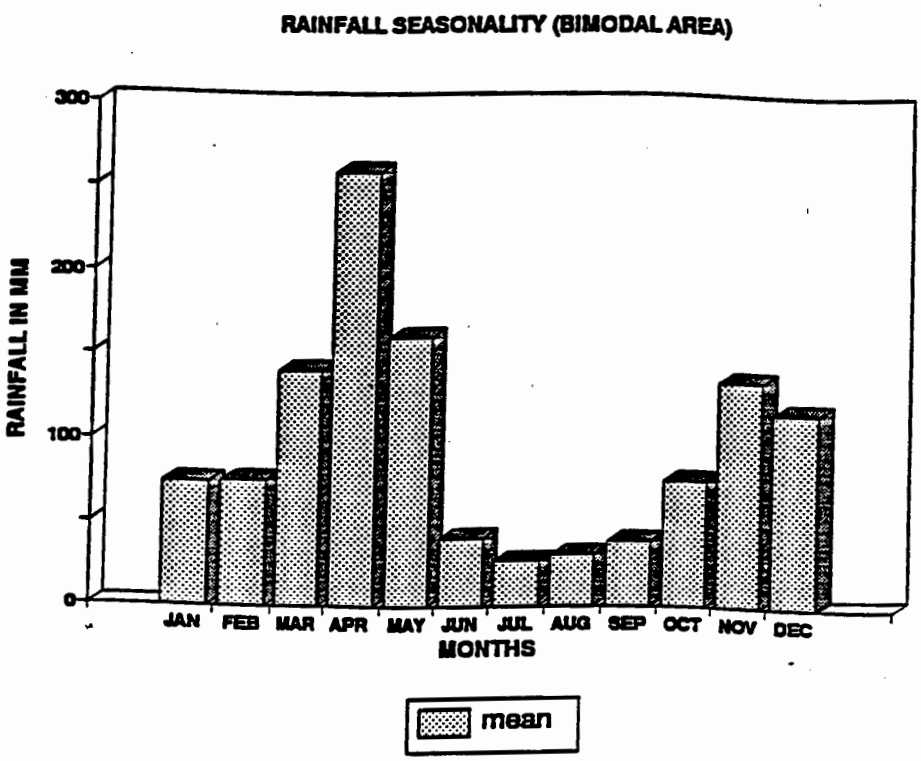

Figure 2.1: Area-averaged rainfall showing seasonality (BIMODAL AREA) for 9 stations in northern Tanzania as in figure 1.1.

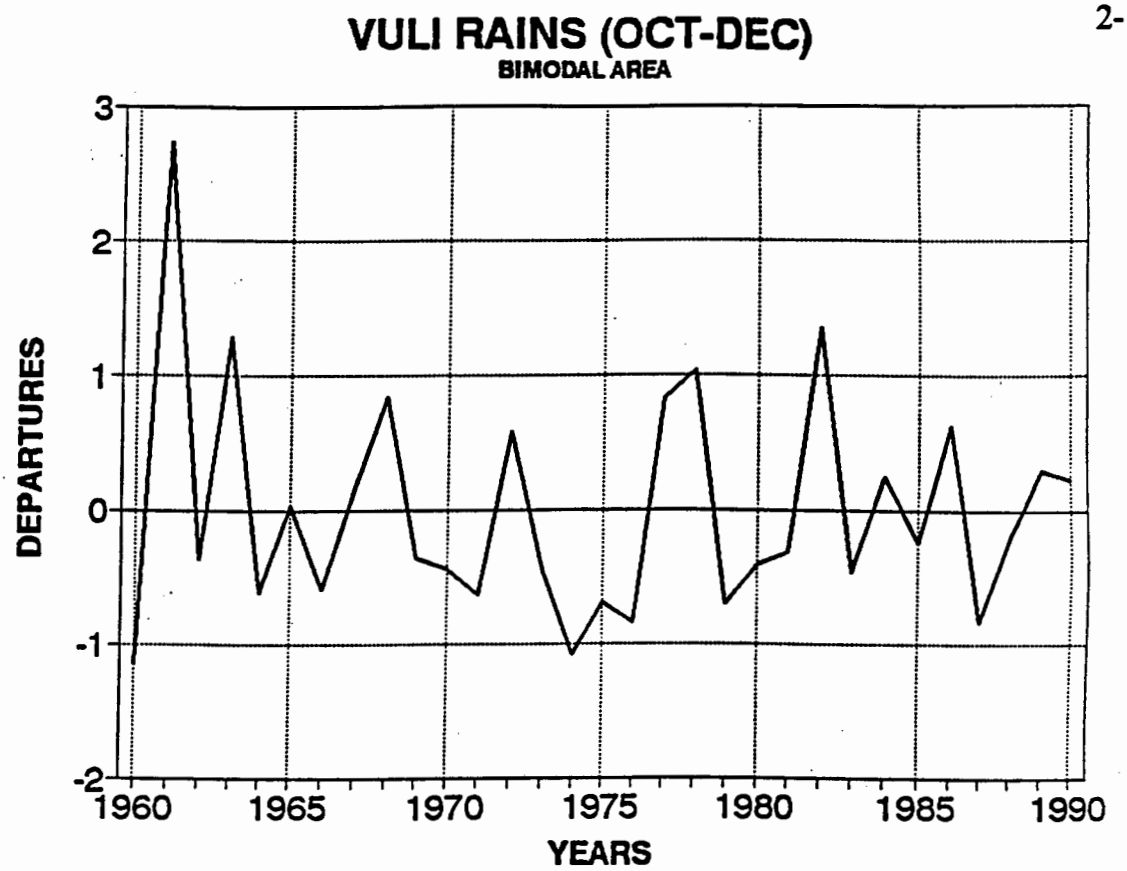

Figure 2.2a: Northern Tanzania 9-station area index (October-December)

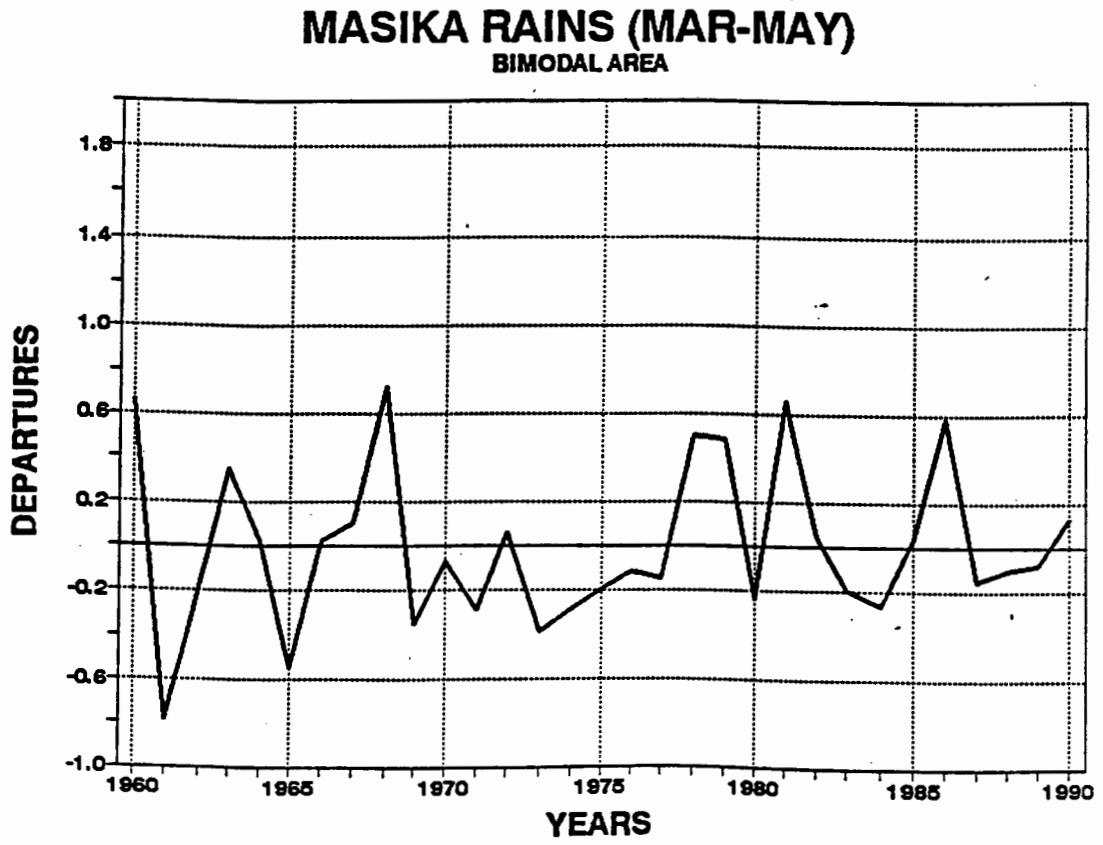

Figure 2.2b: Northern Tanzania 9-station area index (March-May)

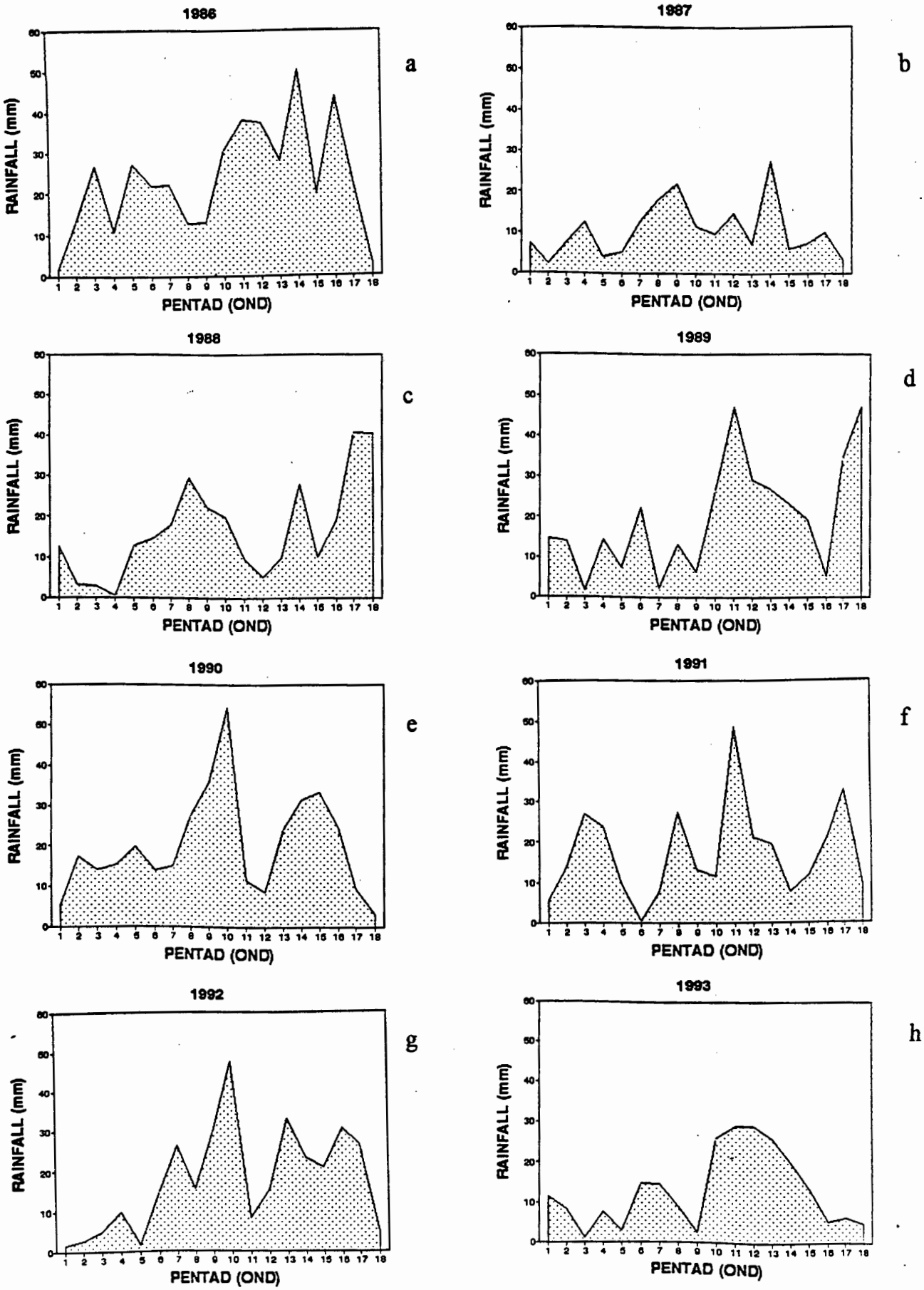

Figure 2.3 : Pentad area-averaged rainfall

Chapter 3: Results of rainfall analysis

Climatology information has a great value especially to the social-economic benefit of farmers, water managers, energy suppliers and public policy makers in Tanzania. In this chapter, results on seasonality, inter-annual rainfall time series and in-seasonal distribution will be illustrated. Another aim will be to test whether significant correlations exist between SOI and QBO and seasonal rainfall.

3.1 Seasonality and distribution

Table 3.1 as extracted from Mhita and Venäläinen (1992), gives the onset and end of rains for selected stations in northern Tanzania.

Table 3.1: Mean week and percentage frequency of start of rains

Season	Masika (MAM)			Vuli (OND)		
Station	25%	50%	75%	25%	50%	75%
Mwanza	Feb- 2	Feb- 3	Feb- 4	Oct- 1	Oct- 2	Oct- 3
Moshi	Feb- 3	Mar- 1	Mar- 3	Oct- 2	Oct- 3	Oct- 4
Tanga	Feb- 3	Feb- 4	Mar- 2	Oct- 1	Oct- 3	Oct- 3
Dar es salaam	Feb- 2	Feb- 4	Mar- 2	Oct- 1	Oct- 3	Oct- 4

Table 3.2: Mean week and percentage frequency of end of rains

Season	Masika (MAM)			Vuli (OND)		
Station	25%	50%	75%	25%	50%	75%
Mwanza	May- 2	May- 4	Jun- 1	Jan- 1	Jan- 2	Jan- 3
Moshi	May- 4	Jun- 1	Jun- 2	Dec- 3	Dec- 4	Jan- 1
Tanga	May- 3	Jun- 1	Jun-2	Dec- 4	Jan- 1	Jan- 2
Dar es salaam	May- 4	Jun- 2	Jun- 3	Dec- 4	Jan- 1	Jan- 2

The percentages in tables 3.1 and 3.2, refers to years of reporting when the rain began or ended on the respective weeks. Some stations started reporting rain as far back as 1893, though data for 1913-1920 is missing due to the first European civil war. The three most rainy months were chosen in this study. March was chosen rather than February as the beginning of Masika season, because by that time rainfall is already distributed to all stations in northern Tanzania. In the first week of October, all stations report rain for the Vuli season. The same reasoning applies to the end of season as illustrated in table 3.2.

Figure 2.1 illustrates monthly area averaged rainfall for the nine stations chosen, namely Dar es Salaam, Tanga, Zanzibar, Same, Moshi, Arusha, Musoma, Mwanza and Bukoba. Two peak seasons centered on April and November, are Masika (March- May) and Vuli (October- December) respectively. It is evident from the

figure that there is no month without rain, however the two major seasons are well defined.

In figures 3.1a-3.1c the seasonal distribution depicts differences from one station to the other. A number of different characteristics affect different parts of the region depending on factors such as local water budget, wind regimes, altitude, and interaction between meso-scale and large-scale weather systems. Coastal stations led by Zanzibar report higher rainfall mainly due to moisture advection from the Indian Ocean. The northeastern highland stations report relatively less rains since the upslope-downslope orographic setting depletes moisture from the incoming moist wind before it is deposited further inland. Lake Victoria basin rainfall is modified by land-lake breezes; Bukoba being on the leeward side of the lake receives maximum moisture. However, these are just meso-scale factors.

3.2 Time series analysis

Figures 2.2 (a) and 2.2 (b), shows the interannual time series analysis for north Tanzania for the two seasons Vuli (October- December) and Masika (March-May) respectively. During Masika season, the year 1968 was the anomalously wet year and 1961 was the most dry year. While in Vuli season, 1961 had the most excessive rainfall and 1960 and 1974 were the driest years. The 31 year period under consideration saw Vuli season experiencing more drier years than Masika. However, the Vuli season of 1961 was remarkable in East Africa, because rainfall

was so excessive that the level of Lake Victoria rose by 2 m and remained so for many years. It was mentioned by Nyenzi (1988), that there are occasions when rainfall for Vuli season has been missed in some areas because the ITCZ passed unnoticed (or diffuse). Stations that fall below -0.2 of the mean normalised departures were classified as dry years while wet years are those above 0.4. The dry years chosen were indeed noted for widespread drought in the region.

3.3 Spectral and correlation analysis

Spectral analysis results are presented in figures 3.2 for Vuli and 3.3 for Masika. The purpose of this analysis is to investigate the presence of any inter-annual periodicities in seasonal rainfall. Vuli season is characterised by peaks around 2.3 year and 5 year period which are associated with Quasi-Biennial Oscillation (QBO) and fluctuation of the Southern Oscillation (SO) respectively. Masika season spectral amplitude peaks around 3.8 years period and with a relatively weak power compared with Vuli season. QBO linkage was clearly illustrated by McQueen and Jury (1993) using November rainfall for Tanga and Arusha. Cycles at the SO frequency are weaker during Vuli when considering stations further inland.

Ogallo (1986) detected significant negative correlation between Vuli rainfall and the SOI when a larger area was used. His study included stations in eastern Kenya and north east coastal Tanzania, these alone are highly negatively correlated with

the SOI. Nicholson (1986), indicated that there is little statistical coherence between the SOI and East African rainfall at 3.5 and 5-6 years, although rainfall and SOI spectra showed a remarkable resemblance.

Hastenrath et al (1993) found that positive correlations between rainfall and SOI do exist in April-May around Lake Victoria and in parts of East African highlands. Negative correlations were prominent along the Tanzanian coast in October-November months; with largest values -0.8. In this work, correlation analysis up to six months lag was done each for QBO, SOI with seasonal rainfall (Masika and Vuli) some of the results are shown in table 3.3.

Table 3.3: Lag-correlation results of seasonal rainfall with QBO and SOI

Season	Masika (MAM)	Vuli (OND)
QBO (Optimum corr.)	+ 0.32 (-6 lag)	+0.22 (0 lag)
QBO (0-lag)	- 0.16	+0.22
SOI (Optimum corr.)	- 0.13 (-6 lag)	- 0.45 (-2 lag)
SOI (0-lag)	+ 0.06	- 0.42

As shown in table 3.3 a positive correlation (0.32) at 95 % confidence limit exists between Masika season and QBO six months before the start of the season, whilst correlation with SOI index is low. Vuli rainfall show a significant negative correlation of -0.45 at 99 % confidence limit with SOI two months prior to the onset of rains. QBO and

Vuli rainfall season show a weak positive correlation. Thus west phase QBO in the southern spring favours Vuli rains and anticipates Masika rains. A warm phase ENSO (-SOI) favours Vuli rains but does not influence Masika. Operationally, prediction using QBO and SOI will need to be supplemented with other teleconnection signals as outlined in the next chapter.

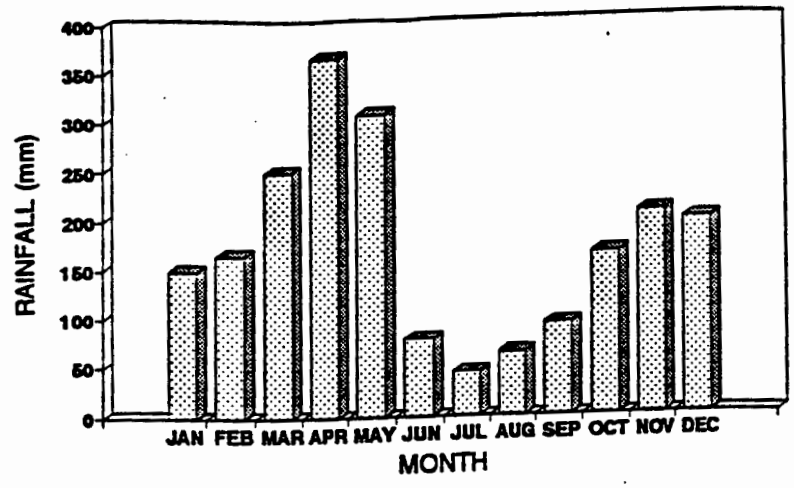

SEASONAL RAINFALL
BUKOBA 1960-92

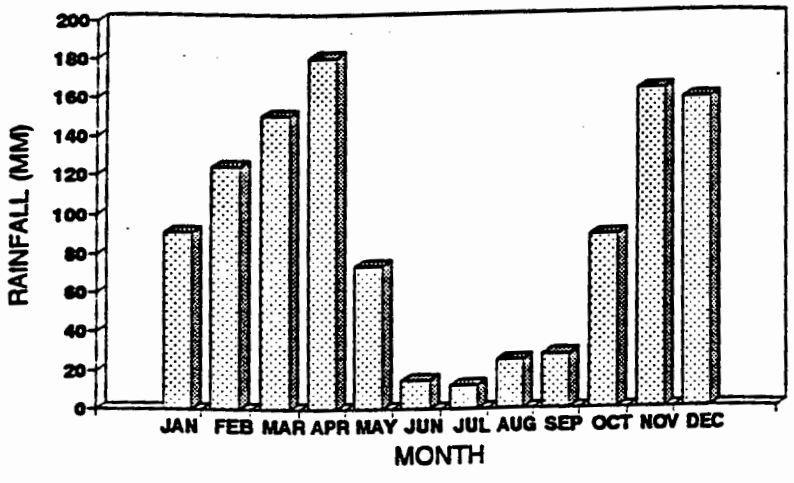

SEASONAL RAINFALL
MWANZA 1960-90

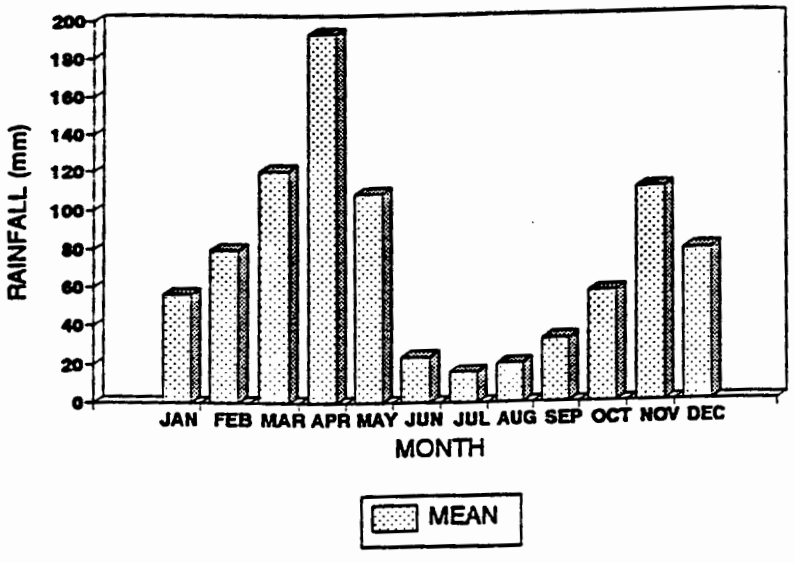

SEASONAL RAINFALL
MUSOMA 1960-90

Figure 3.1a: Seasonal rain distribution over Lake Victoria basin.

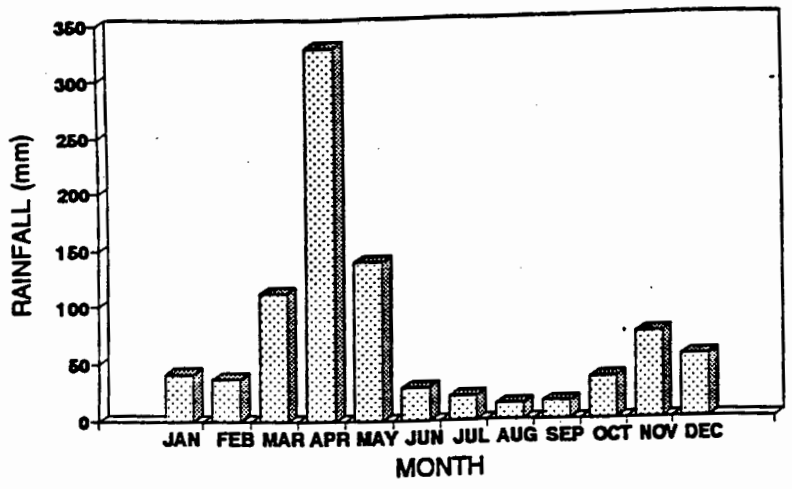

SEASONAL RAINFALL
MOSHI 1960-90

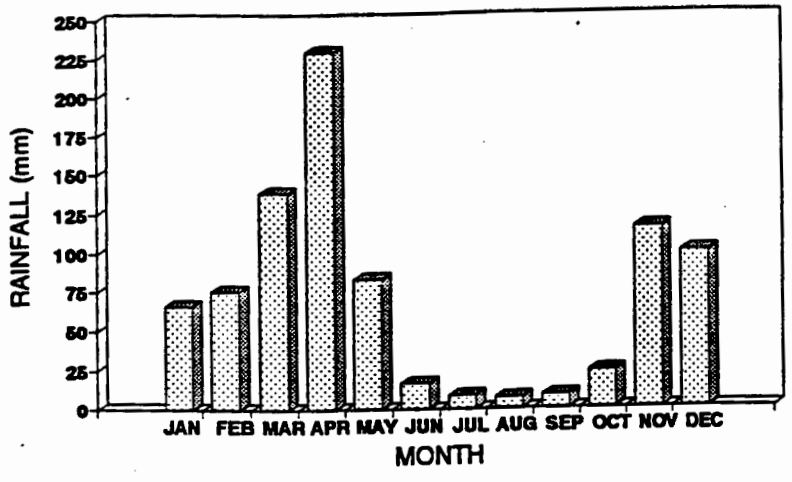

SEASONAL RAINFALL
ARUSHA 59-90

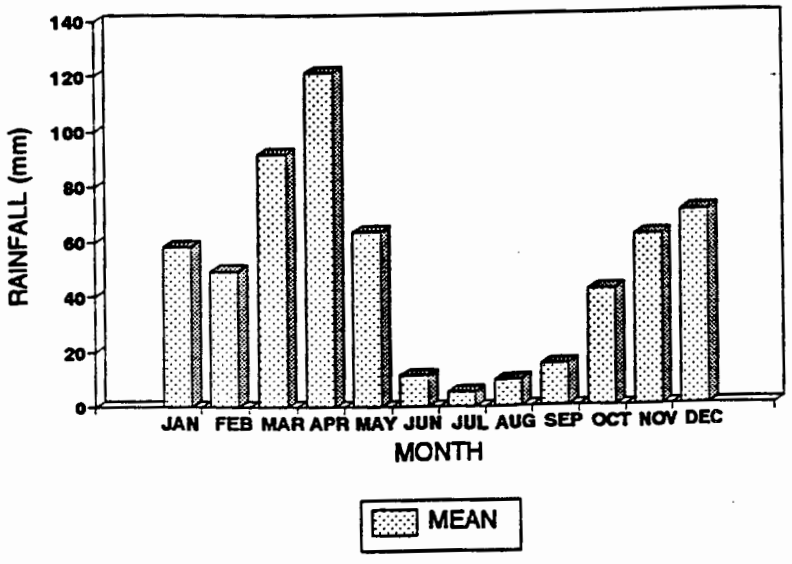

SEASONAL RAINFALL
SAME 1960-90

Figure 3.1b: Seasonal rain distribution over northeastern highlands.

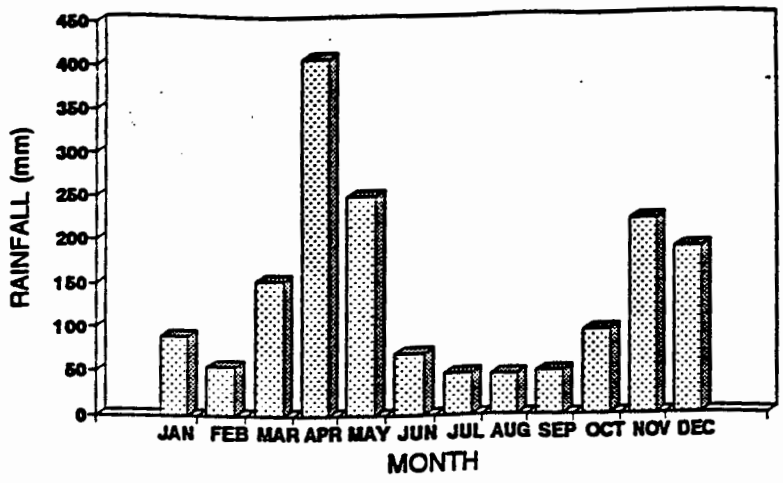

SEASONAL RAINFALL
ZANZIBAR 1960-90

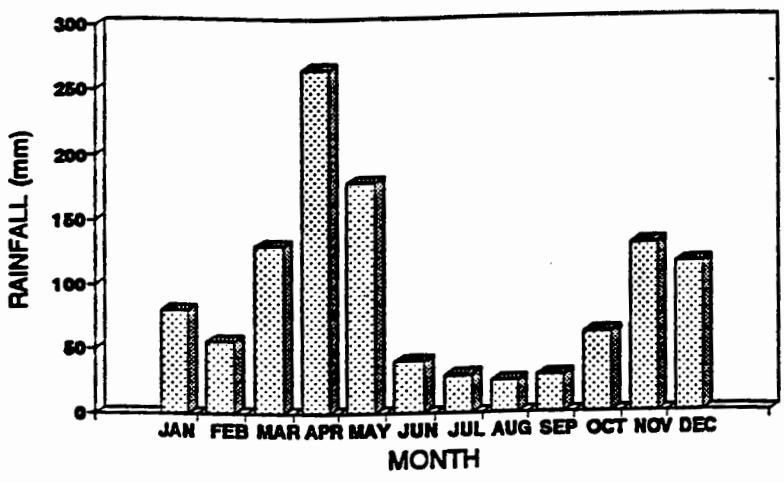

SEASONAL RAINFALL
DAR-ES-SALAAM 1960-92

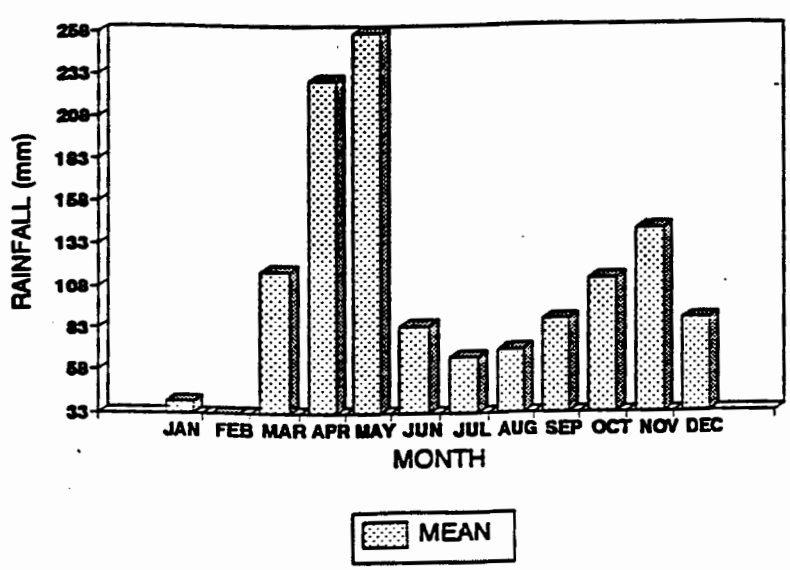

SEASONAL RAINFALL
TANGA 60-90

Figure 3.1c: Seasonal rain distribution over the coastal area.

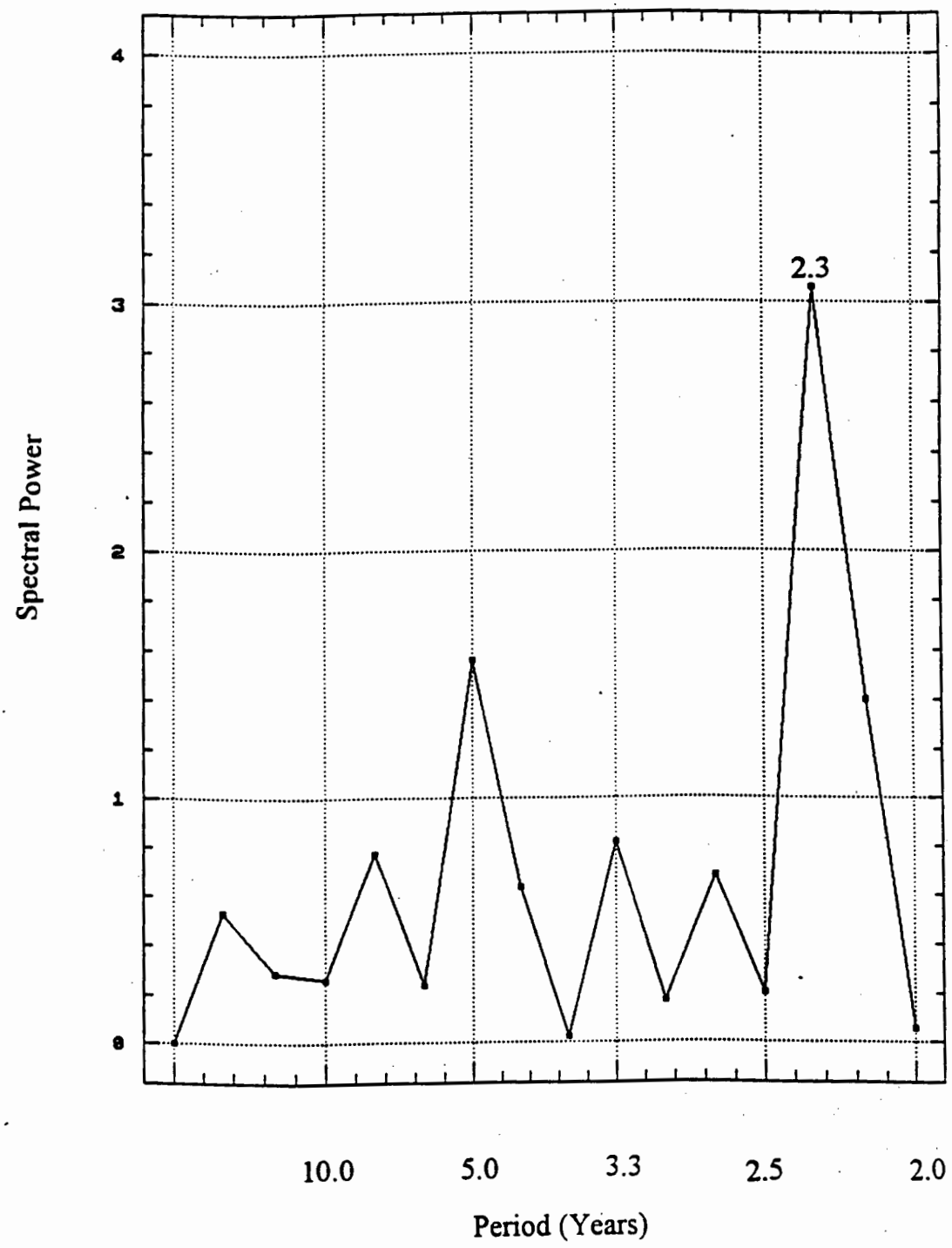

Figure 3.2 : Spectral analysis of VULI rainfall time series.
The period is 1960-1991

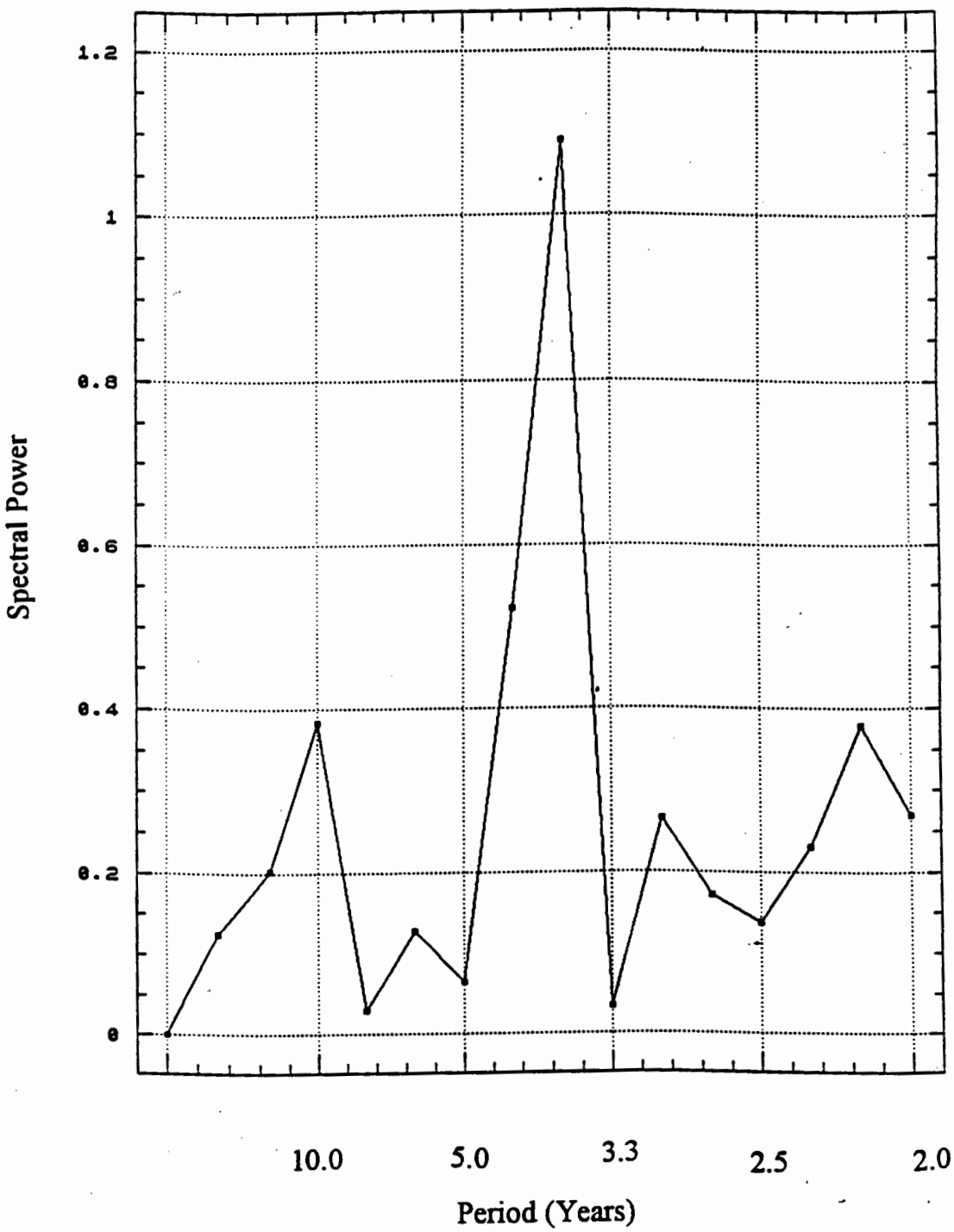

Figure 3.3 : Spectral analysis of MASIKA rainfall time series.
The period is 1960-1991

Chapter 4: Results of seasonal composites and precursors

This section highlights the results obtained in the analysis of sea surface temperature (SST), out-going longwave radiation (OLR), and upper and lower winds. The bimodal area of northern Tanzania that receives rains in October to December (OND) and March to May (MAM), is considered.

Composite analysis offers a way of describing common characteristics of wet and dry seasons. The structure and magnitude of the anomalies will be outlined for predictive purposes using fields at prior lags.

The area rainfall departures as illustrated in chapter 3, are computed and the four wettest and driest years are identified in the period 1975-1987. The precursors of floods and drought seasons are assessed using composite sequences of gridded SST, OLR and winds at 200 and 700 hPa level data. Composites are averaged for the specified season and for periods 2, 4, and 6 months in advance; and the historical mean for the period of overlapping datasets is subtracted to produce anomalies. In this way, evolution of extreme rainfall scenarios is tracked for predictive purposes. The COADS SST dataset extends from 1950 to 1988, OLR extends from 1974 to 1987, and CAC winds extend from 1968-1987. The interest of this chapter however, is to analyse the combined variability of these fields. Statistical significance tests were performed on zones with large SST differences between wet and dry seasons. The statistical method is given in appendix 1. For the Vuli season these differences are significant at the 95% confidence level.

Only the overlapping segment between datasets is considered, so results are pertinent to that period and should not be generalised too much.

4.1 Sea Surface Temperature (SST)

4.1.1 Vuli (OND) Wet composite evolution

Figure 4.1 illustrates the SST composite sequence for wet Vuli seasons at lags 0, -2 , -4 and -6 months. The years composited are 1977, 1978, 1982 and 1986, while the months are October, November and December (Vuli season).

At 6 months before the Vuli season onset (-6 lag), the western coast of Africa in the Atlantic Ocean depicts a cold pool of the order 0.4°C below the 1974-1988 mean from equator to the Namibian coast. Positive anomalies in the Atlantic Ocean are observed off the Brazil coast extending to 10° W. Indian Ocean sea surface temperatures are close to normal except for a cold tongue emerging from western Australia towards the central Indian Ocean.

At -4 months lag, apart from the decrease of SST anomalies in the southeast Indian Ocean, both oceans show a slight warming. In the Indian Ocean, warming is noted along 40° S between 50° E and 90° E, while in the Atlantic Ocean the warm pool off the Brazil coast has intensified in two months to reach 0.4° C above the mean. Generally a northward movement of warm waters is observed as positive temperature anomalies increase with a northward propagation. Two months before, illustrates warming of SST in both tropical and subtropical West Indian Ocean, from near normal (4 months before) to 0.3°C above the mean.

A tongue of negative anomalies from Australia persists and a pool of cold water with SST anomaly in the order of -0.4° C develops around 90° E, 15° S. The area off Brazil remains warm throughout, while the rest of the Atlantic Ocean is below normal.

At 0 lag the western Indian Ocean and the Atlantic Ocean maintain the same configuration. Above normal SST remain along the East African coast, otherwise near normal SSTs occurs.

In this analysis the following observations are ideal for wet Vuli prediction purposes;

- A cold pool emanating from Australia spreading to around 90° E, 15° S, throughout.
- Positive SST anomalies along the eastern African coast, starting 2 months before the season.
- Positive SST anomalies along the Brazilian coast (50°W, 35°S), throughout.

4.1.2 Vuli (OND) Dry composite evolution

Figures 4.2 represent the SST composite sequence for dry Vuli season. Composite years are 1975, 1976, 1979 and 1983, while the precursor months presented are -6 months lag, -4 months and -2 months lag. Patterns at -6 months lag reveal no striking features. The Atlantic, central and southern Indian Ocean show negative

anomalies while SST in the western Indian Ocean along the East African coast are near normal.

A pool of warm water is evident poleward from South Africa. At -4 month lag, the Indian Ocean exhibits near normal temperatures while the Atlantic Ocean SST has decreased with the Gabon coast recording anomalies in the order of -0.6°C. A further decrease of SST two months prior to the onset of a dry Vuli season is recorded in both oceans (-2 lag). A cold pool develops on either side of the tropical African coast extending a total of 50° of longitude. Dry Vuli season SST (0 lag), show below normal SST persisting in both oceans, however a tongue of above normal temperatures is evident in southeast Indian Ocean waters. This warm pool develops gradually throughout the evolution (six months).

Observations which anticipate a dry Vuli season are;

- Persistence of below normal SST throughout the entire period of evolution, notably 2 months prior to Vuli season when tropical SSTs decrease.

4.1.3 Masika (MAM) Wet composite evolution

The Masika rainy season is experienced around March, April and May (MAM) in northern Tanzania and is known as the long rains. In this study, wet Masika composite years are 1978, 1979, 1981 and 1986, while the precursor months are -6 months lag, -4 months and -2 months lag. In figure 4.3, -6 month lag composite structure portray positive SST anomalies in the Mozambique Channel, extending

southwest of Madagascar and the East African coast in the Indian Ocean. Another warm pool is revealed east of Brazil in the Atlantic Ocean (50°W, 35°S). The other parts of the two oceans show negative anomalies.

Four and two months prior to Masika season patterns are similar showing a decrease of SST in the middle of the Atlantic Ocean.

At 0 lag, negative anomalies in the Atlantic Ocean broaden and spread to the southwest African coast. A notable feature that persists throughout evolution is the warm pool off the Somali coast that extends to the Tanzanian coast.

Observations that are ideal for wet Masika prediction purposes are;

- Persistence of positive anomalies poleward from the Mozambique Channel throughout.
- Persistence of a warm pool off the Somali coast that extends to Tanzania throughout.
- Negative (-0.4° C) anomalies in the Atlantic Ocean 4 and 2 months prior to the Masika season.

4.1.4 Masika (MAM) Dry composite evolution

Dry Masika is defined as such, when normalised rainfall departures reach $\leqslant$ -0.2 below the long term mean. The composite years include 1980, 1983 and 1984. Figure 4.4 show the evolution of dry Masika. Prominent features at -6 lag are a cold pool of water off Gabon extending to Angola and along the Brazilian coast in

the Atlantic Ocean. In the Indian Ocean a tongue of positive anomalies from the southeast propagates towards the centre of the Ocean. SST in the western Indian Ocean are near normal.

Four and two months preceding dry Masika season (-4 lag and -2 lag), the patterns are identical showing intensification of the warm tongue from the southeast Indian Ocean first observed at -6 lag. Cold anomalies develop along the East African coast and in the Mozambique Channel. Another striking feature is the warm water pool in the central Atlantic Ocean revealed on both figures. The dry Masika season (0 lag) is characterised by near normal SST in the tropics, and below normal SST in the Indian Ocean subtropics. A persistent warm tongue occurs in the southeast Indian Ocean and southeast Atlantic.

Predictors for a dry Masika season are;

- Consistent warm SST tongue from the southeast of Indian Ocean propagating towards the centre of the Ocean.
- Below normal SST along the East African coast.
- Negative anomalies in the Mozambique Channel throughout.
- A warm pool of water in the middle of the Atlantic Ocean especially pronounced 4 to 2 months preceding the season.

4.2 Out-going longwave radiation (OLR) and winds at 700 and 200 hPa level

Variations in OLR principally reflect cloud amount, heights of cloud tops, and variations of surface temperatures. In the tropics OLR is a function of cloud depth and top temperature. When averaged over large areas, OLR provides a good index for the coverage of those areas by deep convective activity (Gruber et al., 1986). Winds at 700 hPa level, are where the boundary layer noise is minimal and close to the level of maximum water vapour transport; and 200 hPa level winds are where jet streams are found. The wind data were available from March 1968 to February 1987. Results of seasonal composite and lagged composites of OLR and wind anomalies for Vuli and Masika are presented as in the SST analysis. The domain extends from 70°W to 110°E and 20°N to 40°S and composites are averaged for the specified season and for periods 2, 4 and 6 months prior.

4.2.1 Vuli (OND) Wet composite evolution

Figure 4.5 illustrates the OLR composite sequence for wet Vuli season and for periods 2 , 4 and 6 months prior. The years composited are 1977, 1978, 1982 and 1986, while the months are October, November and December (Vuli season). Major zones of convection are readily delineated as regions with low OLR departures. The notable features include a convective area over the Horn of Africa at lag -6, a dry zone in the eastern Indian Ocean from -2 lag and a centre of action (negative values -10 W m^{-2}) over the western Indian Ocean at lag 0 extending westward over Tanzania.

Depicted in figure 4.6, is the composite evolution of the horizontal wind vectors at 700 hPa. Throughout the evolution, easterlies build up over the central Indian Ocean. At -4 lag and eventually during the season, an anticyclone develops east of Madagascar that enhances confluence over the Tanzanian coast and hinterland. Low level convergence over northern Tanzania is improved by the arrival of westerlies from the Congo at 0 lag.

Figure 4.7 illustrates the evolution of horizontal wind vectors at 200 hPa. North westerlies are evident over the study area 6 months prior to the season. These winds are part of a strong flow from the Azores that sweep through the Atlantic Ocean, the Sahara and East Africa. A weak upper cyclonic gyre in the Indian Ocean inhibits moist influx at the Tanzanian coast.

At - 4 lag to 0 lag, cyclonic gyres in the southwest Indian Ocean and over the tropical south Atlantic Ocean are the main features that persist. Southeasterly flow anomalies from south east of Madagascar sweep the east African coast and recurve over northern Tanzania towards the Atlantic Ocean, emerging as northeasterly flow over Angola.

4.2.2 Vuli (OND) dry composite evolution

The OLR analysis for dry Vuli composite evolution is shown in figure 4.8. Positive anomalies are revealed over the northwest Indian Ocean at lag -6 and over tropical South America through the succession. A centre of action is located over the west Indian Ocean (> + 4 W m^{-2}, subsidence) at 0 lag. Few convective (negative anomalies) areas within Africa occur through the sequence. However, negative anomalies are evident in the equatorial western Pacific. Together these suggest a Walker circulation in the atmosphere with rising air over the Pacific and sinking air over the western Indian Ocean.

Lagged composites of wind anomalies at 700 hPa are presented in figure 4.9. Easterly flow anomalies over the Somali coast are persistent at lags -6 to -2 months. However, off the East African coast, a weak cyclonic gyre is present. A weak anticyclonic circulation anomaly is revealed over East Africa with offshore winds during the season (0 lag). In the South Atlantic Ocean, an intense cyclonic gyre oscillating along the 0 meridian remains a notable feature throughout the evolution.

Figure 4.10 illustrates the horizontal wind composite sequence at 200 hPa. South westerlies persistently flow from lags -6 to -4 from the Atlantic Ocean through Angola towards Tanzania at lag -2. Vuli season (lag 0) shows westerlies dominating in East Africa and the west Indian Ocean. An anticyclonic flow in the southwest Indian Ocean from lag -2 to lag 0 is also notable.

4.2.3 Masika (MAM) Wet composite evolution

During wet Masika and 4 months prior (Figure 4.11), the whole of East Africa is covered by enhanced (negative OLR anomalies). At lag - 2 the centre of action is over Kenya (< -4 W m^{-2}), whilst sympathetic response is revealed over central Africa and the central Indian Ocean. During Masika season (lag 0), negative anomalies are shown in a northwest- southeast alignment pattern with a centre (< -6 W m^{-2}) over East Africa.

Winds during wet Masika at 700 and 200 hPa are presented in figures 4.12 and 4.13 respectively. 700 hPa winds reveal enhanced westerly flow over the tropical Atlantic Ocean and locally (northern Tanzania). Another remarkable feature is a meridional (northern Hadley) circulation anomaly along 40° E.

Winds at 200 hPa show a meridional oscillation of cyclonic gyres in the south west Atlantic Ocean and south Indian Ocean. The one in the Indian Ocean, moves westward and occupies the African continent south of equator and indicates increased westerlies aloft at lag 0 (Masika season).

4.2.4 Masika (MAM) Dry composite evolution

Figure 4.14 to 4.16 indicates dry composite evolution patterns for Masika for the OLR, 700 hPa and 200 hPa winds.

Figure 4.14 shows a convective area (negative) over the central Indian Ocean at lags -6 to -4 months. There is a gradual eastward movement of cells during the

sequence. At lag 0 (Masika season), the dry region shifts from central and southern Africa to north-eastern Africa (> + 4 W m^{-2}), while a centre of convective action reaches the equatorial western Pacific. This is attributed to a Walker circulation having the descending arm over northeast Africa and an ascending arm possibly over the equatorial western Pacific. Another notable feature is that circulation anomalies for the dry Masika season are of a greater intensity than for the wet season.

Wind anomalies at 700 hPa are shown in figure 4.15. Large anticyclonic gyres are present in the south Atlantic, while local easterly flow develops during the season. Anticyclonic flow develops in the south-western Indian Ocean and may create local diffluence.

Figure 4.16 exhibits lagged composites of wind anomalies at 200 hPa. Persistent anticyclonic gyres and enhanced subtropical westerlies are depicted at lag -4 to lag 0. Northeasterly anomalies flow toward the study area during the season.

Summary of structural patterns and predictors:

- Wet Vuli (OND) convection over Tanzania is controlled by a centres of action in the western and eastern Indian Ocean, with lower (upper) level confluence (diffluence) off the east African coast.

- Dry Vuli (OND) circulation patterns do not necessarily oppose the wet composite; a Walker cell anomaly in the central Indian Ocean develops well in advance, with low level easterlies and upper westerlies evident.
- Wet Masika (MAM) shows a northwest-southeast tilted convective region over Tanzania with confluent northwesterlies in the low levels and diffluent southerlies aloft; cyclonic 200 hPa wind gyres in the southwest Atlantic and south Indian Ocean at -4 months are useful predictors.
- Dry Masika (MAM) circulation patterns are nearly opposite to the wet with anticyclonic gyres in the southwest Atlantic and south Indian Ocean and diffluent equatorial easterly flow during drought.

This chapter has highlighted inter-annual variabilities which are significant both for seasonal prediction and as a tool for understanding in-seasonal behaviour. No skilful prediction of in-seasonal rainfall can be anticipated without clear a understanding of inter-annual fluctuations. Chapters 5 to 7 will study intra-seasonal variations and predictions within the Vuli season.

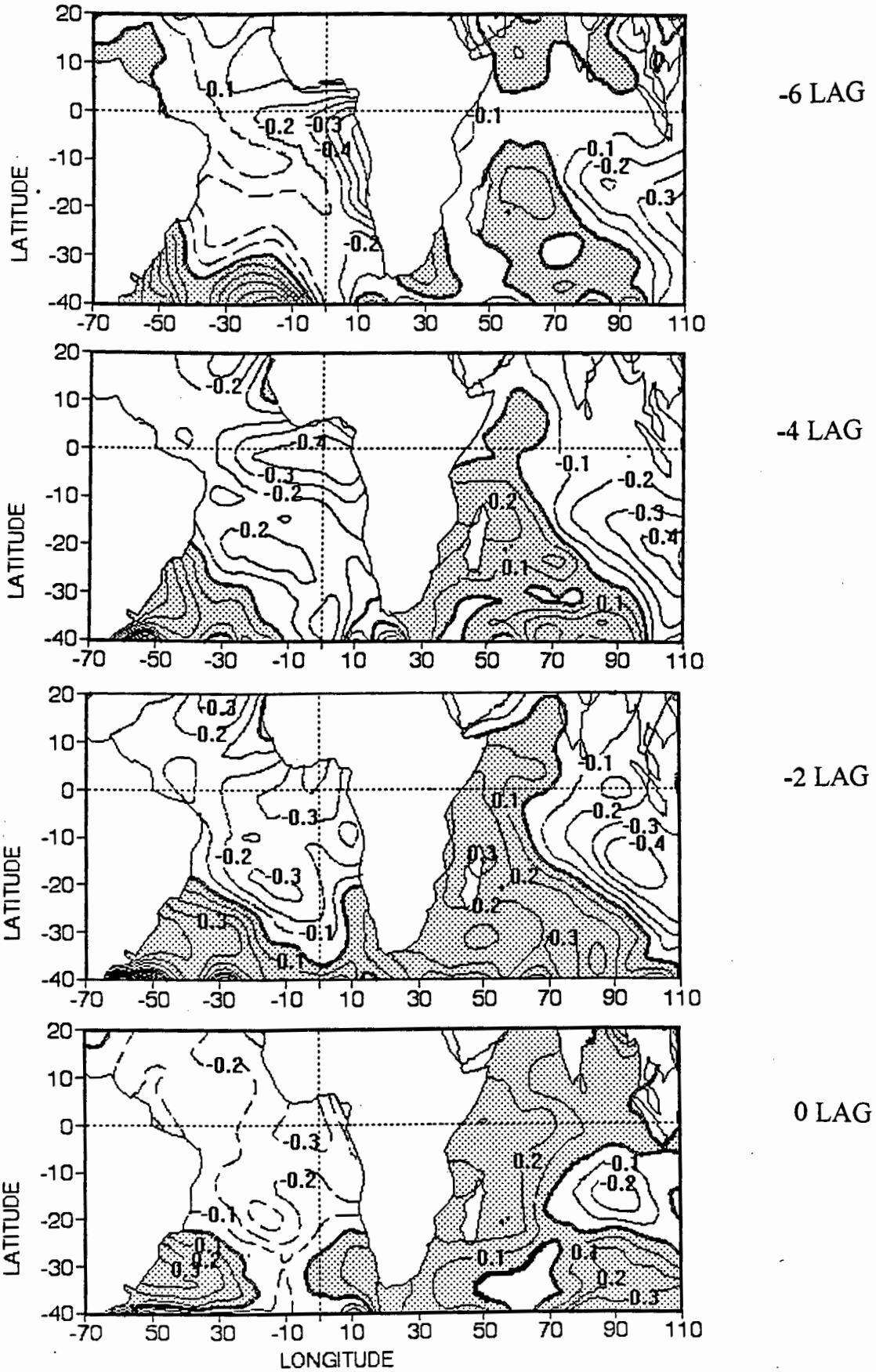

Figure 4.1: SST composite anomalies for wet Vuli season
Contour Intervals are 0.1° C

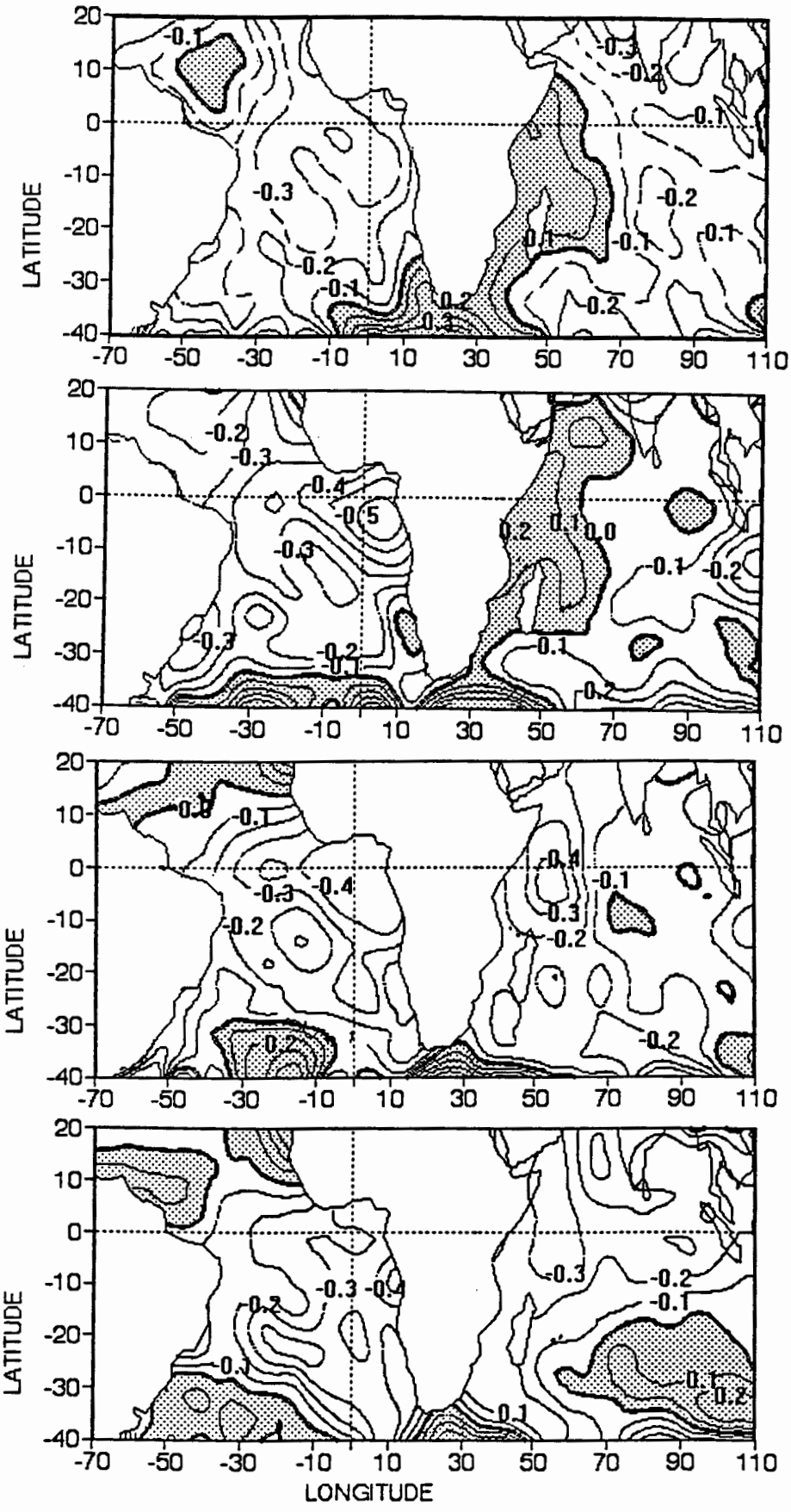

Figure 4.2: SST composite anomalies for dry Vuli season
Contour Intervals are 0.1° C

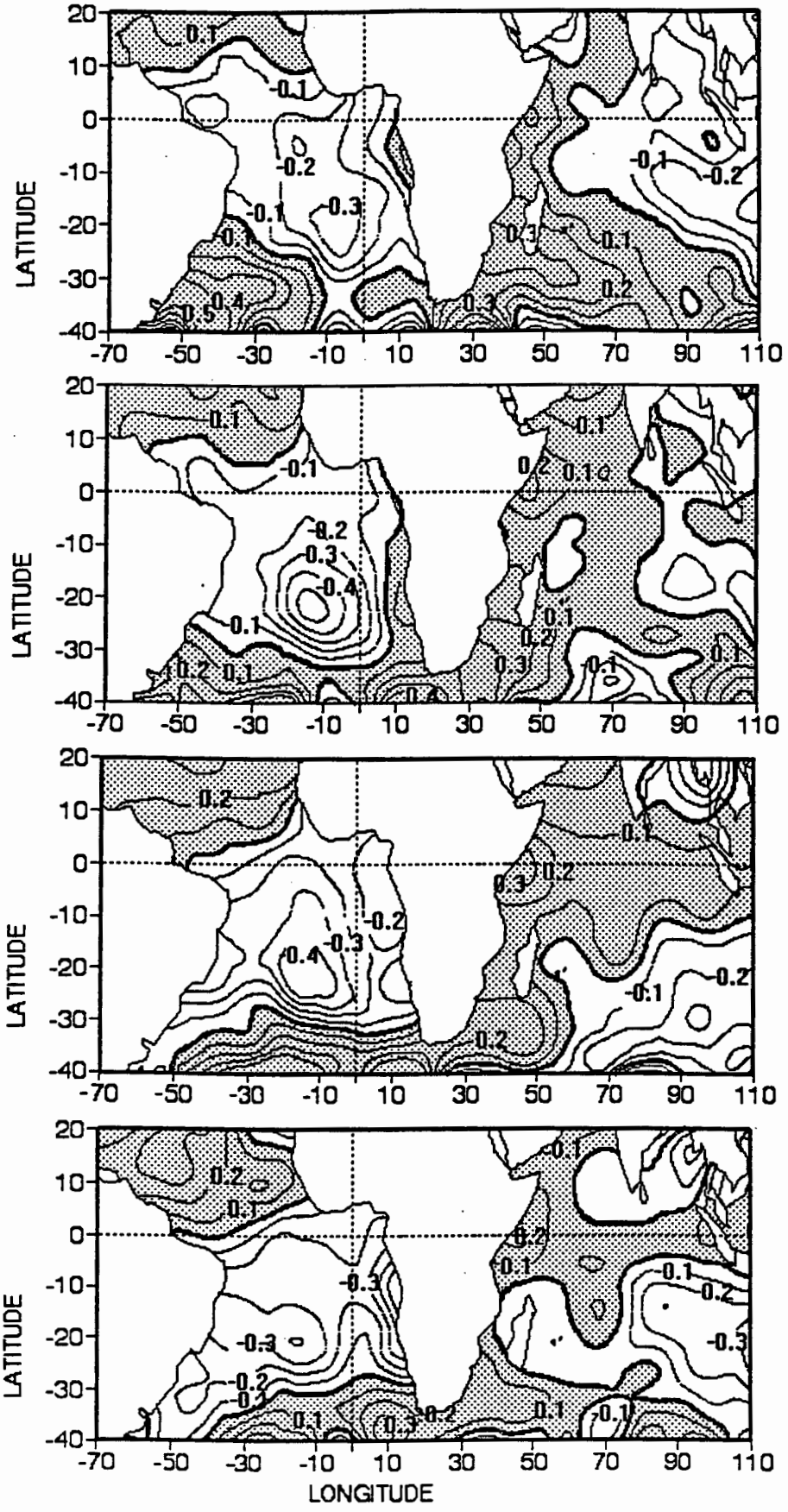

Figure 4.3: SST composite anomalies for wet Masika season
Contour Intervals are 0.1° C

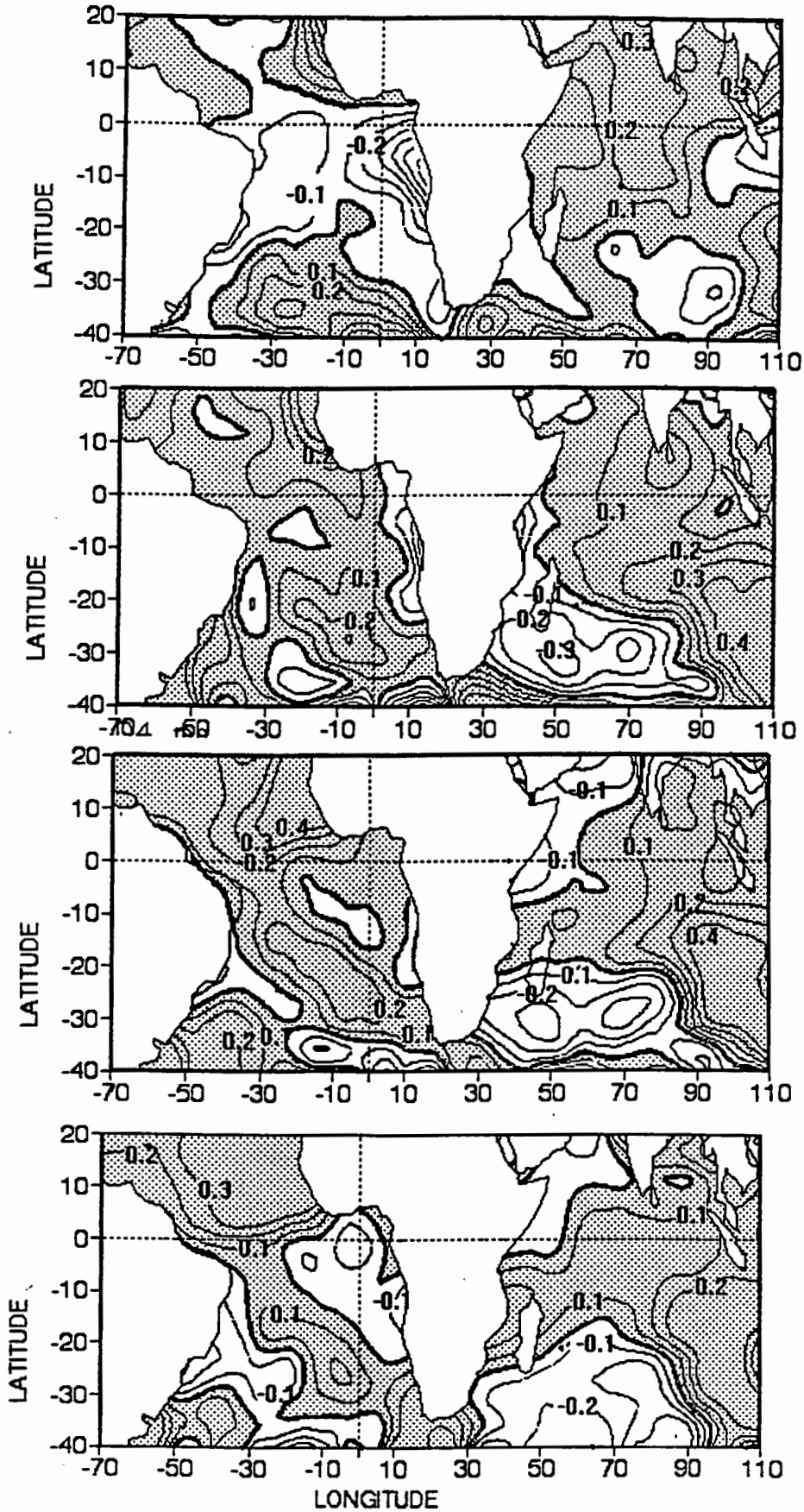

Figure 4.4: SST composite anomalies for dry Masika season
Contour Intervals are 0.1° C

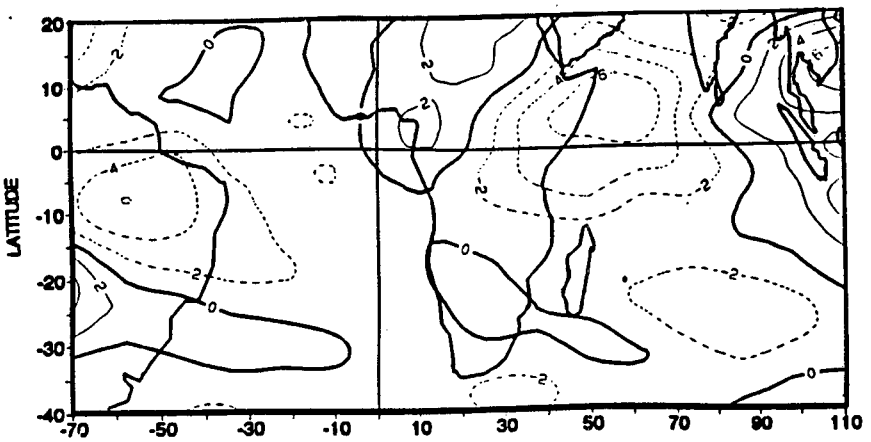

-6 LAG

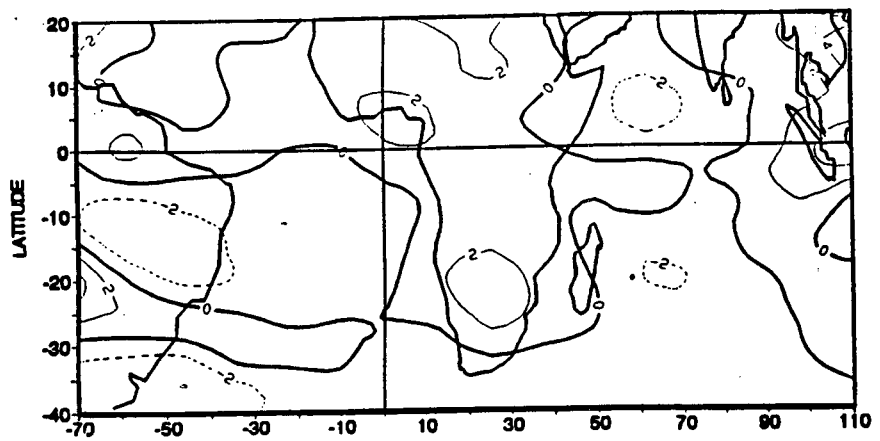

-4 LAG

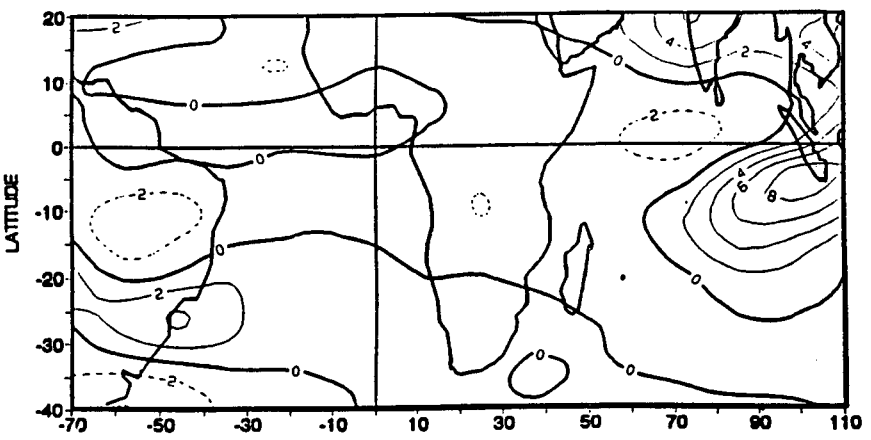

-2 LAG

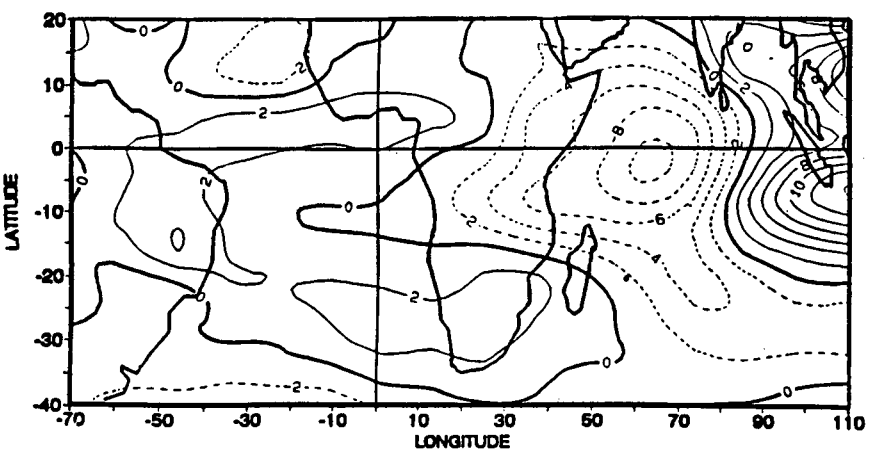

0 LAG

Figure 4.5 : Lagged Composite of outgoing longwave radiation (OLR) anomalies for ; wet VULI

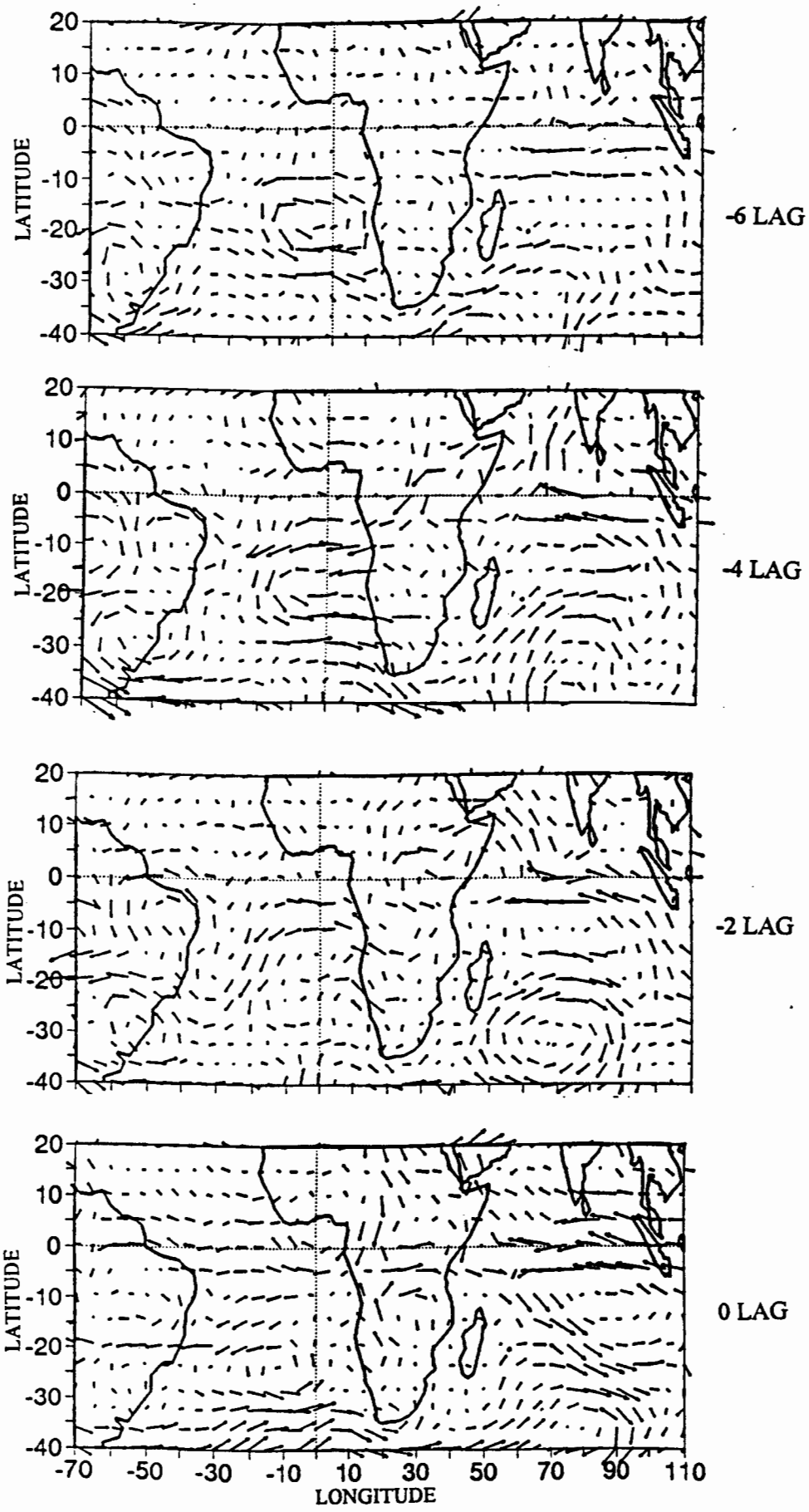

Figure 4.6 : Lagged Composite of wind anomalies at 700 hPa
for ; wet VULI
Vector : ⟶ 2.5 m s^{-1}

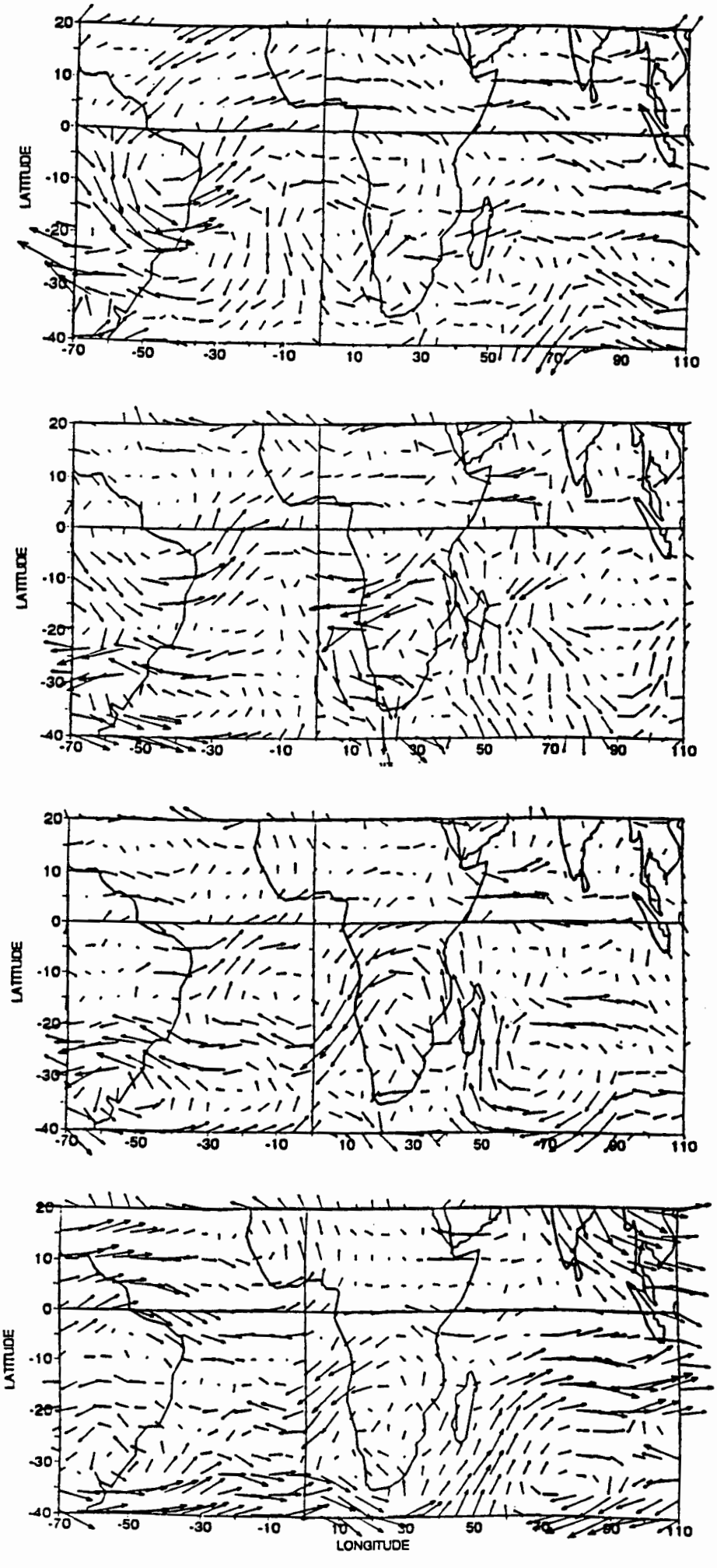

Figure 4.7 : Lagged Composite of wind anomalies at 200 hPa
for ; wet VULI
Vector : — 2.5 m s^{-1}

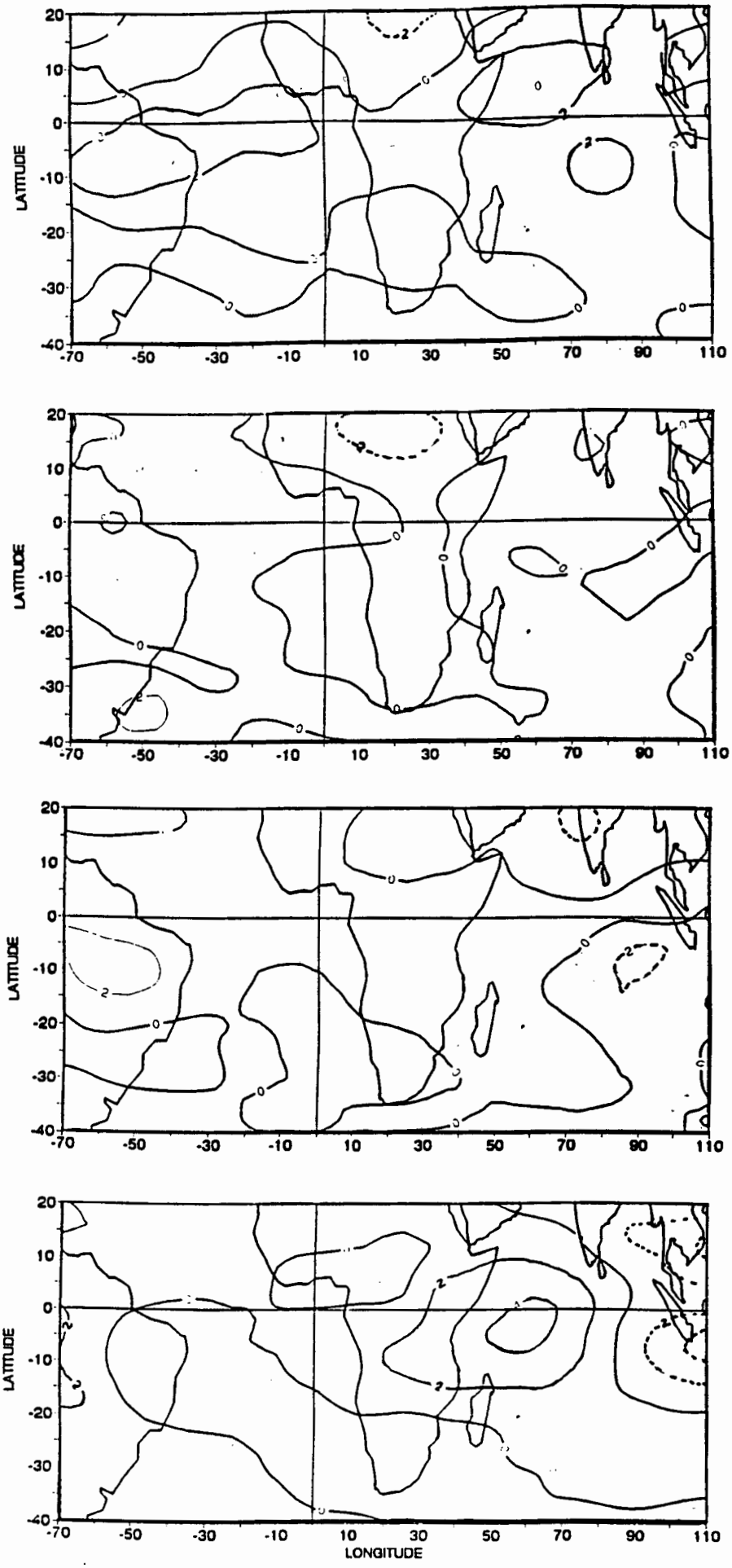

Figure 4.8 : Lagged Composite of outgoing longwave radiation (OLR) anomalies for ; dry VULI

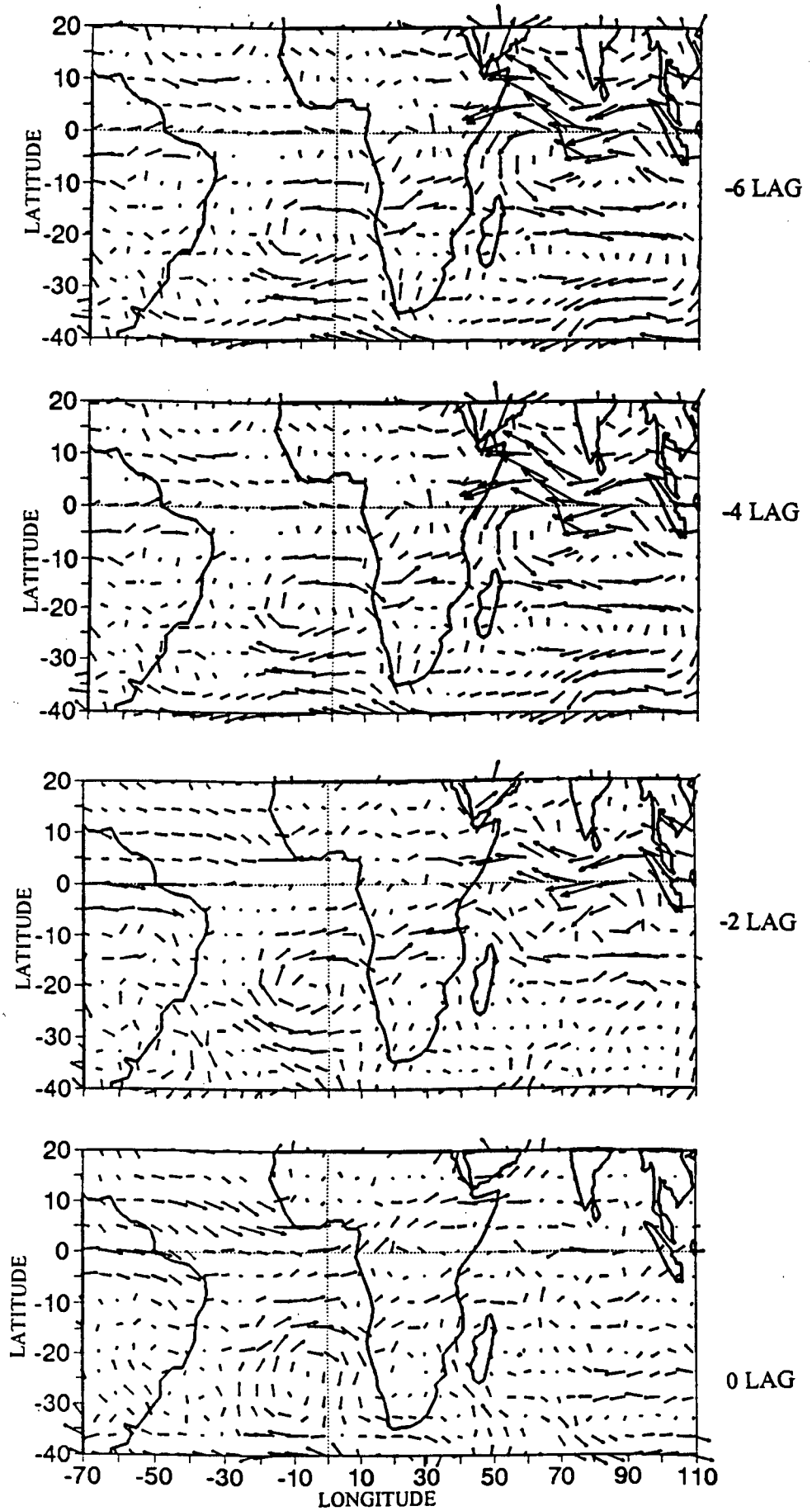

Figure 4.9 : Lagged Composite of wind anomalies at 700 hPa
for ; dry VULI
Vector : — 2.5 m s^{-1}

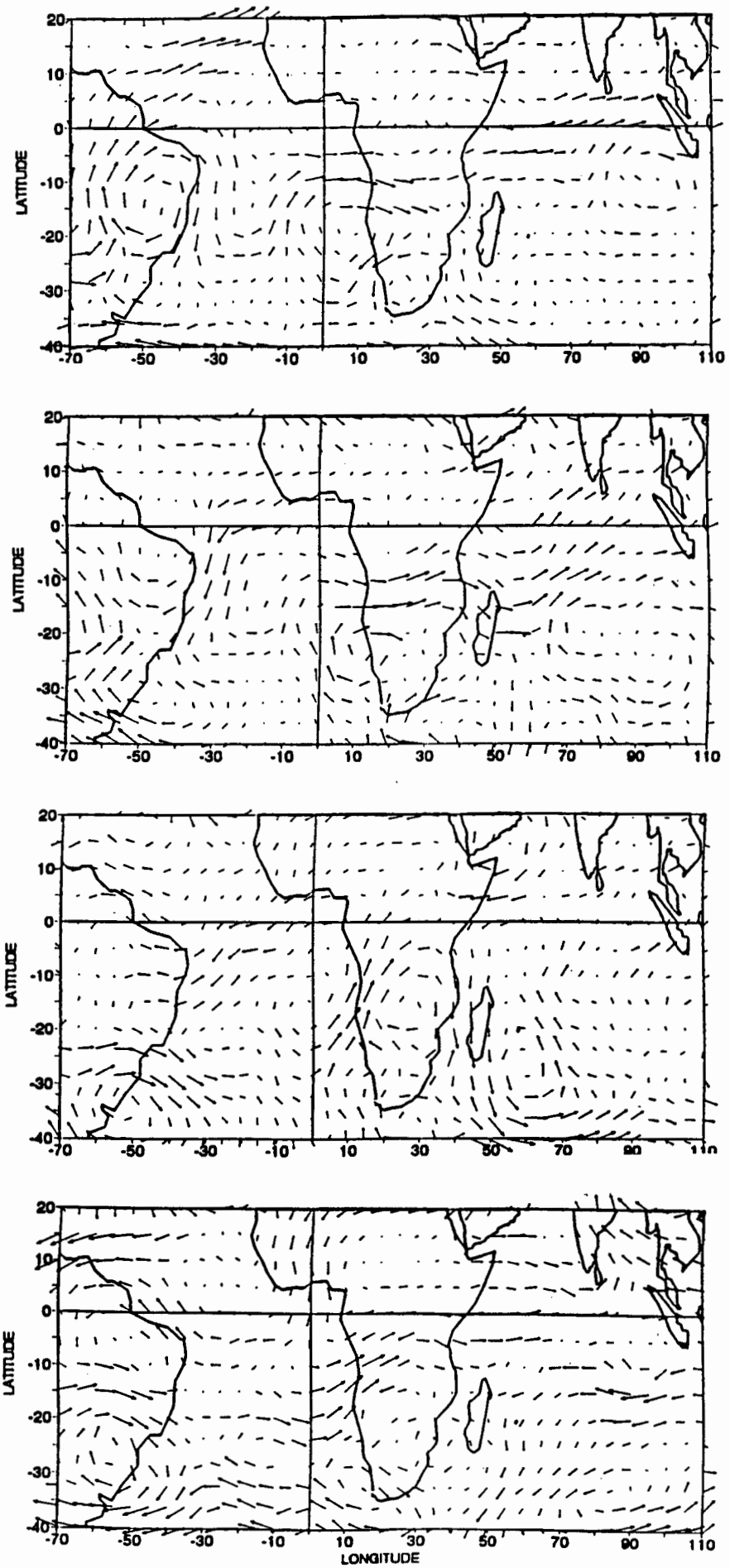

Figure 4.10 : Lagged Composite of wind anomalies at 200 hPa
for ; dry VULI
Vector : ⟶ 2.5 m s^{-1}

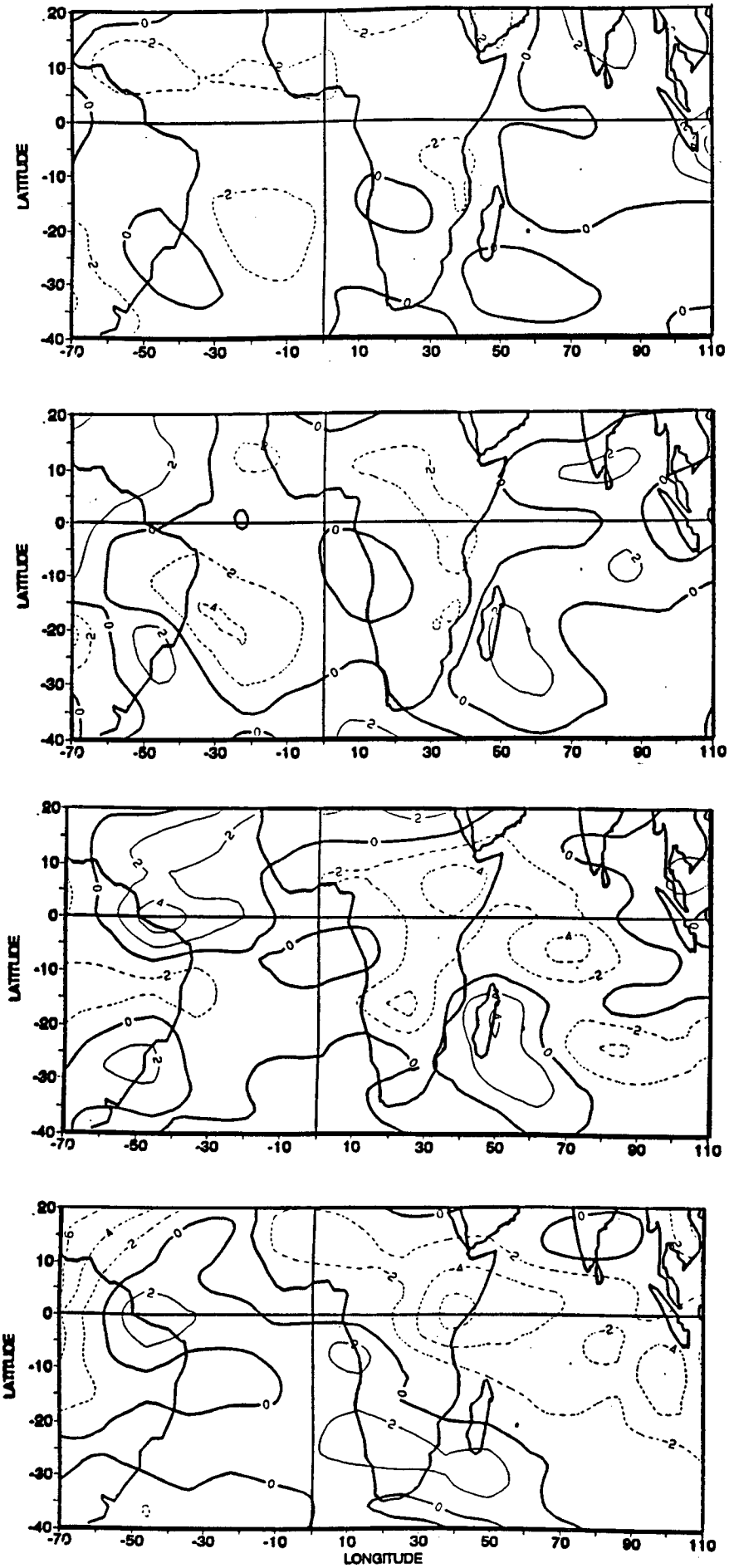

Figure 4.11 : Lagged Composite of outgoing longwave radiation (OLR) anomalies for ; wet MASIKA

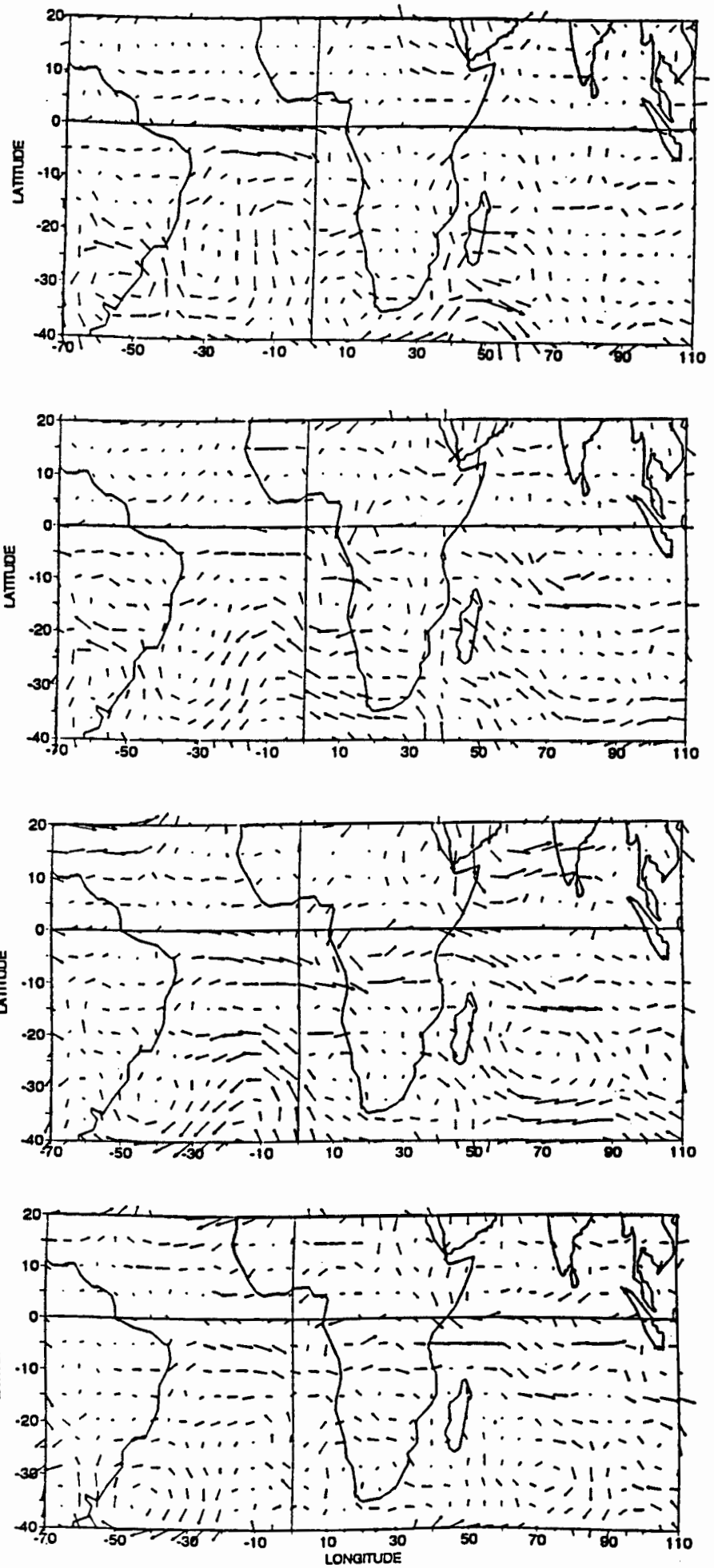

Figure 4.12 : Lagged Composite of wind anomalies at 700 hPa for ; wet MASIKA
Vector : — 2.5 m s^{-1}

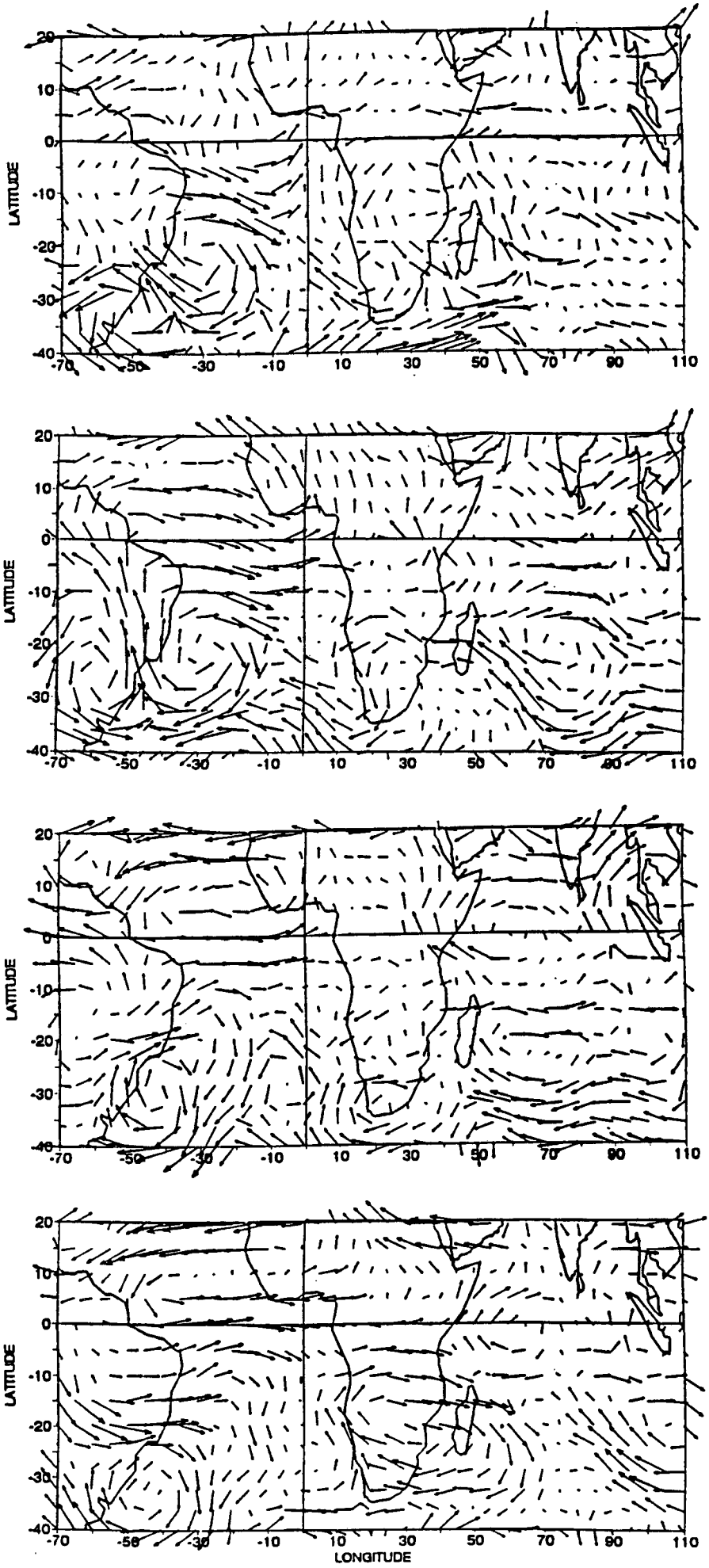

Figure 4.13 : Lagged Composite of wind anomalies at 200 hPa for ; wet MASIKA
Vector : ⟶ 2.5 m s^{-1}

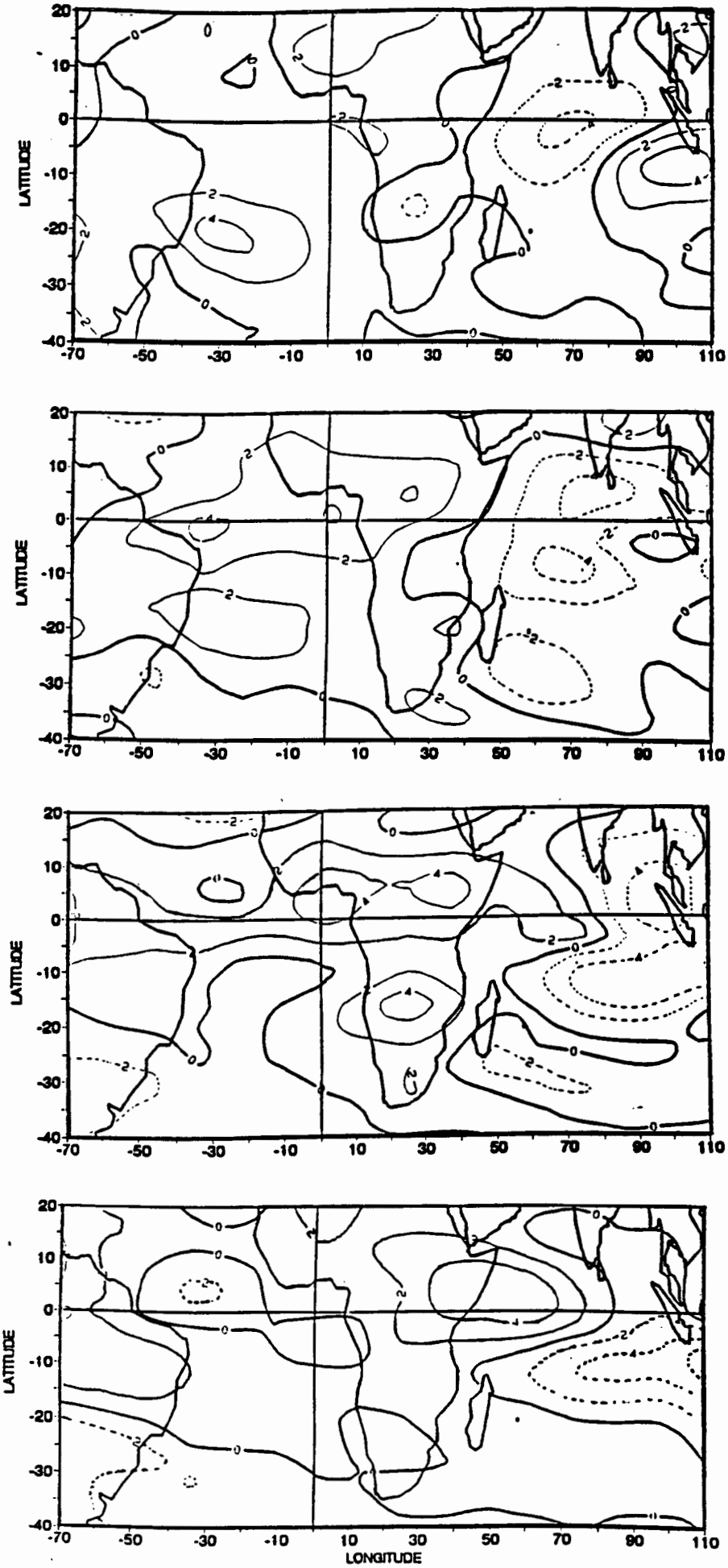

Figure 4.14 : Lagged Composite of outgoing longwave radiation (OLR) anomalies for ; dry MASIKA

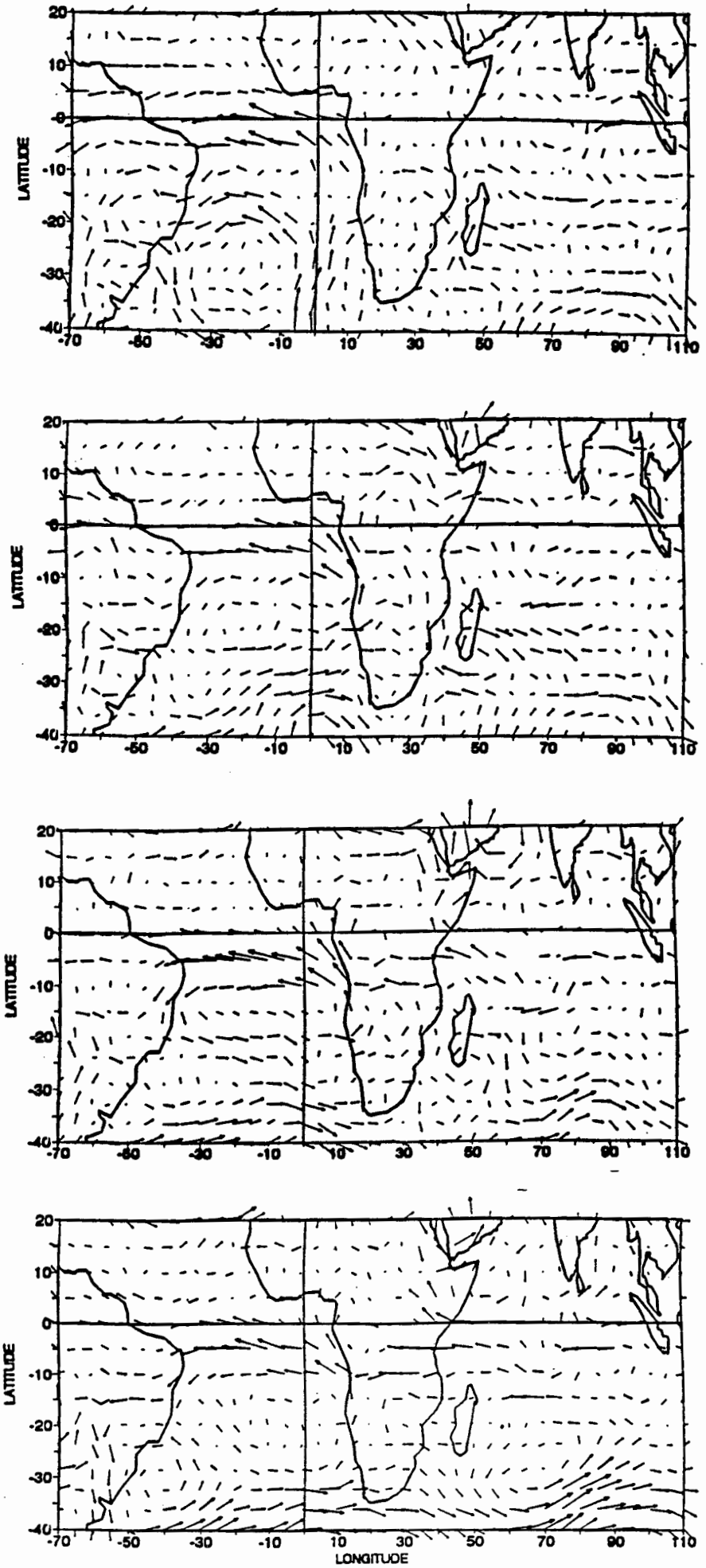

Figure 4.15 : Lagged Composite of wind anomalies at 700 hPa
for ; dry MASIKA
Vector :⟶ 2.5 m s^{-1}

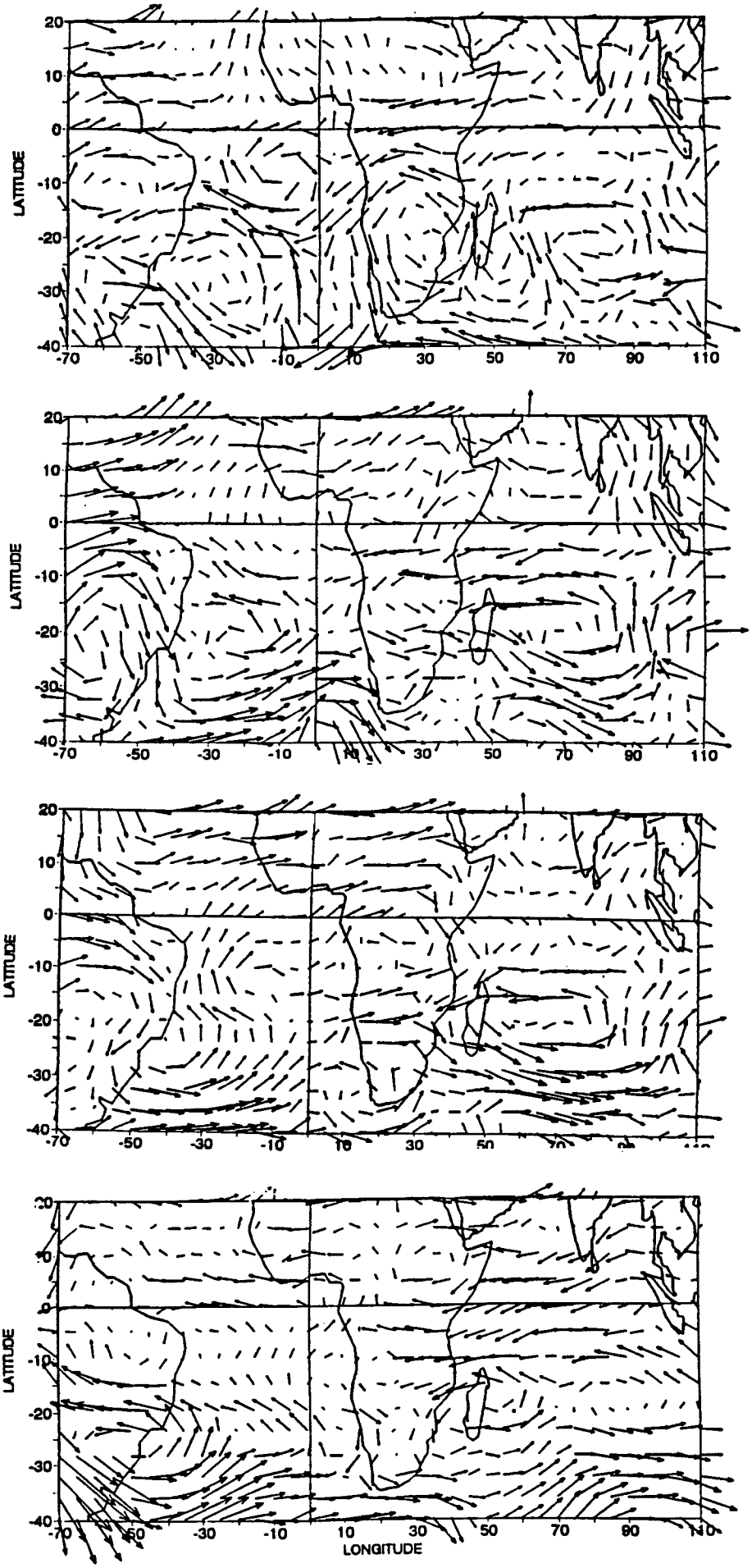

Figure 4.16 : Lagged Composite of wind anomalies at 200 hPa for ; dry MASIKA

Vector : ⟶ 2.5 m s^{-1}

Chapter 5: The background climate and Vuli wet spell

5.1 Introduction

This chapter is divided into two sections, the first section looks at mean characteristics of selected long-term meteorological fields for Vuli (October-December). It is presupposed that the general weather producing systems such as the sub-tropical anticyclones, tropical depressions, the inter-tropical convergence zone (ITCZ) etc., will be detected. Anomaly results from chapters 6, 7, and 8 will be inferred with respect to the background climate. The mean circulation patterns are computed from a six-year ECMWF data set as detailed below.

The second part of this chapter is to give insight to composite mean characteristics of selected pentad meteorological fields according to onset of the wet spell, and one and two pentads before. This will lead into anomalies in chapter six, thus illustrating fluctuations with frequencies shorter than the seasonal cycle. This type of analysis is known as intra-seasonal scale analysis.

Due to significant improvement in ECMWF data after 1985, a six year (1986-91) dataset was used to compute the mean patterns for each phase of the Vuli convective optimum. From each major wet spell (>25 mm/pentad) determined from pentad area-averaged rainfall as illustrated in figures 2.3 (a-h), precursor patterns in terms of onset and dry phase were established. A mean was then determined by averaging ECMWF data for all pentads comprising each phase, results of which are indicated in table 5.1. The mean composite analyses generally

display small changes in the temporal progression from formation stage (P2) to mature stage (P0). In this respect, the discussion will emphasis these stages, but for continuity all three stages will be presented. Chapter 6 will discuss all composite phases in terms of departures from the seasonal mean.

Table 5.1: Evolution of Wet spells

P2 Dry Pentad-Year	P1 Onset Pentad-Year	P0 Wet Pentad-Year
9 - 1986	10 - 1986	11 - 1986
6 - 1988	7 - 1988	8 - 1988
9 - 1989	10 - 1989	11 - 1989
7 - 1990	8,9 - 1990	10 - 1990
10 - 1991		11 - 1991

5.2 Mean Circulation patterns for Vuli

5.2.1 Geopotential Height:

The mean geopotential height field at 850 hPa is presented in figure 5.1.1. Revealed are two distinctive areas of low gpm, one over eastern Africa and another in the northern Indian Ocean sector extending from southeast Asia. Sub-tropical high pressures; St. Helena in the Atlantic Ocean and Mascarine in the Indian Ocean exist while the Arabian ridge which emanate from the Siberia high is

absent. Figure 5.1.2 shows the 200 hPa geopotential height and indicates the equatorial region is overlaid by high geopotentials while low values are revealed south of 10°S. The upper and lower levels show opposing geopotential patterns which suggest vertical convective overturning and warm cored barotropic weather systems.

5.2.2 Precipitable Water:

Figure 5.1.3 shows two areas of high precipitable water, having origins over the Indian and Atlantic Oceans respectively. The Sahel and South Atlantic Ocean show dryer atmospheric conditions mainly due to the desert air and upwelled water respectively. Of the two sources of moisture, the Indian Ocean "pool" spreads over the study area as illustrated by the 40 mm contour.

5.2.3 Mean Water vapour flux and Horizontal wind at 200 hPa.

Figure 5.1.4 summarises the vertically integrated water vapour flux between the surface and 500 hPa. The moisture flux over northern Tanzania is adivected from the Indian Ocean (southeasterlies) as a result of established Mascarene anticyclone cell east of Madagascar. North easterly flow from the Arabian peninsula has no influence on Tanzania, the flow curves both east and westward on reaching the Kenyan coast, thus creating a slight diffluence. There is little influence from the Atlantic Ocean flux since the little moisture that advects from the ocean converge

along 20°E. The 200 hPa level is used since it is the level closest to convective outflow in the tropics. Also the association of divergence-convergence may be related directly to tropical heating-cooling (Sardeshmukh and Hoskins,1988).

The 200 hPa winds in figure 5.1.5 shows a westerly duct pattern over the Atlantic. Thus geopotentials are high either side of the equator. Over the Indian Ocean easterly winds occur. A subtropical westerly trough extends northward towards Tanzania. Both tropical regions display strong westerly flow.

5.2.4 Divergence and Vorticity

The low-level divergence and vorticity are illustrated in figures 5.1.6 and 5.1.8 respectively, significant convergence is over the Congo basin, central Madagascar and eastern South Africa. However, intense low-level convergence (-6×10^{-5} s^{-1}) is revealed over the Ethiopian highlands. The Angolan and Namibian coast depict divergent regions.

The mean vorticity field at 850 hPa displays cyclonic band that extends from the equator to 10°S in the Indian Ocean. Cyclonic flow is found over the eastern Atlantic Ocean. Upper- tropospheric (200 hPa) fields of divergence and vorticity are illustrated in figures 5.1.7 and 5.1.9. Strong divergence (6×10^{-5} s^{-1}) exists over the central equatorial African region. While the southwest Indian Ocean, Mozambique Channel and the Atlantic Ocean display upper-level convergence. Vorticity fields show anticyclonic (+ve) values over southern central Africa and in

the Indian Ocean east of 55°E between 10°S and 20°S. The sign of vorticity in the northern hemisphere is negative and therefore anticyclonic in the band 0-20°N.

5.2.5 Mean vertical motion

Figure 5.1.10 illustrates vertical motion patterns in the middle-levels (500 hPa). Apart from northern Africa which shows strong subsidence, the rest of Africa experiences uplifting motion. There is a center of relatively greater uplift of order of -10×10^{-4} Pa s^{-1} over the Congo basin (Zaire). The southwest Indian Ocean, western Atlantic Ocean and the Arabian Sea are other areas of significant subsidence.

5.2.6 Mean Velocity Potential

Mean divergent water vapour flux (WVF) and velocity potential are derived assuming irrotational motion (in the domain). Positive WVF indicates low-level large scale convergence and in figure 5.1.11, strong convergence (80×10^{8} kg s^{-1}) is shown over northern Tanzania and south of India in the central Indian Ocean. The Atlantic Ocean and southeast Indian Ocean are covered by divergence (negative mean divergent WVF). Figure 5.1.12 exhibit upper tropospheric mean velocity potential, negative values indicate large-scale upper divergence. As expected, the area occupied by convergent/divergent fields in the lower levels has divergent/ convergent fields aloft (200 hPa) with a westward shift or tilt.

Maximum divergent motion occurs over the Congo, whilst the upper convergent maximum occurs over the south Indian Ocean.

5.2.7 Summary and discussion

The mean circulation analysis have disclosed the characteristics of Vuli season. The major points observed will provide useful background for discussing intra-seasonal scale anomalies in the second part of this chapter and in chapters 6 and 7. Major points observed from the analysis are:

- Southern subtropical highs are conspicuous in the low-level geopotential fields. The Arabian ridge is weak to the northeast. Ogallo (1994) indicated that the seasonal rainfall during Septermber-November was attributable to the inter-tropical convergence zone over East Africa. Consequently, convergence of the north-easterly and south-easterly winds occur over the region.Vertically integrated water vapour flux analysis and the presence of easterly flow over the equatorial Indian Ocean suggests two separate cells of high pressures exist on either side of the equator, hence two separate low-level sources of moist unstable air.

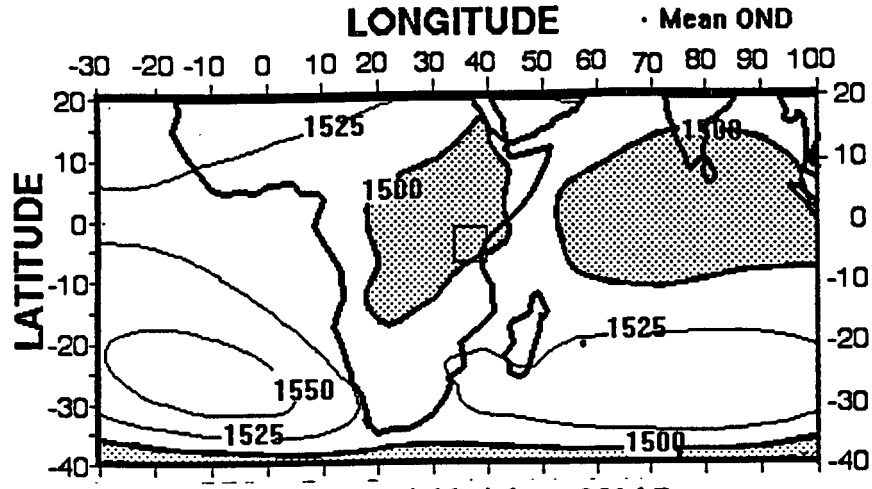

Figure 5.1.1: Mean Vuli Geopotential height at 850 hPa
Contour intervals are 25 gpm.

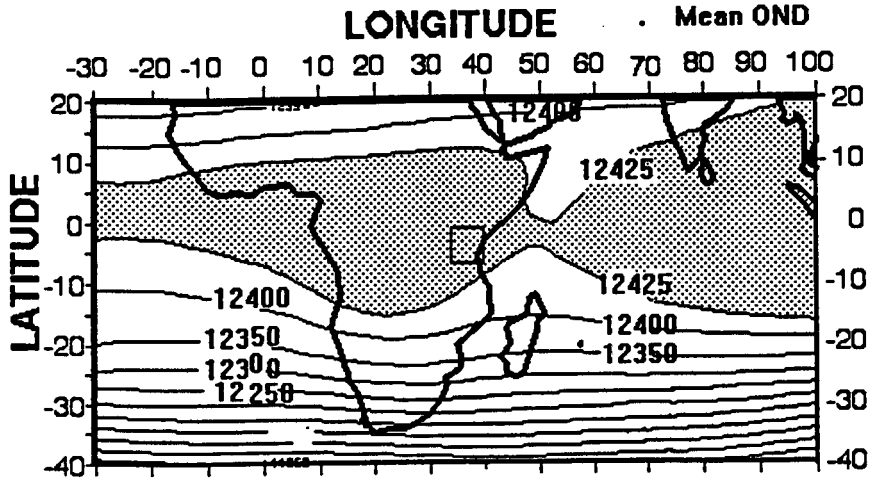

Figure 5.1.2: Mean Vuli Geopotential height at 200 hPa
Contour intervals are 25 gpm.

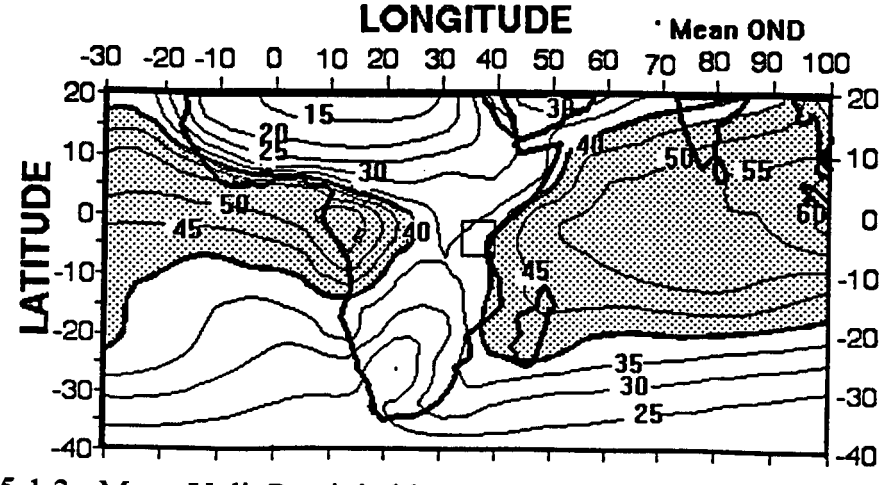

Figure 5.1.3: Mean Vuli Precipitable water between surface and 300 hPa
Contour intervals are 5 mm.

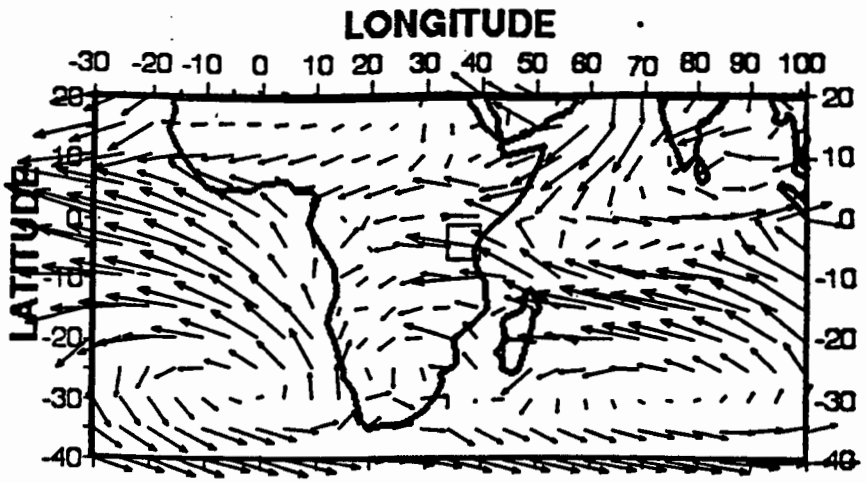

Figure 5.1.4: Vertically integrated water vapour flux
⟶ vector is equivalent to 240 kg m^{-1} s^{-1}

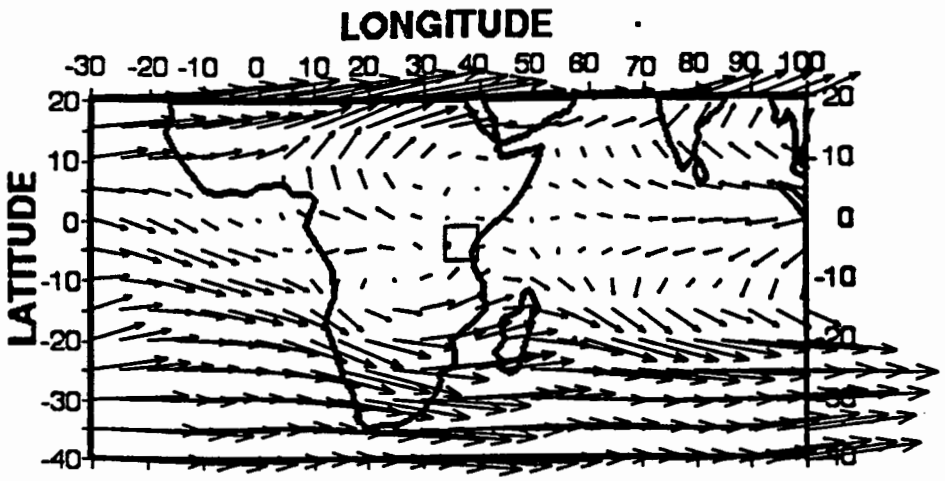

Figure 5.1.5: Mean Vuli Horizontal wind vector at 200 hPa
⟶ vector is equivalent to 40 m s^{-1}

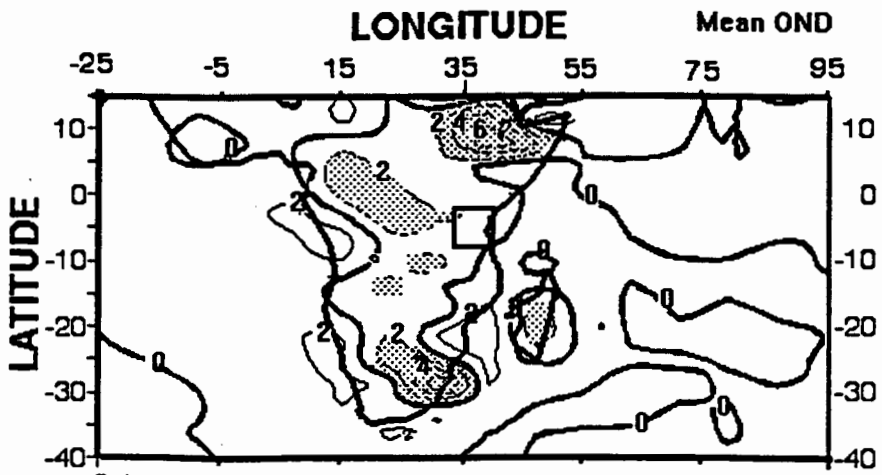

Figure 5.1.6: Mean Vuli Divergence field at 850 hPa
Contour interval is 2×10^{-5} s^{-1}

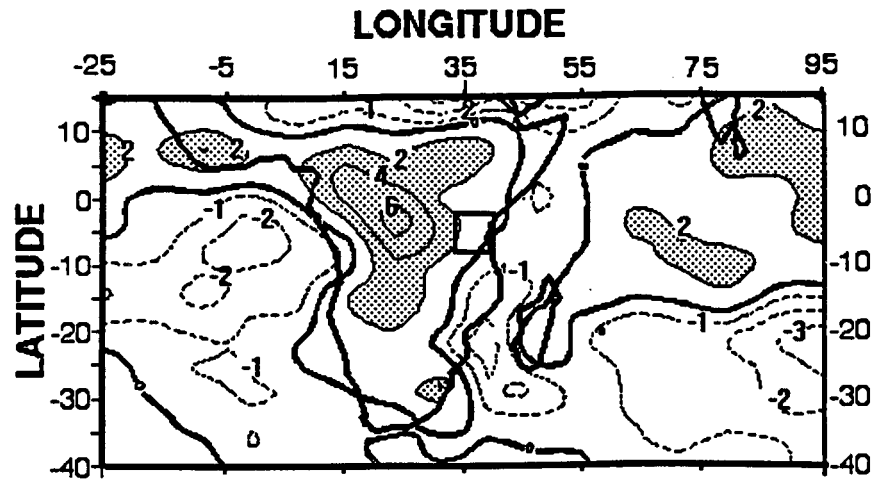

Figure 5.1.7: Mean Vuli Divergence field at 200 hPa
Contour interval is 2×10^{-5} s^{-1}

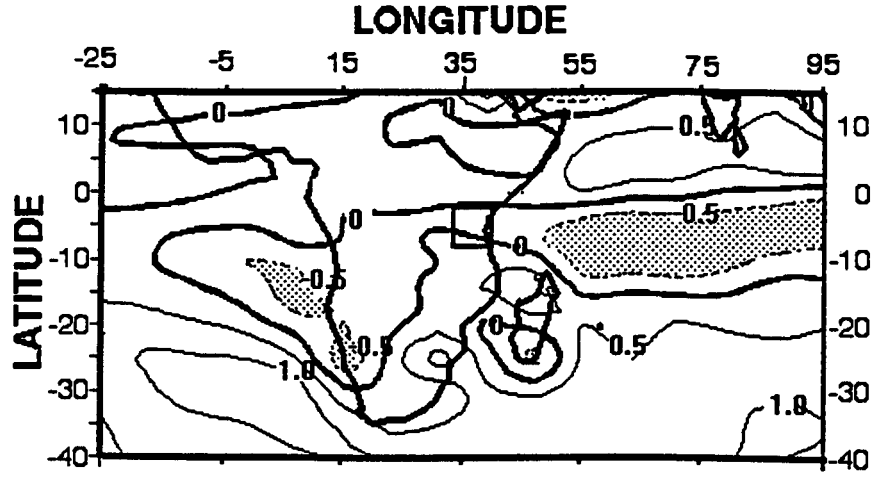

Figure 5.1.8: Mean Vuli Vorticity field at 850 hPa
Contour interval is 0.5×10^{-5} s^{-1}

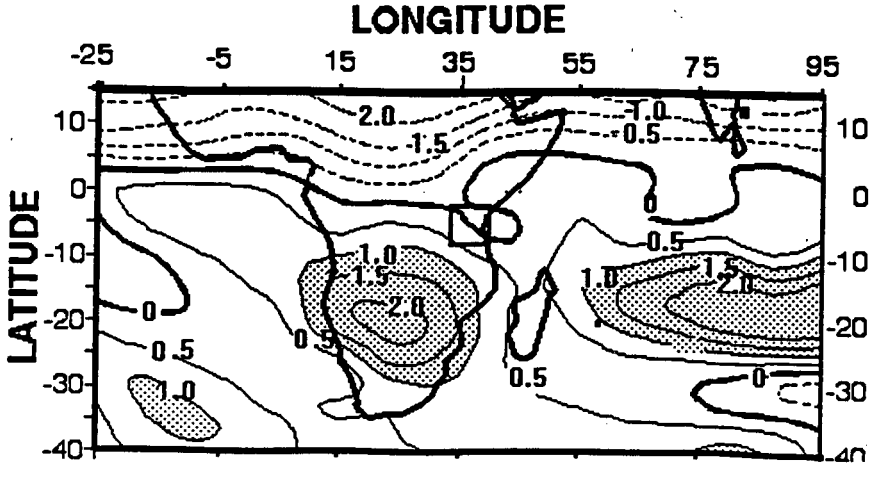

Figure 5.1.9: Mean Vuli Vorticity field at 200 hPa
Contour interval is 0.5×10^{-5} s^{-1}

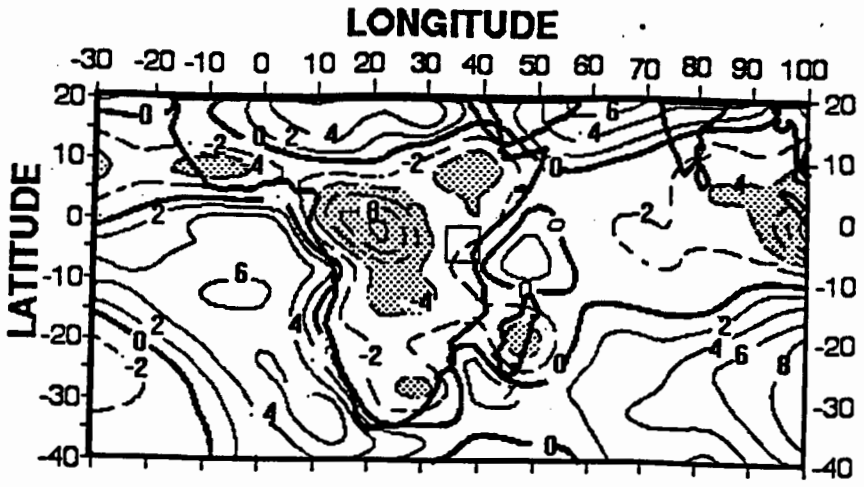

Figure 5.1.10: 500 hPa Vertical motion
Contour interval is 2×10^{-4} Pa s^{-1}

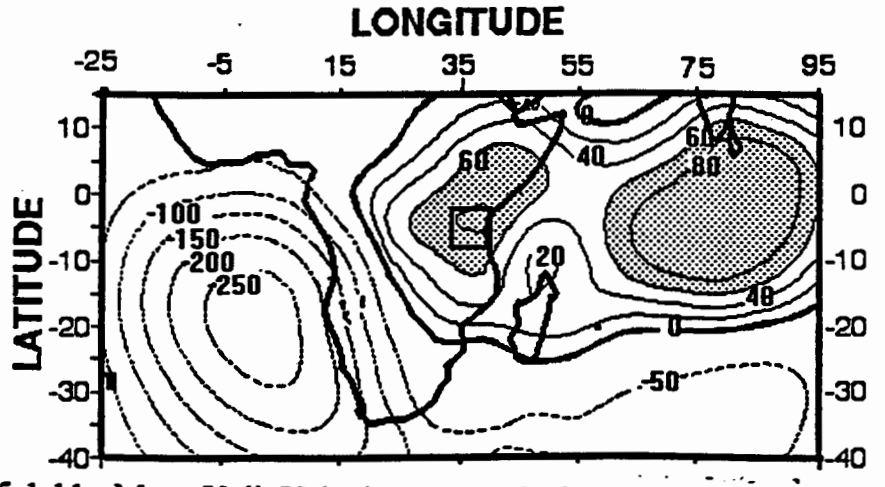

Figure 5.1.11: Mean Vuli Velocity potential of WVF,
integrated for surface to 500 hPa
negative contour interval is 50×10^6 kg s^{-1}
positive contour interval is 20×10^6 kg s^{-1}

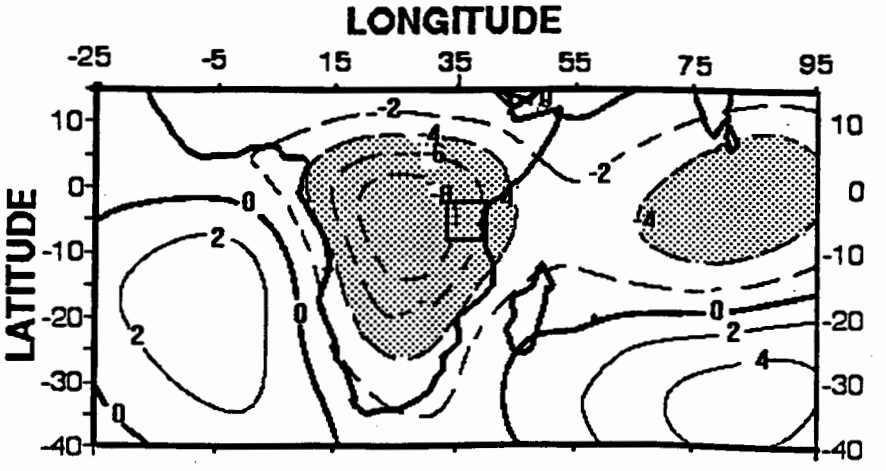

Figure 5.1.12: Mean Vuli Velocity potential field at 200 hPa
Contour interval is 2×10^6 m^2 s^{-1}

5.3 Composite mean analysis of Vuli wet spells

5.3.1 Geopotential Height:

The equatorial region east of 10° E to Indonesia in the Indian Ocean, reveals low pressure at 850 hPa on both P2 and P0 (Figure 5.2.1). At maturity, the subtropical anticylone cell in the Atlantic and Indian Oceans centered along 25° S retains the same intensity although with a northeastward propagation. The anticyclonic centers oscillate from 25° S to 15° S and shift 5° eastward.

At 200 hPa (Figure 5.2.2) the upper level anticyclone is maintained over the equatorial zone where low pressures are revealed at 850 hPa. However there is a more eastward shift of upper level anticyclones compared to the low level troughs and cyclonic centers. This is shown by the position of an upper level trough axis which shifts from the South to East African coast and the axis of the southern ridge on the accompanying lower level analysis.

5.3.2 Precipitable Water (PW):

Figure 5.2.3 shows a maximum composite pentad PW east of latitude 70° E with a closed center over Indonesia at the formative stage. Over Africa the maximum PW of 60 mm is positioned over Angola. South Africa and North Africa over the Sahara and local minimums of mean PW. At the mature stage the composite PW reveals a build up of moisture from the Indian Ocean to the East African coast and interior. Moisture from the Angolan center extends eastward but does not merge

with moisture from the Indian Ocean. This observation suggests that moisture contributing to Vuli rains is predominantly from the east.

5.3.3 Composite water vapor flux and Horizontal wind at 200 hPa.

The composite pentad water vapor flux sequence is illustrated in figure 5.2.4. Notable features which prevail throughout the life cycle over East Africa include moisture advection by monsoon winds and by southeasterly trade winds with an origin east of Madagascar. The driving force in the southern hemisphere is the anticyclone situated southeast of Madagascar. Atlantic Ocean fluxes are largely confined to the western coastal regions. By maturity stage moisture flux affecting northern Tanzania is mainly from the southern hemisphere. Equatorial convergence is also contributed from the northern hemisphere.

Figure 5.2.5 shows composite horizontal wind vectors at 200 hPa. A distinctive near equatorial duct is caused by an upper trough over Madagascar. The duct exit is over East Africa where westerlies prevail aloft and correspond to low- level moisture flux convergence there. At P0 new features include a change of wind flow in the Arabian Sea from southeasterly at P2 to southwesterly and a collapse of the upper- level ridge in the Atlantic Ocean.

5.3.5.1 Mean Divergence and Vorticity: 850 hPa

In the tropics divergence is contributed by vorticity forcing (Sardeshmukh and Hoskins, 1988), therefore in this and the following sub-section, these two parameters will be discussed together.

Figure 5.2.6, indicates the mean low- level tropospheric divergence during wet spell progression (P2, P1 and P0). At P2, apart from areas of significant divergence just off the east African coast, Mozambique Channel, and eastern Atlantic Ocean, the rest of Africa exhibits convergent flow. Strong lower level convergent centers are over Ethiopia, east Africa, eastern South Africa and Madagascar. India and the equatorial Indian Ocean east of 55° E display weak convergent flow.

At maturity stage (P0), East Africa and Madagascar convergence cells deepen and shift southward. The Mozambique Channel divergence pattern is intensified and extends inland to Botswana. Other patterns displayed at formation stage are either maintained or slightly transposed at maturity stage.

Figure 5.2.7 displays the progression of mean vorticity fields from formation to maturity. There exist only minor changes from P2 to P0. A feature exhibited during all stages is the existence of a cyclonic vorticity band in the Indian Ocean south of Equator associated with the ITCZ. The southwest coast of Africa displays another area of relatively weak cyclonic vorticity. Anticyclonic vorticity north of

the Equator off the Somali coast extends towards India and intensifies at maturity. Generally there is southward movement and some intensification at all stages.

5.3.5.2 Mean Divergence and Vorticity: 200 hPa;

Shown in figure 5.2.8 and figure 5.2.9 are 200 hPa composite divergence and vorticity for P2 to P0 respectively. Particularly impressive in the divergence field, is a confluent circulation that exists along the eastern coast of Africa at P2. It extends into the interior of Mozambique and towards Madagascar. Divergence occurs over Equatorial Africa. This increases at P0 and shifts southward. An intrusion into East Africa that spreads to cover the coast is evident. However, compensating convergence occurs in the Mozambique Channel and interior (section 5.2.4.1).23

Figure 5.5b displays vorticity fields which change only slightly in progression from P2 to P0. Two subtropical anticyclonic cells are found south of the equator and a band of cyclonic vorticity exists north of the equator. Eastward movement of anticyclonic vorticity cells is revealed over Namibia at P2 and over Zimbabwe at P0. Anticyclonic vorticity in the Indian Ocean is separated from that over central Africa.

5.3.4 Vertical motion at 500 hPa:

The entire African continent displays mid-tropospheric upward motion except over north Africa throughout the sequence (P2 to P0) presented in figure 5.2.10. However, equatorial East Africa and the Congo Basin are centers of strong uplift

(-16×10^{-2} Pa s^{-1}). At P2 the Mozambique Channel, western Indian Ocean, Madagascar and the Atlantic Ocean show subsidence (positive values). These areas correspond to the existence of anticyclones and ridge influences (see 5.3.1) in the lower level. A tongue of persistent uplifting with origin in the far east exists throughout the period and extends to the western Indian Ocean.

5.3.6 Velocity Potential anomalies:

In this sub-section divergent WVF and velocity potential at 200 hPa are investigated within the domain 20°N - 40°S, 30°W - 100°E. Figure 5.2.11 portrays the evolution of composite divergent WVF. At P2, east of 15° E in equatorial Africa and the Indian Ocean, distinctive convergent flow is noted. While the Atlantic Ocean exhibits strong low level divergent flow that extends into Namibia and South Africa. Little change occurs throughout the evolution, the major features at P0 are the intensification of a low level convergent center over east Africa and a marked southeastward propagation.

At upper levels (200 hPa, Figure 5.2.12) mean velocity potential fields oppose the patterns of the mean divergent WVF discussed above, but with a slight southwestward tilt. Intensification of the upper level divergent cell over Zambia is observed during the maturity stage. From the viewpoint of divergent WVF and upper tropospheric velocity potential, it is consistent that convective activities develop over the target region of northern Tanzania.

5.3.7 Mean divergent WVF / wind at 200 hPa.

This section deals with irrotational components of the circulation for water vapour flux and wind at 200 hPa. It is recognised that the boundaries affect this analysis, causing regional balance and compensation which may be somewhat artificial. Figure 5.2.13 reveals a meridional convergence flux zone from South Africa to the equator along 30°E. A quasi-stationary divergent centre over the Atlantic Ocean is maintained throughout the cycle. At maturity, a low level divergent area southwest of Madagascar shifts eastward and collapses. A localised convergent flux develops over northern Tanzania.

Composite divergent vectors at 200 hPa are illustrated in figure 5.2.14. All stages are dominated by upper divergence across the interior of Africa. The oceans obtain a consistent upper-level convergence where low-level response is exactly opposing. Little propagation through the successive stages is noted. These observations suggest that the tropical east Atlantic and particularly the southwest Indian Oceans are important sources of moisture convergence across the interior of Africa.

5.4 Discussion

The Vuli season is characterised by dry and wet spells. In part one of this chapter the analysis was based on the 1986-1991 mean that contains both dry and wet years. Part two dealt with selected wet spells using pentad composites. The mean and the composite patterns show only slight differences which can be highlighted

by differencing. The knowledge gained in this chapter will help in interpreting the anomaly patterns of wet and dry events discussed in chapters 6 and 7 respectively. Attention will be focused on:

- Development and persistence of upper-anticyclonic cells on either side of equator over East Africa.
- Southeasterly and northeasterly flow confluence over northern Tanzania.

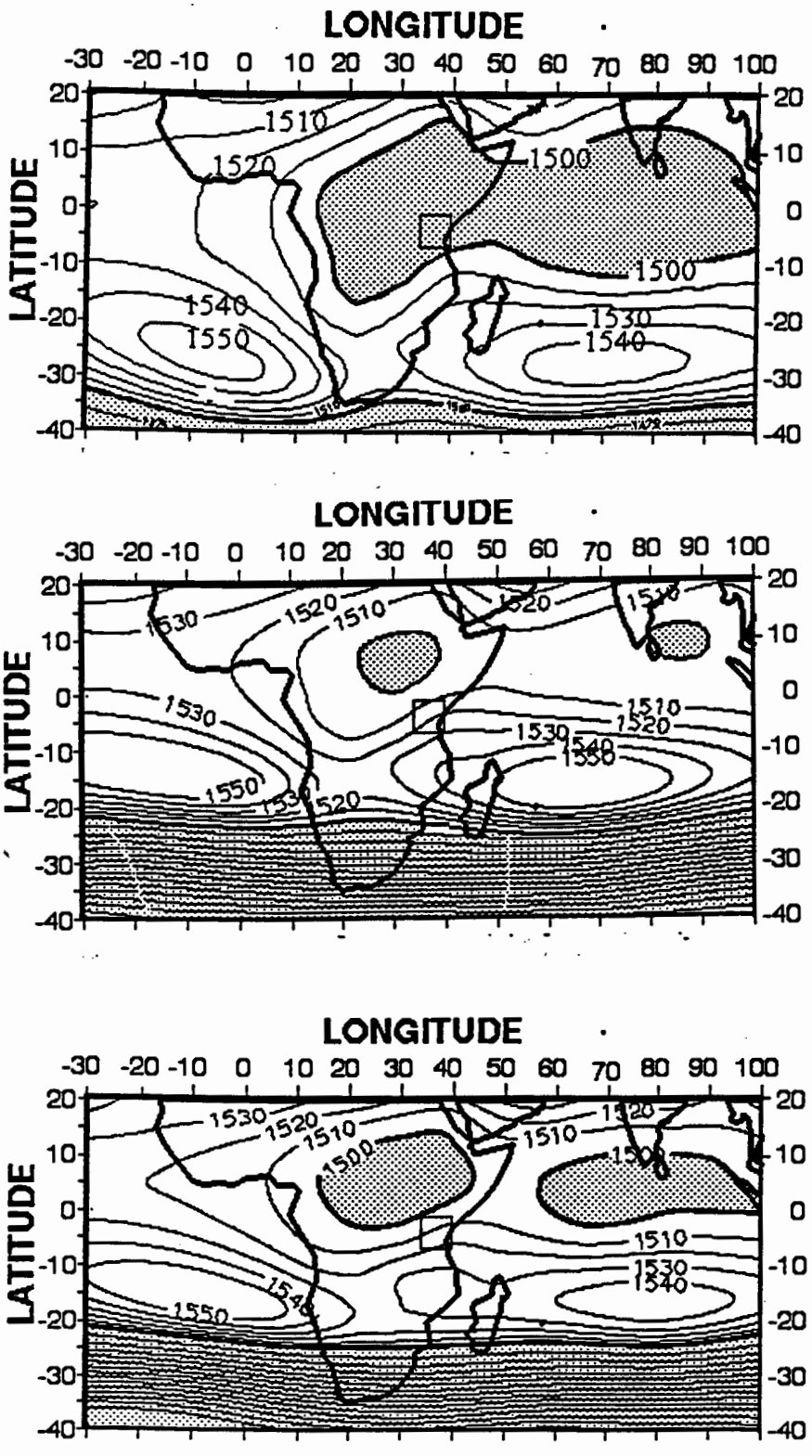

Figure 5.2.1: Mean composite Geopotential height at 850 hPa
Contour intervals are 10 gpm.

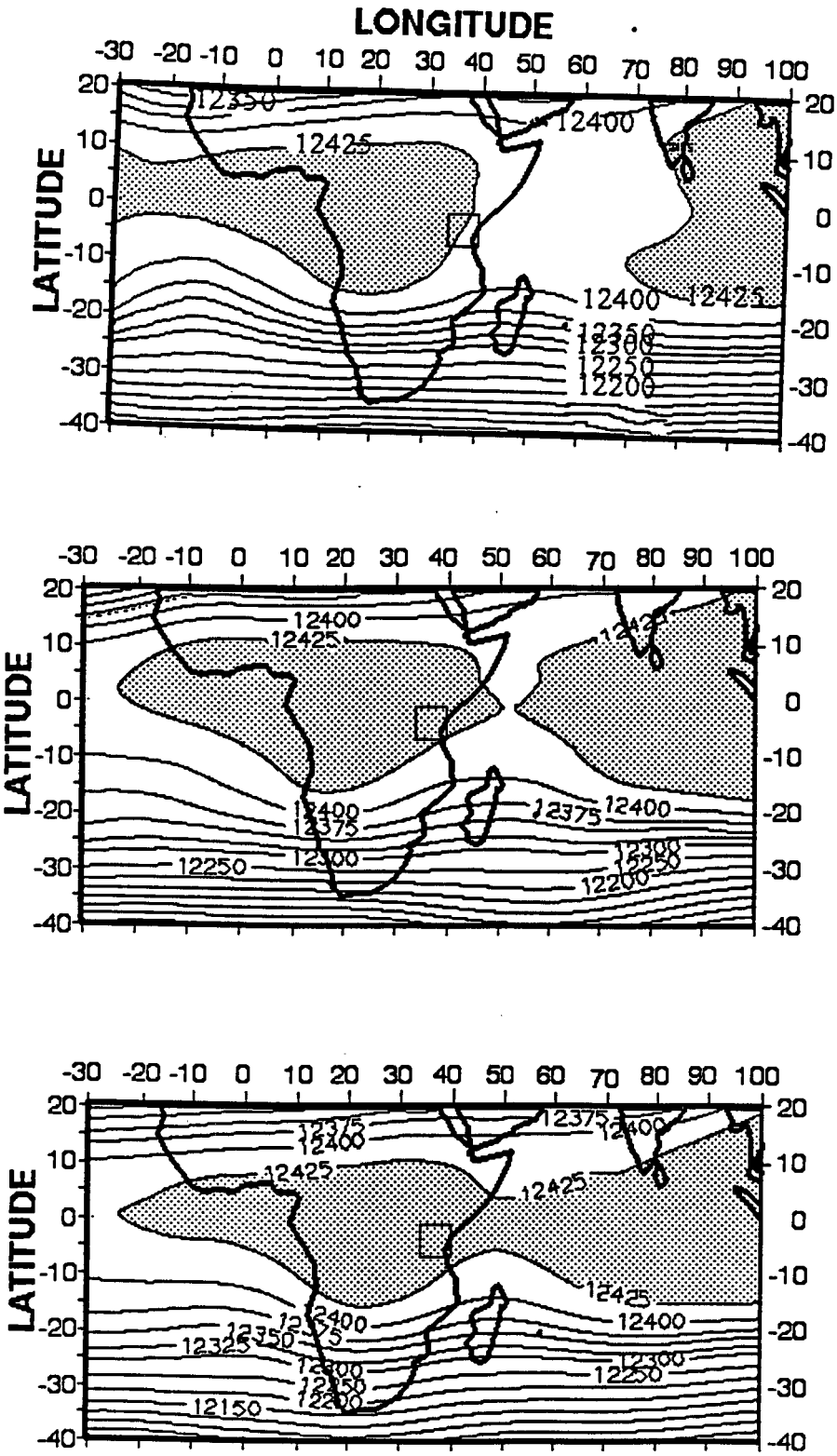

Figure 5.2.2: Mean composite Geopotential height at 200 hPa
Contour intervals are 25 gpm.

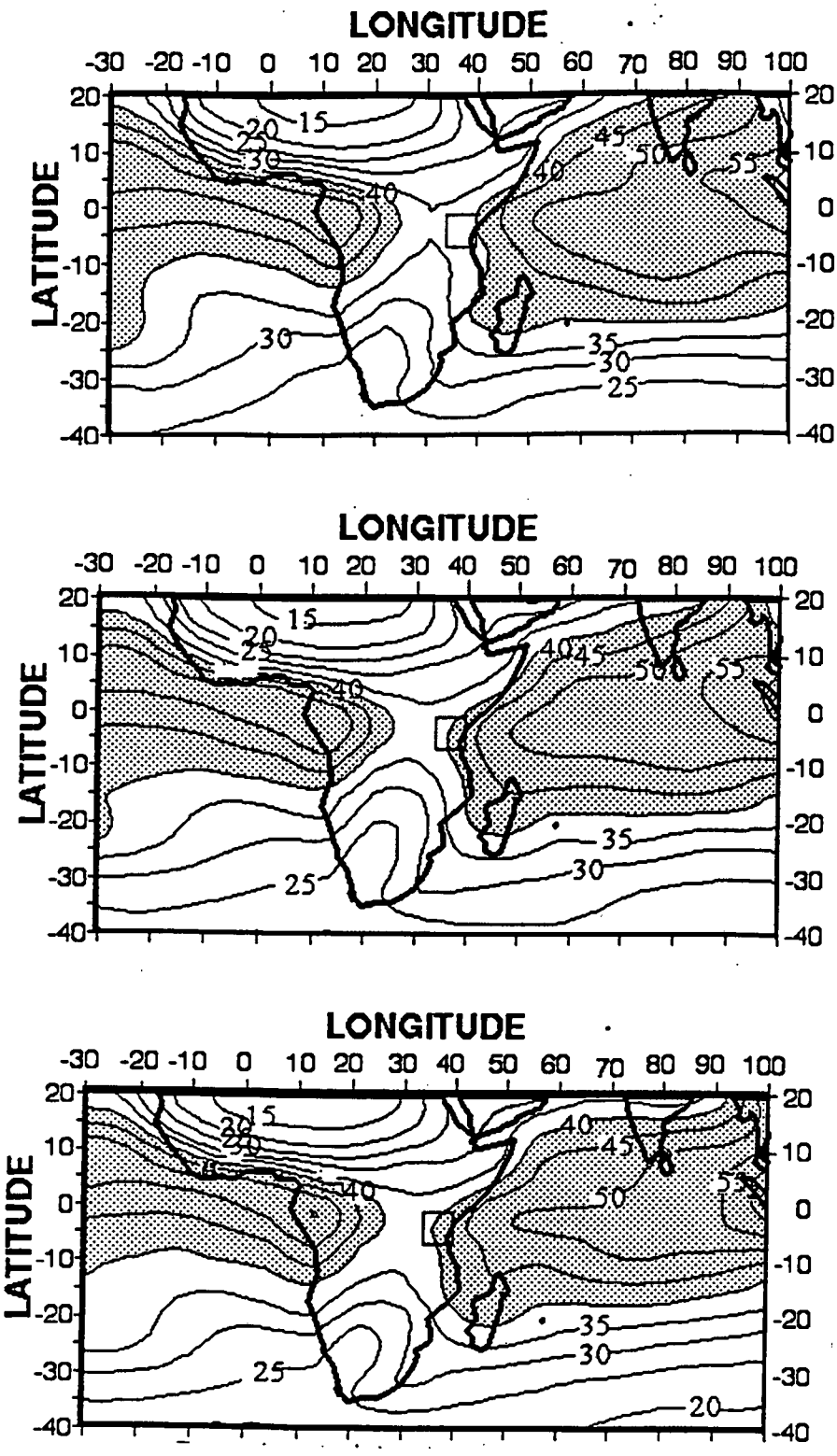

P2

P1

P0

Figure 5.2.3: Mean composite Precipitable water between surface and 300 hPa
Contour intervals are 5 mm.

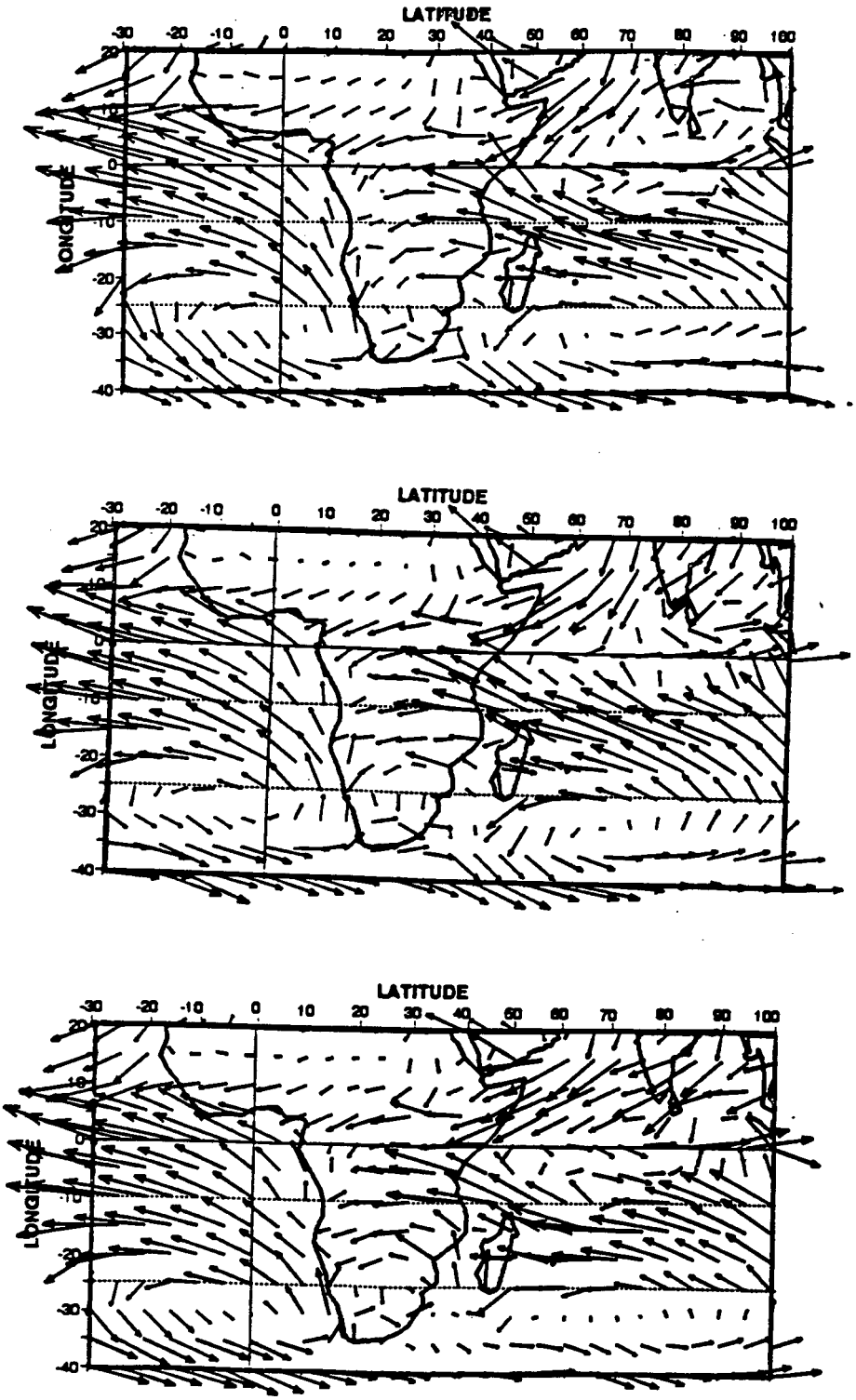

Figure 5.2.4: Mean composite Vertically integrated water vapour flux
⟶ vector is equivalent to 300 kg m^{-1} s^{-1}

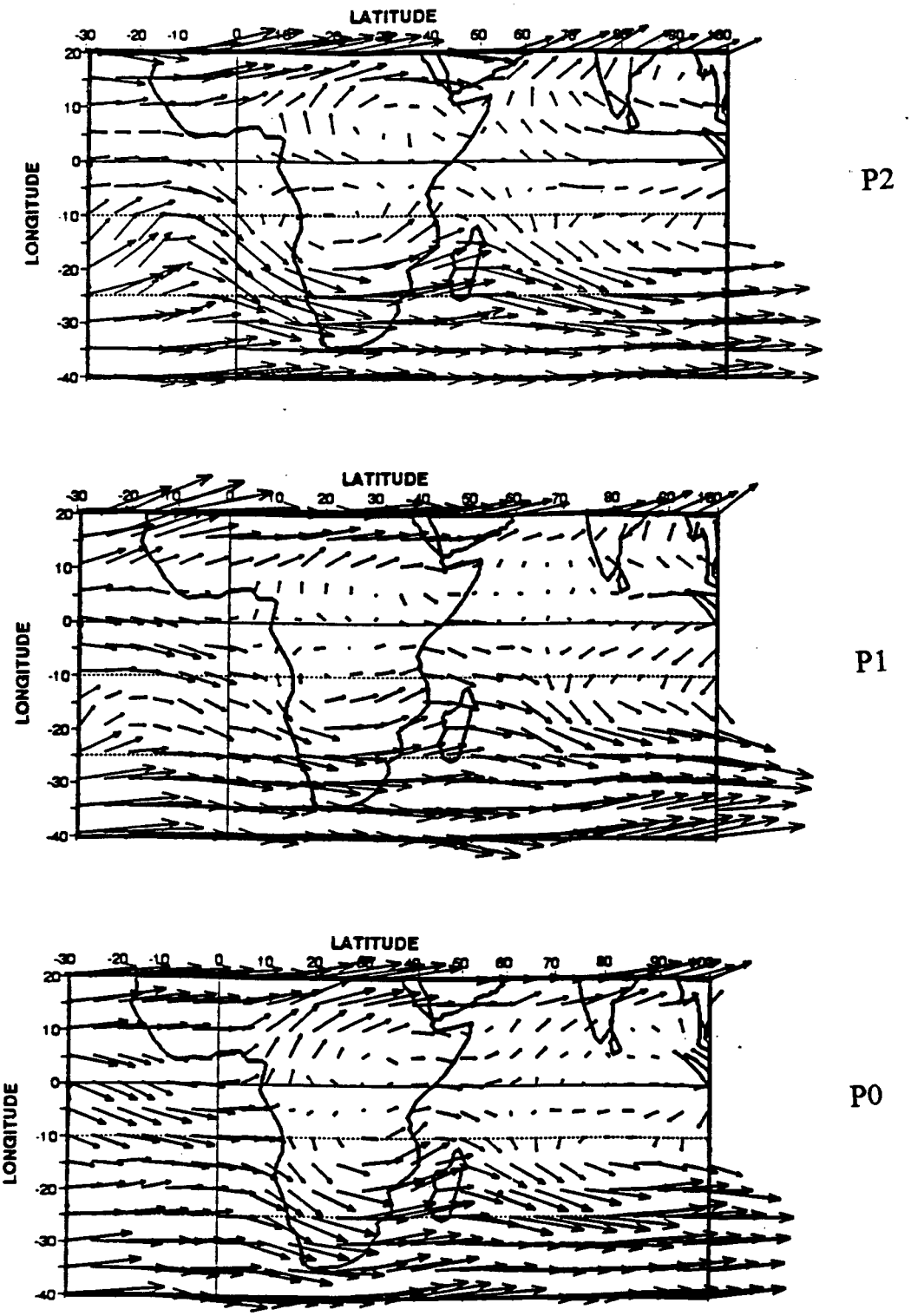

Figure 5.2.5: Mean composite Horizontal wind vector at 200 hPa
⟶ vector is equivalent to 30 m s^{-1}

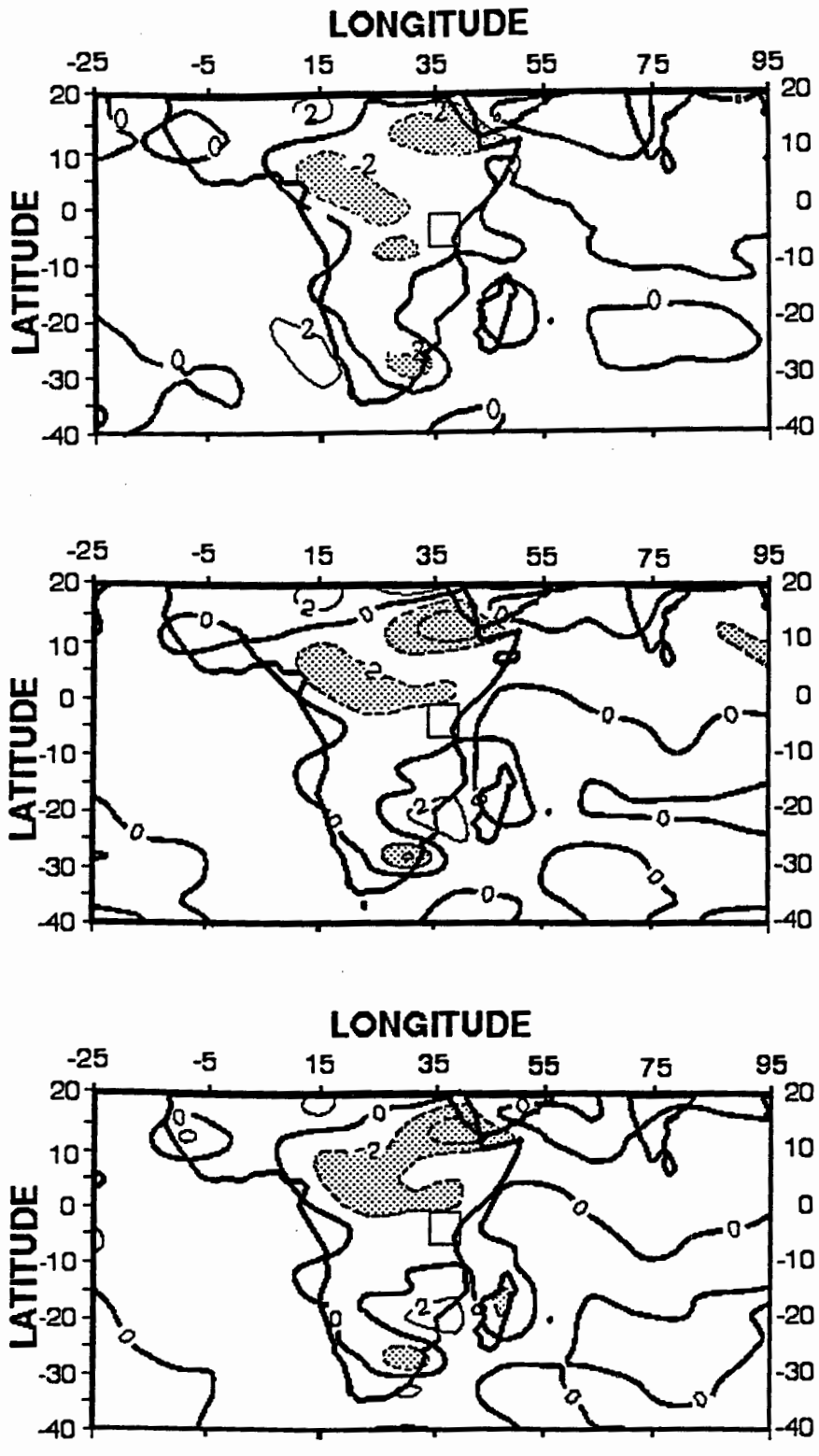

Figure 5.2.6: Mean composite Divergence field at 850 hPa
Contour interval is 2×10^{-5} s^{-1}

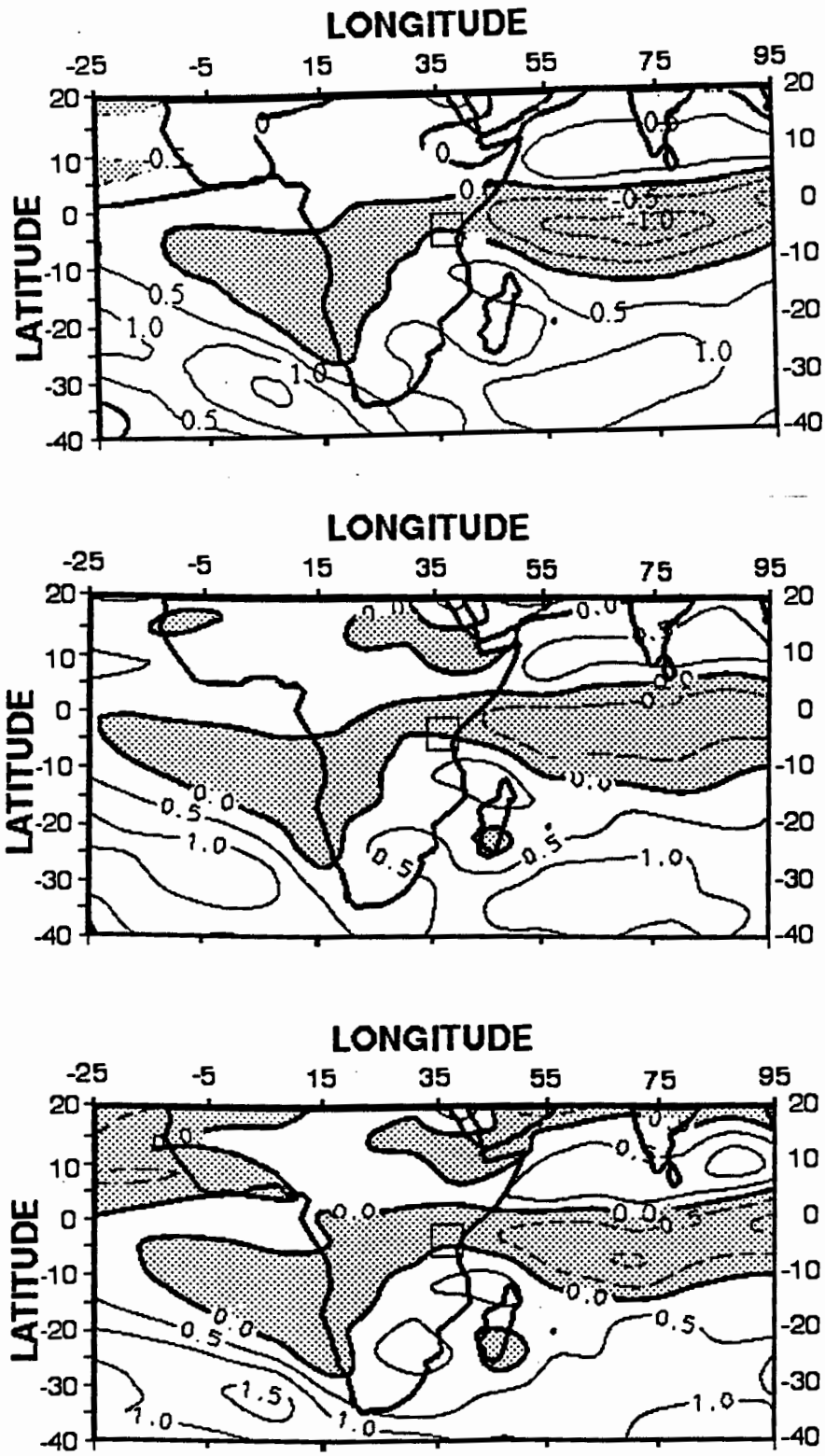

Figure 5.2.7: Mean composite Vorticity field at 850 hPa
Contour interval is 0.5×10^{-5} s^{-1}

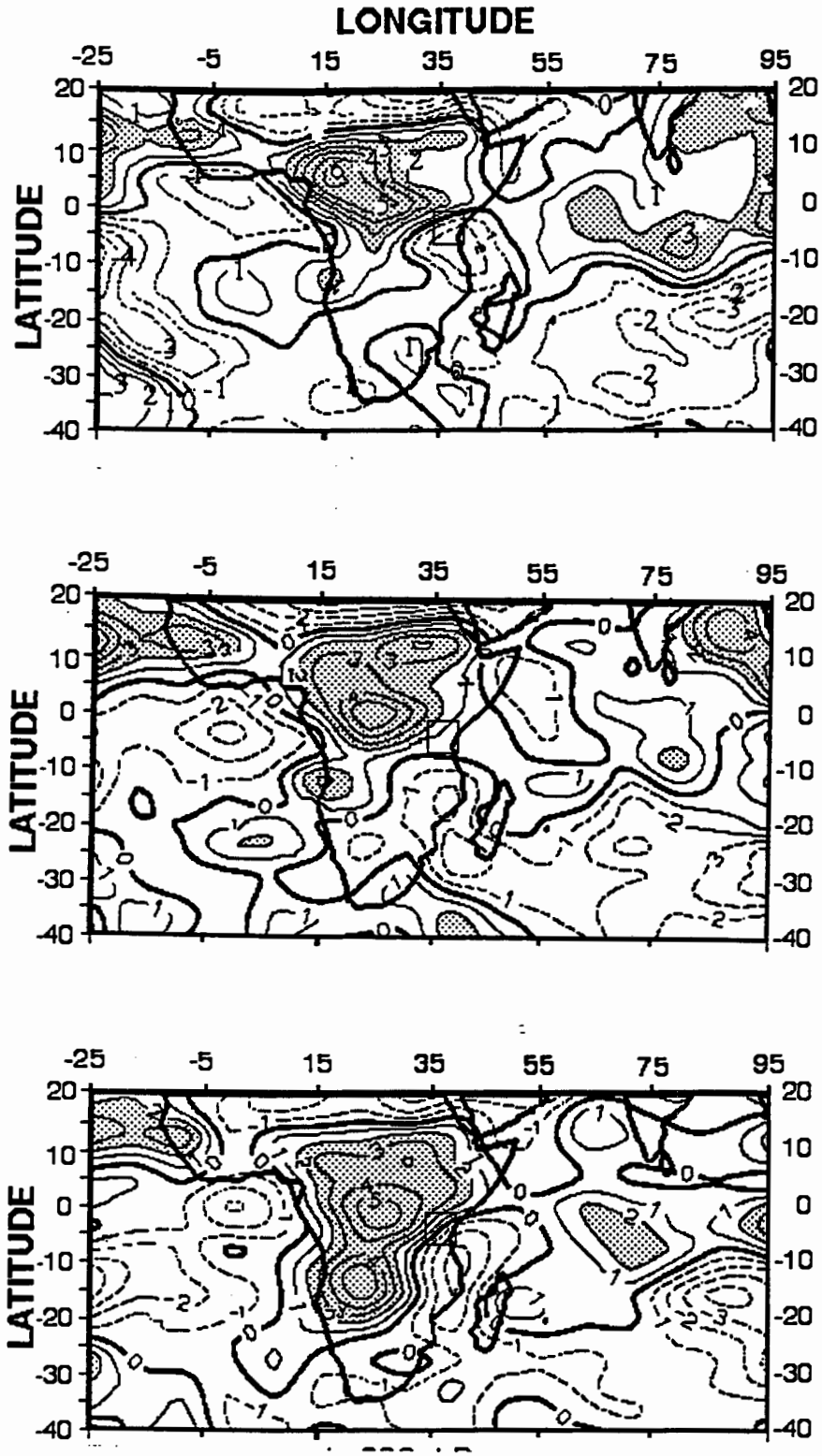

Figure 5.2.8: Mean composite Divergence field at 200 hPa
Contour interval is 1×10^{-5} s^{-1}

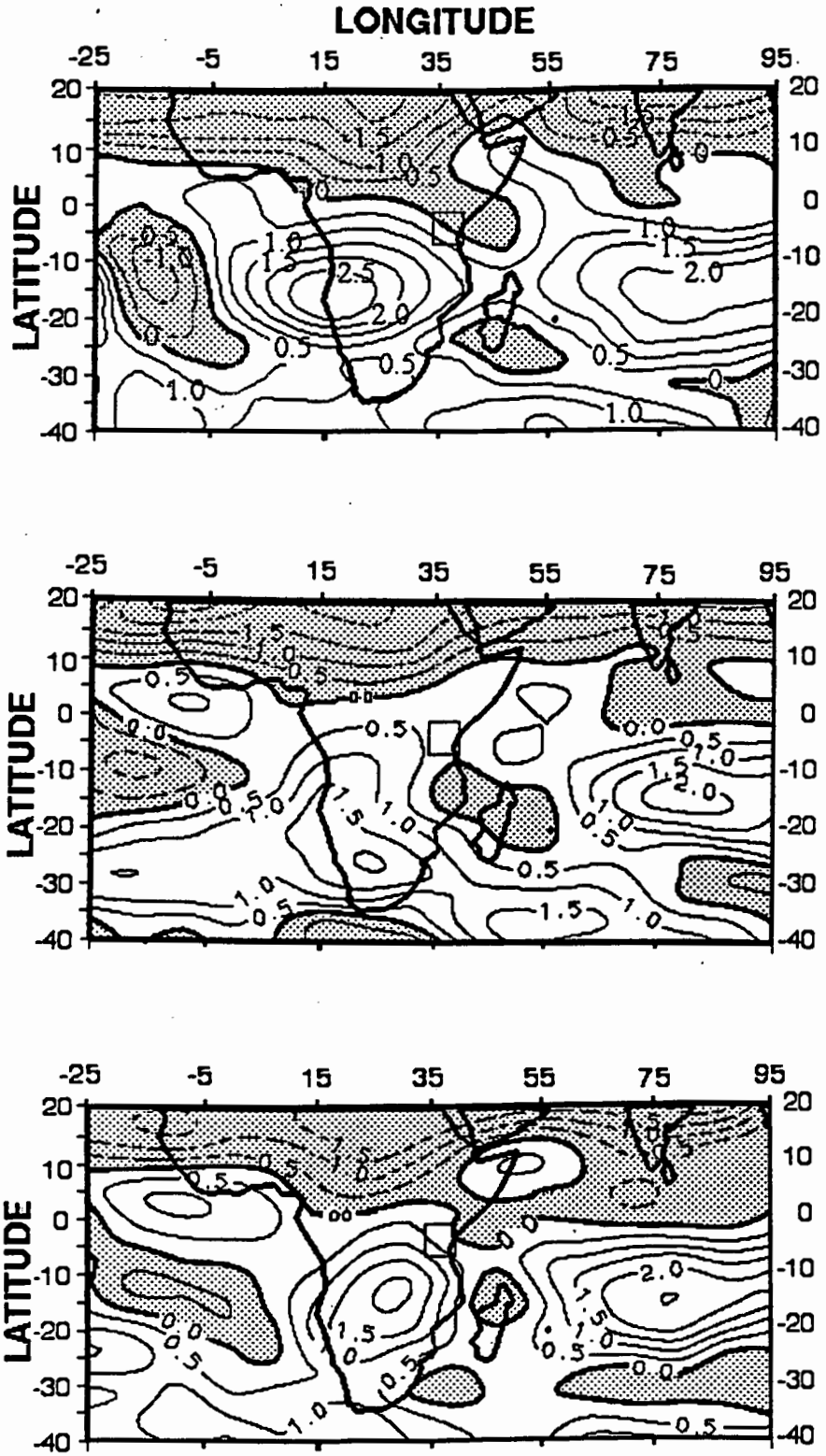

Figure 5.2.9: Mean composite Vorticity field at 200 hPa
Contour interval is 0.5×10^{-5} s^{-1}

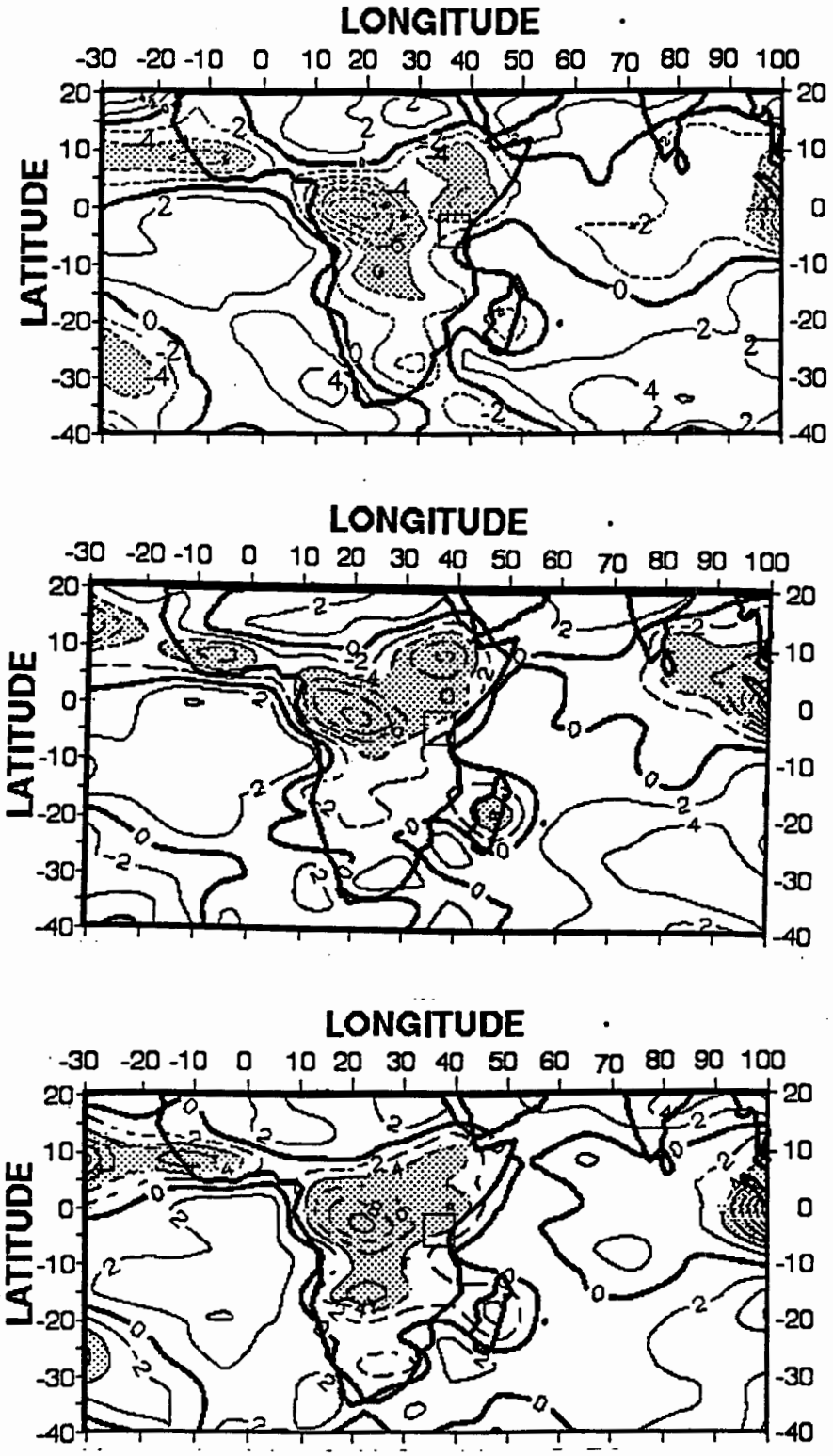

Figure 5.2.10: Mean composite 500 hPa Vertical motion
Contour interval is 2×10^{-4} Pa s^{-1}

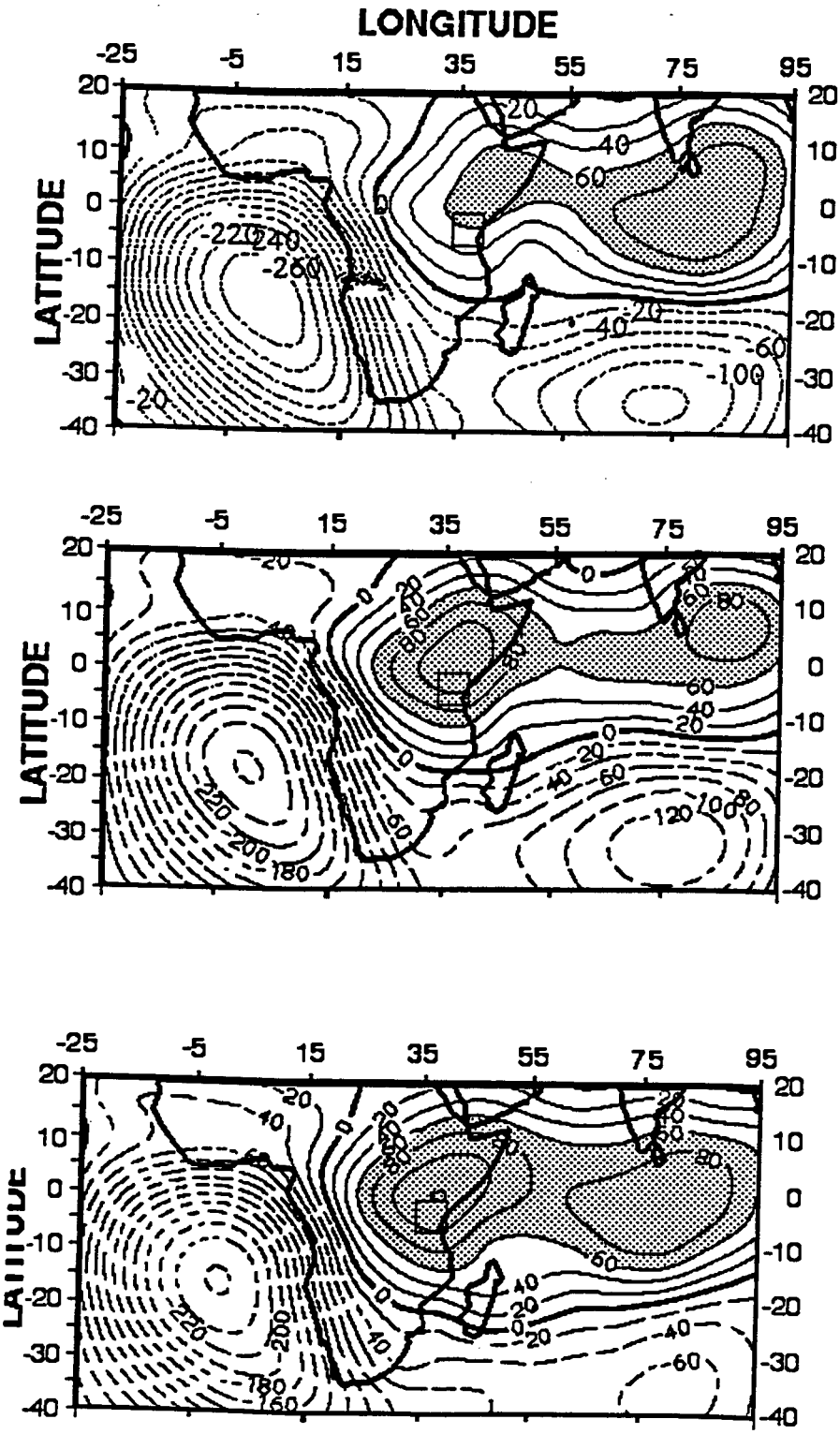

Figure 5.2.11: Mean composite Velocity potential of WVF integrated from surface to 500 hPa
Contour interval is 20×10^6 kg s^{-1}

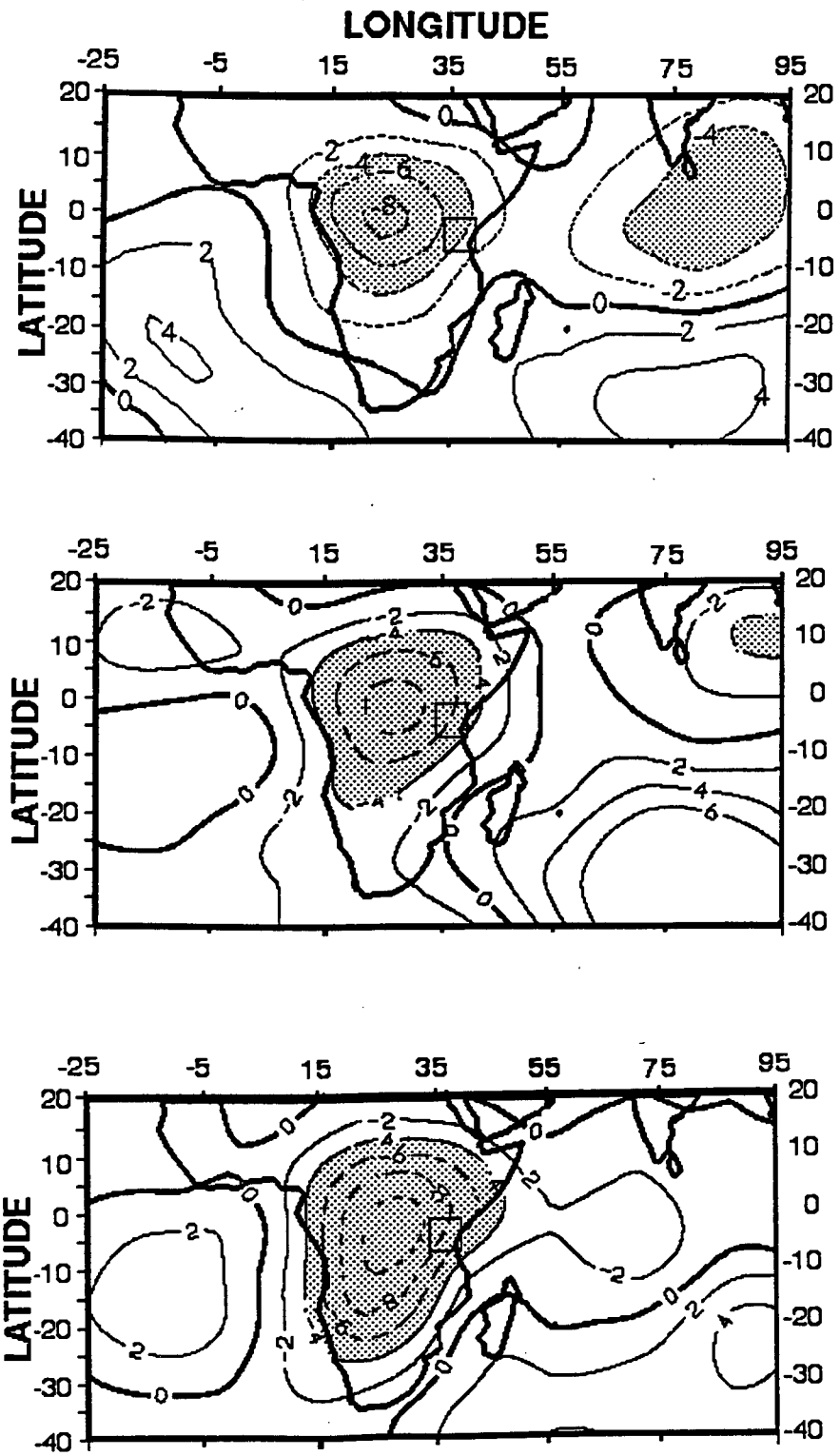

Figure 5.2.12: Mean composite Velocity potential field at 200 hPa
Contour interval is 2×10^6 m^2 s^{-1}

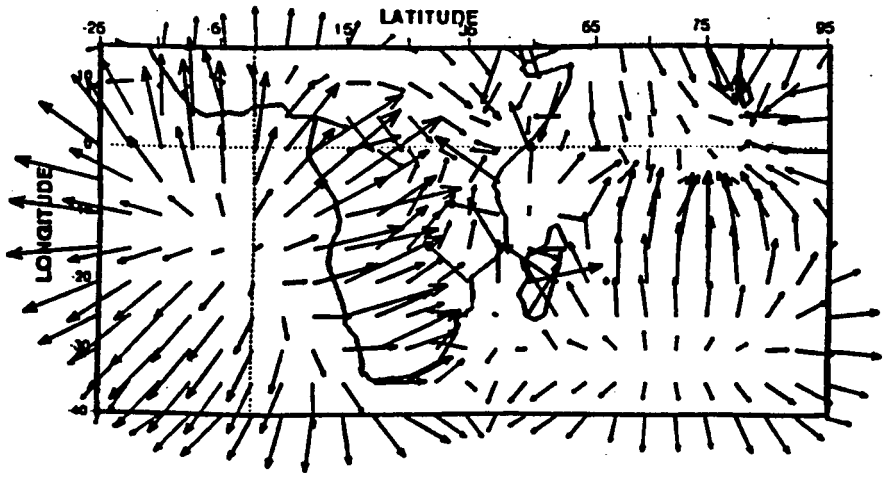

P2

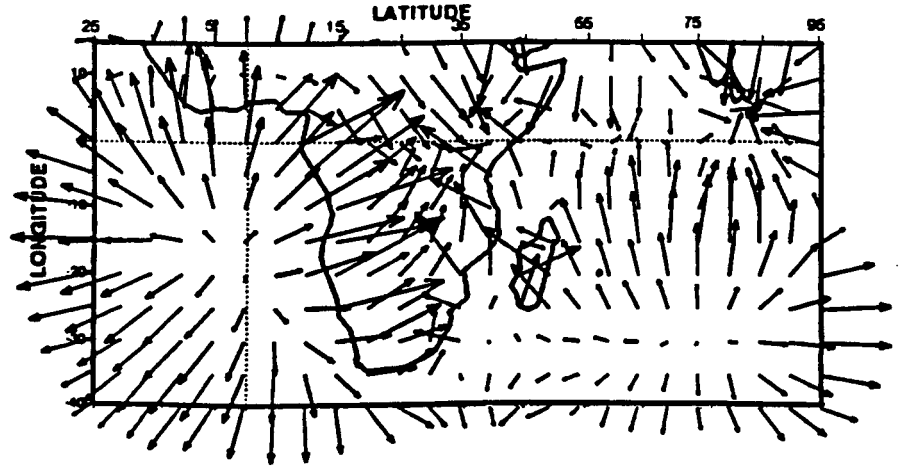

P1

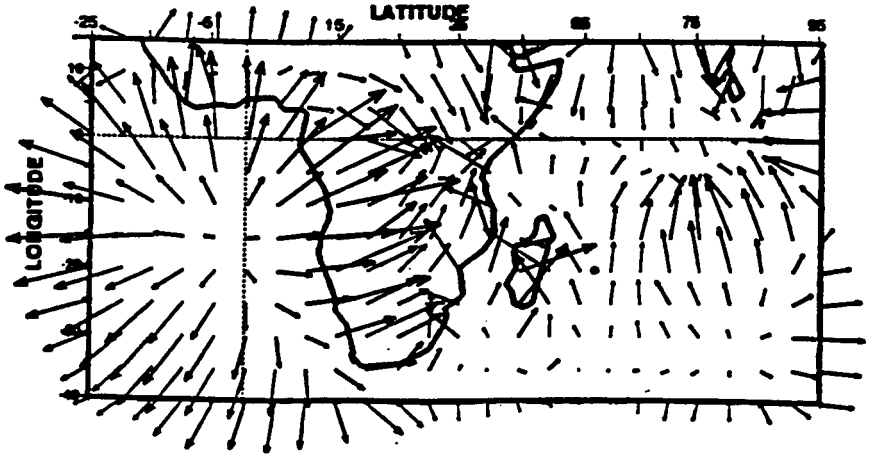

P0

Figure 5.2.13: Mean composite Divergent water vapour flux
⟶ vector is equivalent to 80×10^6 kg m^{-1} s^{-1}

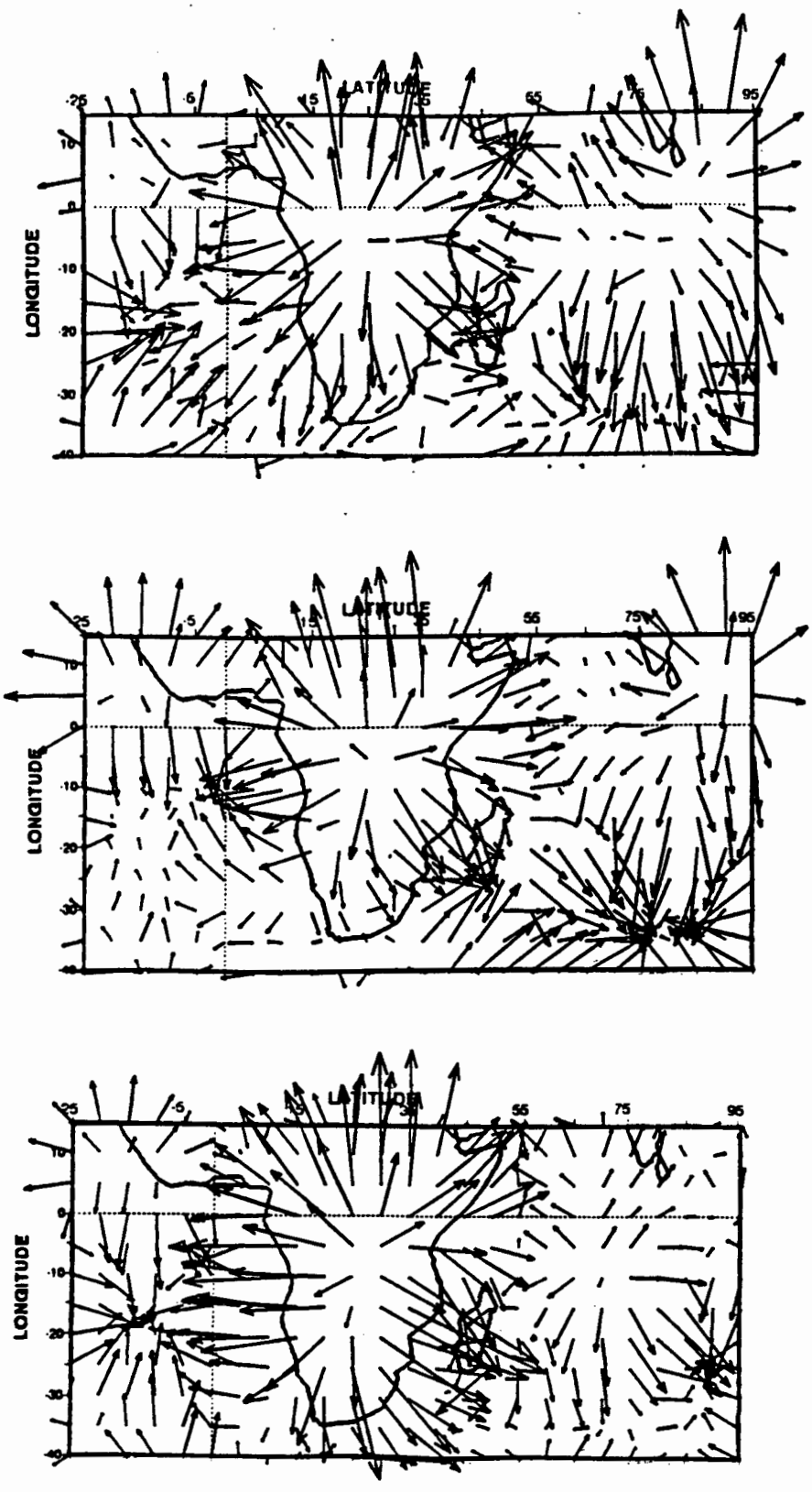

Figure 5.2.14: Mean composite Divergent wind
⟶ vector is equivalent to 5.0 m s^{-1}

Chapter 6: Intra-Seasonal Oscillations: Vuli wet spells and evolution:

The "Vuli" October to December season in Tanzania is when rains affect the northern part of the country, assisting in agricultural production and the replenishing of water resources. These rains are often associated with the retreat of the summer monsoon over India (Asnani 1993). To diagnose the mechanisms underlying intraseasonal variability, ECMWF data of horizontal winds and derivertives, vertical motion, heating, divergence, atmospheric moisture, etc., are used. In the literature, an example of this type of work is Bengtsson and Shukla (1988) on blocking in mid-latitudes and 30 to 60 day oscillations in the tropics. Here ECMWF data for the period 1986- 1991 in the months October to December provide insight to processes responsible for the formation, development, and maturity or persistence of Vuli wet spells.

Vuli wet spells are hypothesized to be related to:

I) moisture advection from the western Indian Ocean and Congo Basin.

ii) enhanced southeasterly flow across the Mozambique Channel converging with northeasterlies from the Arabian sea over East Africa.

iii) in-situ convection due to localised instability and heating.

In this chapter characteristics of selected meteorological fields in terms of pentad anomalies are used to focus on the evolution of Vuli wet spells in three stages, namely formation stage (P2), development stage (P1), and maturity stage (P0). The

aim is to gain a better understanding of precursors, structures and factors prevailing at each stage. More specific aims are to:

I) determine moisture sources, sinks and propagation over Northern Tanzania and immediate environs;

ii) investigate observed pentad anomalies with respect to the OND mean for use in medium-range weather forecasting.

6.1 Methodology:

Major wet spells (>25 mm/pentad) were determined in the middle of the Vuli season. Following identification, the preceding pentads were identified in terms of onset and dry phase. These were usually one and two pentads before the wet spell, respectively. Table 5.1 illustrates the cases selected to form pentad composites for analysis of the surrounding weather patterns using ECMWF data in the period 1986-1991. Pentad anomalies were computed in respect of the Vuli season OND mean for each stage for each parameter and level. Hence, the composite anomalies are based on 5 individual cases (25 days) minus the seasonal mean: (90 days x 6 yr. or 540 days). Anomalies are computed for P2, P1 and P0 and presented and interpreted below.

6. 2 Results of ECMWF pentad analysis

6.2.1 Geopotential Height:

At P2, geopotential height anomalies at 850 hPa (fig 6.1) are weakly positive in both hemispheres. Negative anomalies (-25 gpm) lie along 40°S in a wavy pattern. At upper levels (200 hPa, fig 6.2), a large negative anomaly is located southeast of Africa in the mid-latitudes and extends northwards along the coast of east Africa.

At the onset stage (P1) lower levels illustrate the growth of a positive anomaly (+25 gpm) south east of Madagascar which is reflected in the northern hemisphere at similar longitudes 40 - 90° E. 200 hPa patterns show strong positive anomalies in the southern subtropics with a peak of +70 gpm at 40° S, 60° E and in the South Atlantic Ocean. Areas of the southwest Indian Ocean and northeast Africa all lie under negative values.

During maturity stage (P0), a cell of positive anomaly extends zonally over and to the southeast of southern Africa at lower levels. Also apparent is the Arabian ridge over India. The tropical region displays weak geopotential anomalies. The upper level geopotential anomalies are positive in the tropics and therefore oppose the lower level. An upper ridge is noted south of Cape Town. The area south of Madagascar and in the northern subtropics along 15°N is occupied by negative anomalies.

A major feature is the build up of the Mascarene high and positive anomalies over the Indian Peninsula and Arabian Sea in the lower levels.

6.2.2 Precipitable Water:

Precipitable water is one of many derived variables used in this thesis. It is an integrated measure of specific humidity between the surface and 300 hPa and is considered to be more useful than a single level humidity analysis (Klinker 1990), particularly for deep tropical convection.

Figure 6. 3 shows, in the formation stage (P2), a thin NW-SE band of positive precipitable water anomalies located over equatorial East Africa and extending into the Indian ocean. Most of southern Tanzania is covered by negative anomalies.

At development stage (P1), the thin band of moisture expands into a big cluster of positive PW anomalies covering East Africa and extending offshore to 60° E. In its near-equatorial position, the central value is 3 mm higher than the mean. Negative values cover central and southern Africa and the rest of the Indian Ocean, while the Atlantic Ocean maintains positive anomalies throughout formation and development stages.

A gradual merging of positive anomalies from Atlantic and Indian Oceans occurs. By the mature stage (P0), a large zone of positive PW values forms between 20°S and 10°N. Negative anomalies are found in the Mozambique Channel (-4 mm) and also in the central Indian Ocean and across the Sahara.

6.2.3 Water vapor flux and Horizontal wind anomalies at 200 hPa.

Water vapour flux (WVF) parameter is the advection of precipitable water by the horizontal wind. Since moisture is concentrated in the lower levels, the weighted vector average reflects flow in the levels below 500 hPa. Figure 6.4 (a) represents water vapour flux anomalies integrated from surface to 500 hPa. The objective of using horizontal 200 hPa wind vectors figure 6.4 (b) together with water vapour flux in this analysis, is chiefly to infer the mass flux, vertical overturning, and kinematic forcing.

It is evident from the figure that weak northeasterly and southeasterly (WVF) winds converge onto the east African coast near the equator at formation stage (P2). The flow is weak owing to the disorganised structure of the Mascarene anticyclonic and northeasterly flow from the Arabian sea. Horizontal wind vectors (200 hPa) at formation stage reveal a strong anticyclonic circulation over Angola and a cyclonic cell over the Arabian peninsula. Weak westerlies prevail along the equator of East Africa. Water vapour flux of magnitude 100 g kg^{-1} m s^{-1} prevails along the east African coast and its hinterland during development stage (P1) as revealed in figure 6.4(a). The Mascarene anticyclone is more dominant. Convergent flow anomalies shift over East Africa during this phase.

During the maturity stage (P0), water vapour flux vectors show northeasterlies dominating as southeasterlies weaken. Convergence is pushed south of the equator approximately to 5°S. Equal strength of flow anomalies from each

hemisphere maintains a convergence line near the equator. Horizontal wind vectors (200 hPa) during development (P1) and maturity stage (P0) show upper westerly flow to be dominant over tropical Africa, with a source area from north Africa and the Atlantic Ocean.

6.2.4 Divergence and Vorticity: 850 and 200 hPa

In figure 6.5(a), low level convergence anomalies (negative) are maintained over the western Indian Ocean and Namibian escarpment throughout the sequence (P2, P1 and P0). At the development stage convergence extends to the Mozambique Channel from the Sudan. Maturity stage (P0) commences with a deep convergent center over Madagascar and intensification over East Africa.

Low level vorticity anomalies (figure 6.5(b)) are located off the east African coast in the western Indian Ocean, with opposing signs in each hemisphere at all stages. At maturity, the northern anticyclonic cell off the Somali coast intensifies at the expense of the southern cyclonic gyre. This vortex pair, located over the ocean to the east, refers to convergent meridional flow to the west. The vortex pair anomaly gradually shifts southward through the sequence. Another cell of strong anticyclonic vorticity lay in the ocean south of India. In the Mozambique Channel, anticyclonic anomalies are replaced by cyclonic vorticity.

Reference to the upper divergence figure 6.6 (a) and vorticity patterns figure 6.6 (b), show that in the formation stage upper convergent anomalies are prevalent

over the east, central and southern Africa except the Lake Victoria basin and Mozambique. At P2 a closed cyclonic cell over the East African coast extends westward to join another over South Africa and the Mozambique Channel. Anticyclonic vorticity anomalies are found in the East Atlantic Ocean, Angola, Namibia and Zaire. At development, upper level divergence anomalies increase to a central value of 4 $x10^{-5}$ s^{-1} over a NNW-SSE axis across East Africa and Madagascar. Cyclonic vorticity is featured over Botswana, in a meridional band in the central Indian Ocean and over the Sahara.

At maturity stage two centers of strong upper level divergence are noted over East Africa and Botswana (20° S, 24° E). These join in a NE-SW axis. Upper level convergence occurs over the bulge of West Africa, South Africa and Zimbabwe. Vorticity anomalies are anticyclonic over the Somalia and Malawi, elsewhere cyclonic vorticity is found. Intense cyclonic centers are located over Madagascar and on the South African southeast coast. The latter cyclonic area appears as a band extending into the South Indian Ocean. In general upper anticyclonic vorticity anomalies are small over Tanzania, while upper divergence values are relatively larger and dynamically more significant.

6.2.5 Vertical Motion Anomalies at 500 hPa

The vertical motion field indicates areas of subsidence (sinking motion) and ascent (rising motion) where diabatic heating is efficient. During formation stage (P2)

figure 6.7, strong rising motions occur over East Africa with a center near the equator. Coastal regions are subsident, while offshore in the Indian Ocean rising motion is displayed in a NW-SE band.

At development stage (P1), centres of vertical uplift are displaced westward. Most of Tanzania is under rising motion, while sinking motion intensifies in the Indian Ocean. A few pockets of rising motion are found over Namibia, over the Sudan and equatorial West Africa. The whole of East Africa, Angola and Congo develop strong uplift during maturity stage (P0). The Atlantic Ocean maintains rising motions, compared with the Indian Ocean which remains more quiescent throughout the sequence (P2 to P0). Westward coalescence of the NW-SE band from the Indian Ocean with uplift over the Mount Kilimanjaro region appears as the main feature of vertical motions.

6.2.6 Velocity Potential anomalies:

Divergent WVF is useful in identifying cumulus convection and atmospheric energy sources and sinks, hence effective in assessing intra- and inter-annual oscillations at global and regional scales (Krishnamurti, 1978; Salsten et al., 1980; Chen, 1985; Rosen et al., 1980; Peixoto et al., 1980; Peixoto and Oort, 1983; Chen and Tzeng, 1990). In figure 6.8 (a), positive values imply water vapour convergence and ascent, while negative values are divergent areas where sinking

motions prevail. Divergent WVF is also a more useful diagnostic tool than velocity potential alone, since the effects of moisture advection are included.

At formation stage (P2) the entire African continent is under large scale divergence with the exception of a positive convergent area in the NW Indian Ocean extending to the equator near 60°E. A center of divergence is situated in the south Indian Ocean (at 67°E, 35°S).

At 200 hPa figure 6.8 (b) the velocity potential anomalies show a divergent cell in the Atlantic Ocean, and convergent anomalies over the African continent and western Indian Ocean. Strongest upper convergence anomalies occur over southern Africa and spread into the southwest Indian Ocean.

The development stage (P1) pattern reveals strong centers of upper divergent and lower convergent anomalies over equatorial Africa, with one center over East Africa and Angola. The WVF divergent cell in the South Indian Ocean is intensfied and moves slightly northeastward to 77°E, 25°S. Upper convergence overlies this zone and extends to southern Africa.

During maturity stage (P0), convergent WVF anomalies are positioned off the East African coast, extending south to Madagascar and zonally across East Africa towards the Congo. The center of negative anomalies buds-off and shifts northeast towards India. Velocity potential anomalies at 200 hPa become negative (divergent) over Tanzania in an axis extending northeast from Botswana and the South Atlantic. Thus a condition of lower convergence and upper divergence

conducive to heavy rainfall occurs over East Africa. In contrast, the Bay of Bengal and Mozambique Channel show upper convergence and convective suppression.

6.2.7 Divergent WVF and 200 hPa wind anomalies.

Verticaly integrated (from surface to 500 hPa) divergent water vapor flux anomalies are illustrated as vectors in figure 6.9 (a). At the formative stage (P2) a divergent center occurs southwest of Madagascar in the Indian Ocean. A line of lower convergence occurs off the Somali coast; convergence dominates the Atlantic Ocean. However, at development stage (P1), divergence in the Indian Ocean southwest of Madagascar intensifies and shifts northward, enhancing convergence in East Africa south of the equator. Weak divergence east of South Africa, in the Atlantic Ocean and West Africa is in contrast with convergence over the Congo and Angolan coast. The Indian Ocean divergent cell collapses at maturity stage (P0) to be replaced by a weak convergence, while convergence over East Africa is found along the Tanzanian coast and hinterland and the Lake Victoria basin. Divergent wind vector anomalies at 200 hPa figure 6.9 (b), at all stages, reveal characteristics opposite to their counterpart of water vapour flux vectors. In the Indian Ocean along 85° E latitude, a convergence line exists which enhances strong upper-level divergence over East Africa. This supports lower level convergence in those areas. We may summarized as follows. Circulation systems over the southwest Indian Ocean prepare the onset of the Vuli wet spell

by supplying the moisture, while systems over the Arabian Sea act to trigger convection over East Africa.

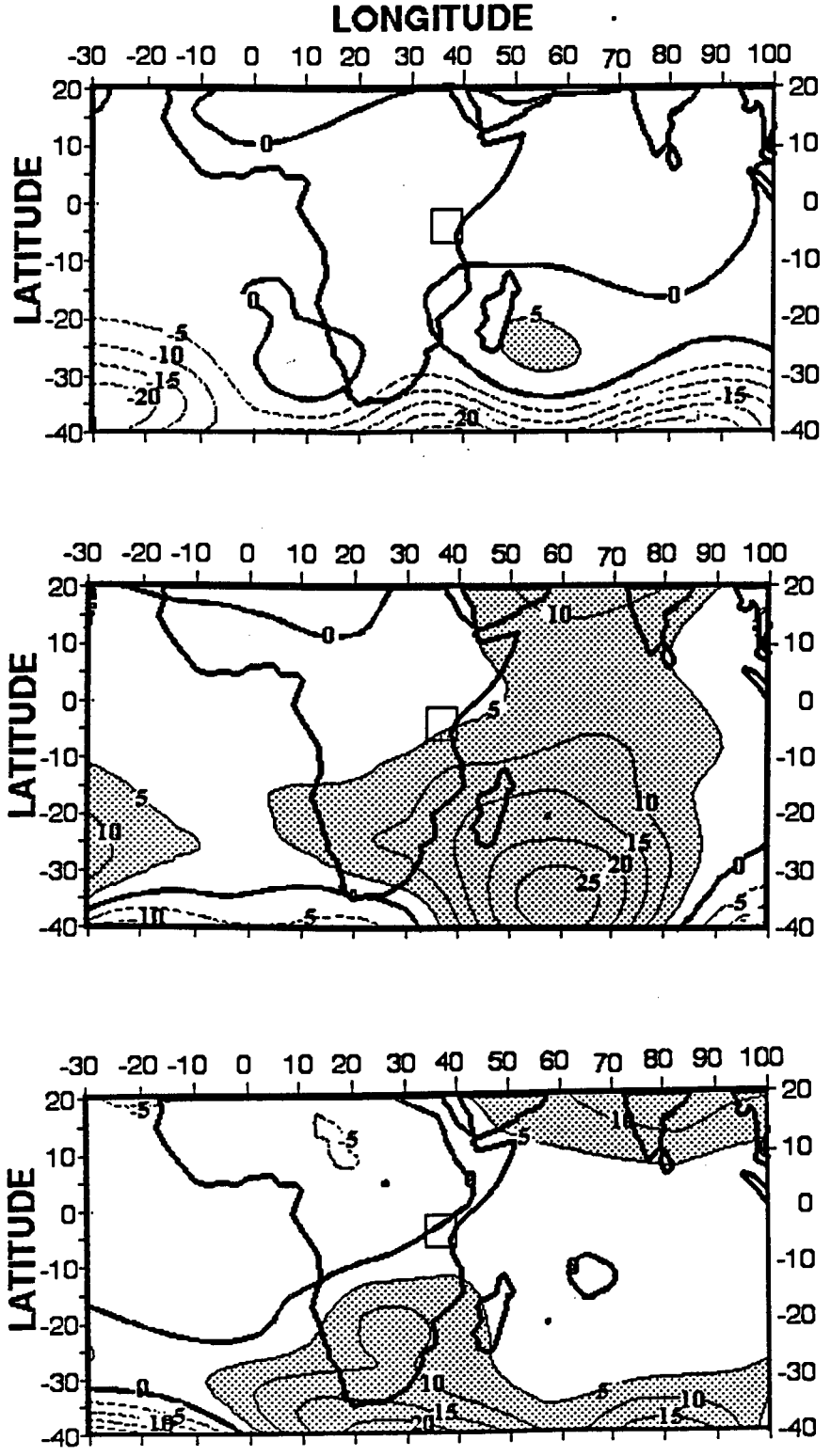

Figure 6.1: Geopotential height anomalies at 850 hPa for Vuli wet spell
Contour intervals are 5 gpm.

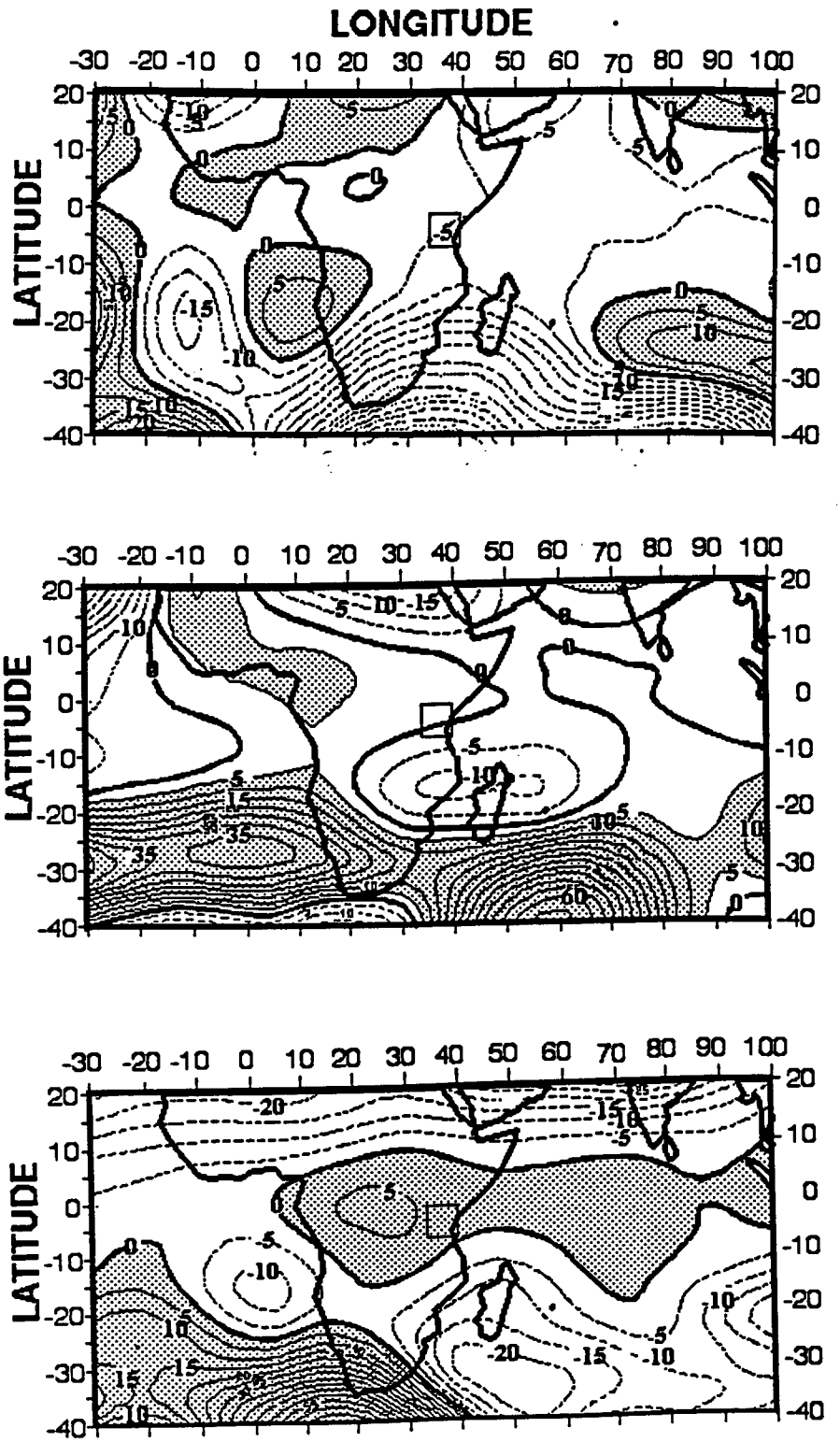

Figure 6.2: Geopotential height anomalies at 200 hPa for Vuli wet spell
Contour intervals are 5 gpm.

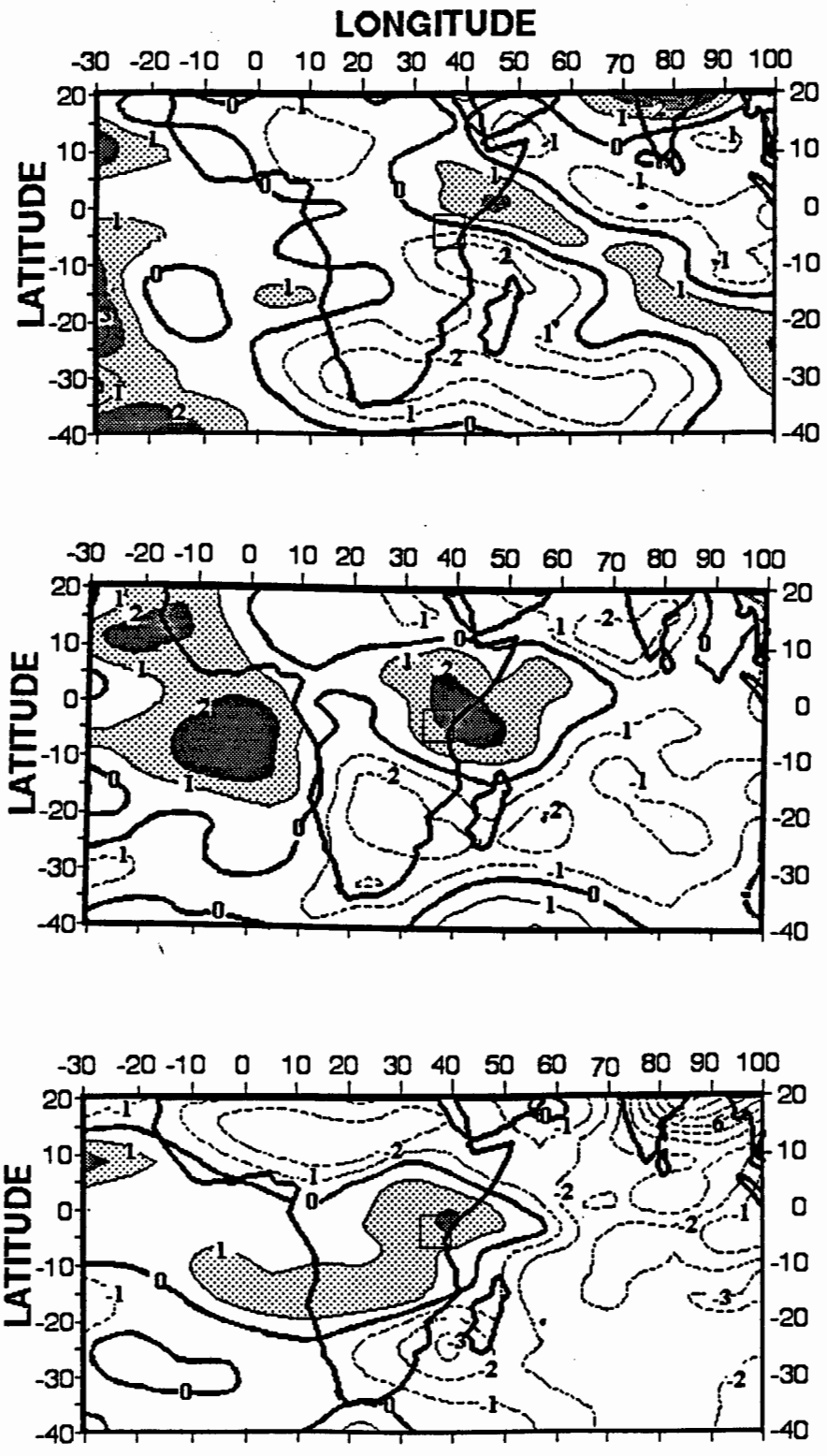

Figure 6.3: Precipitable water anomalies between surface and 300 hPa for Vuli wet spell

Contour intervals are 1 mm.

≥ 1 mm.

≥ 2 mm.

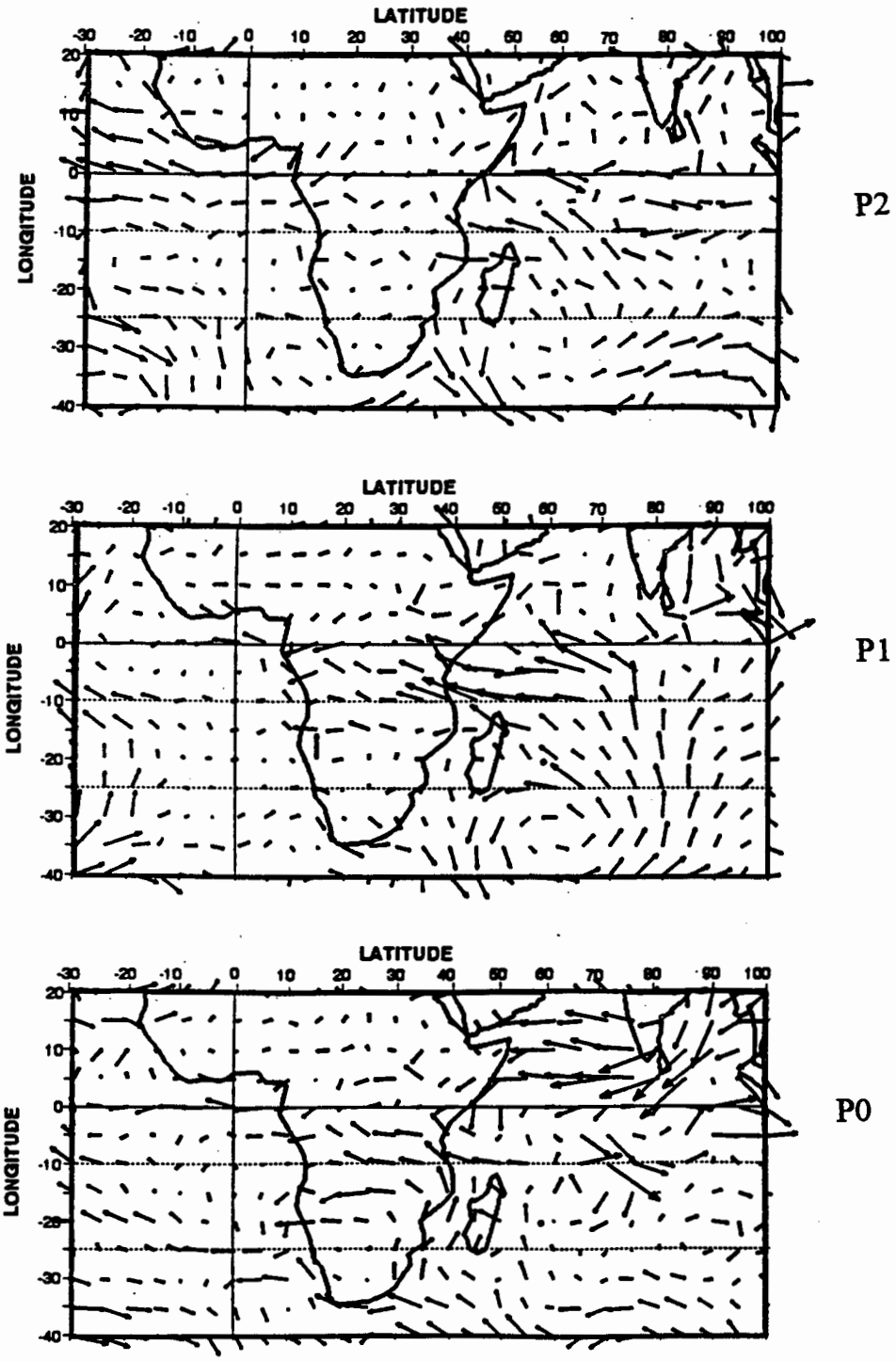

Figure 6.4 (a): Vertically intergrated water vapour flux anomalies.
⟶ vector is equivalent to 100 kg m^{-1} s^{-1}

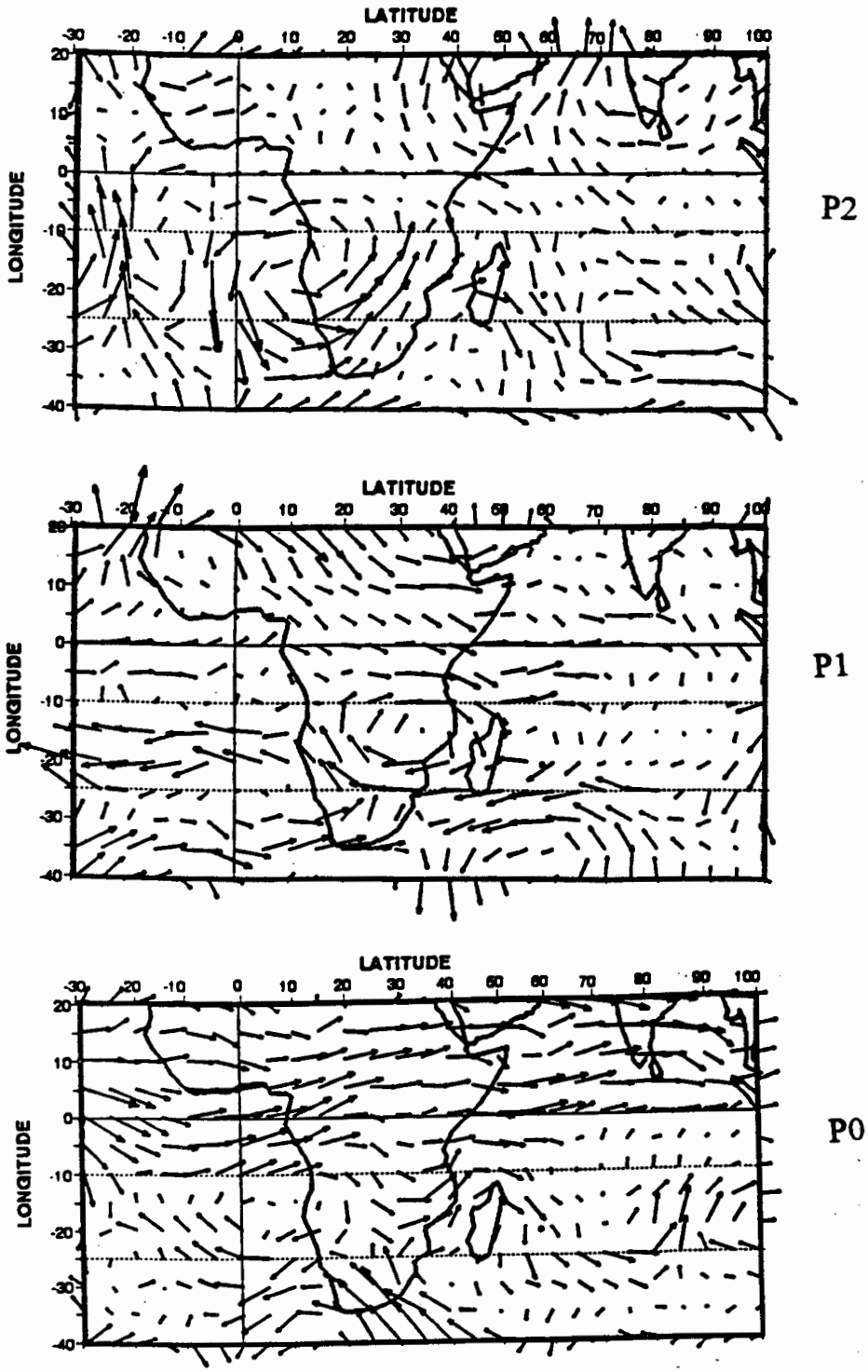

Figure 6.4 (b): Horizontal wind vector anomalies at 200 hPa for Vuli wet spell
⟶ vector is equivalent to 10 m s^{-1}

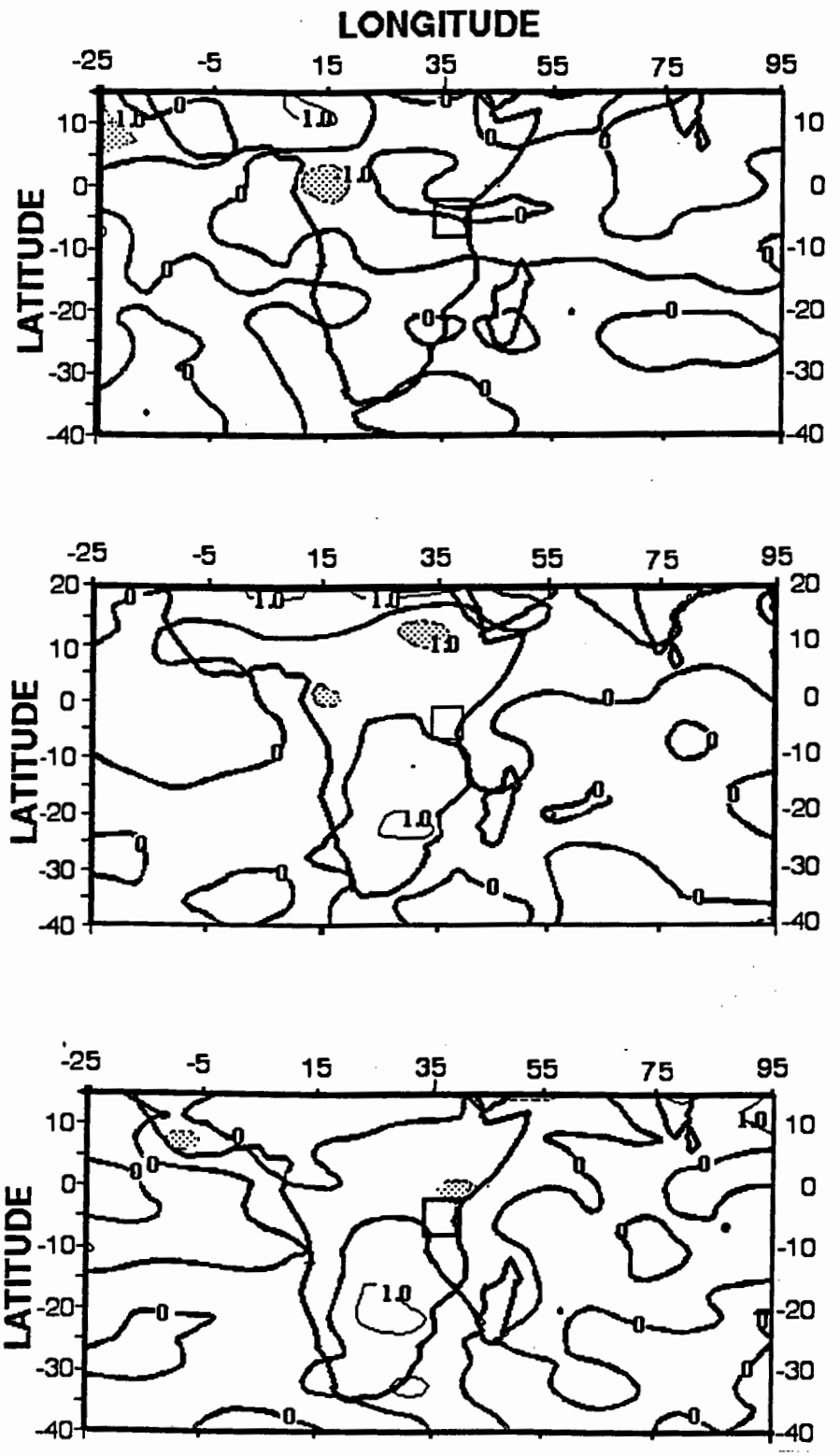

Figure 6.5(a): Divergence field anomalies at 850 hPa for Vuli wet spell
Contour interval is 1×10^{-5} s^{-1}

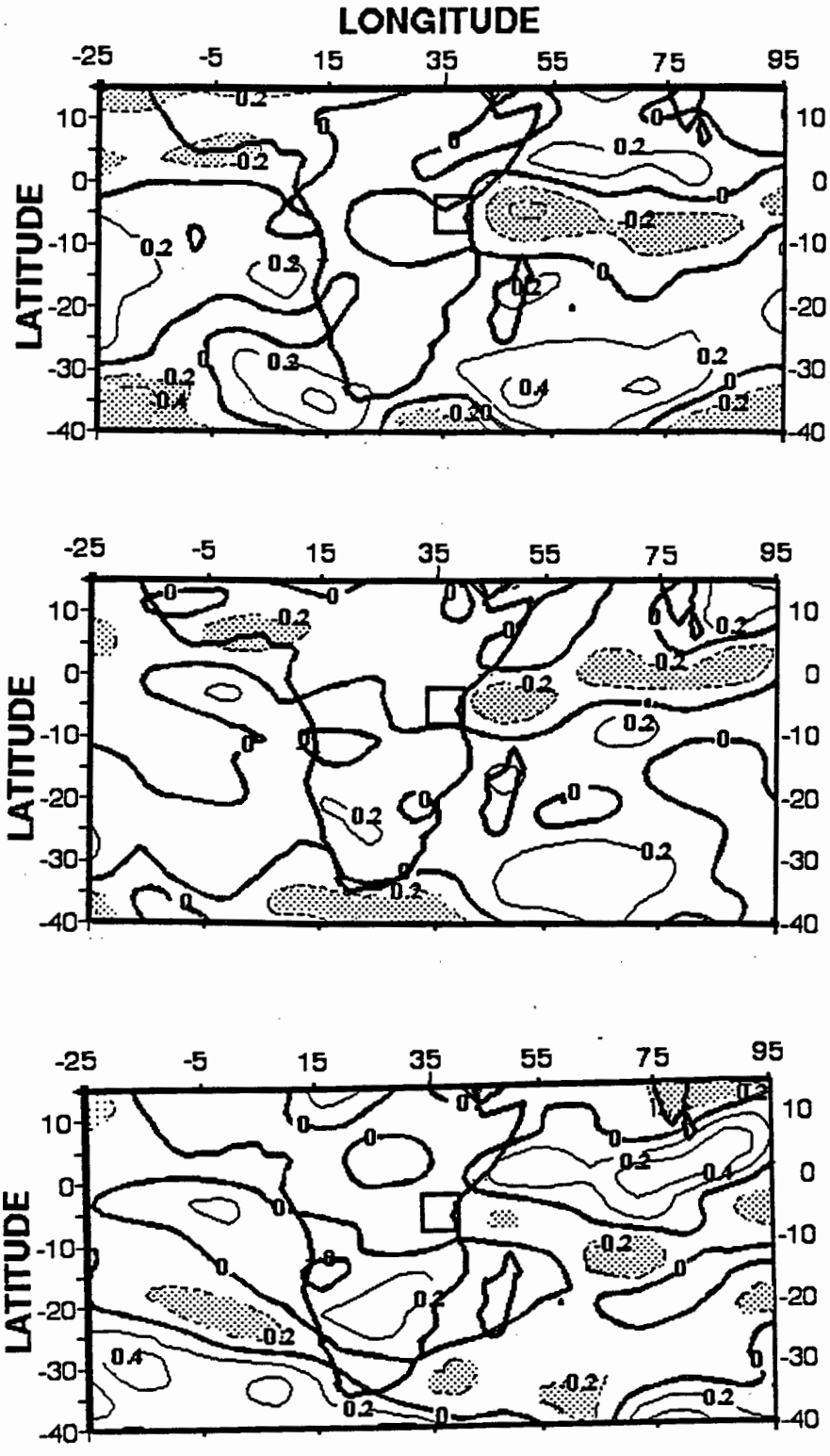

Figure 6.5(b): Vorticity field anomalies at 850 hPa for Vuli wet spell
Contour interval is 0.2×10^{-5} s^{-1}

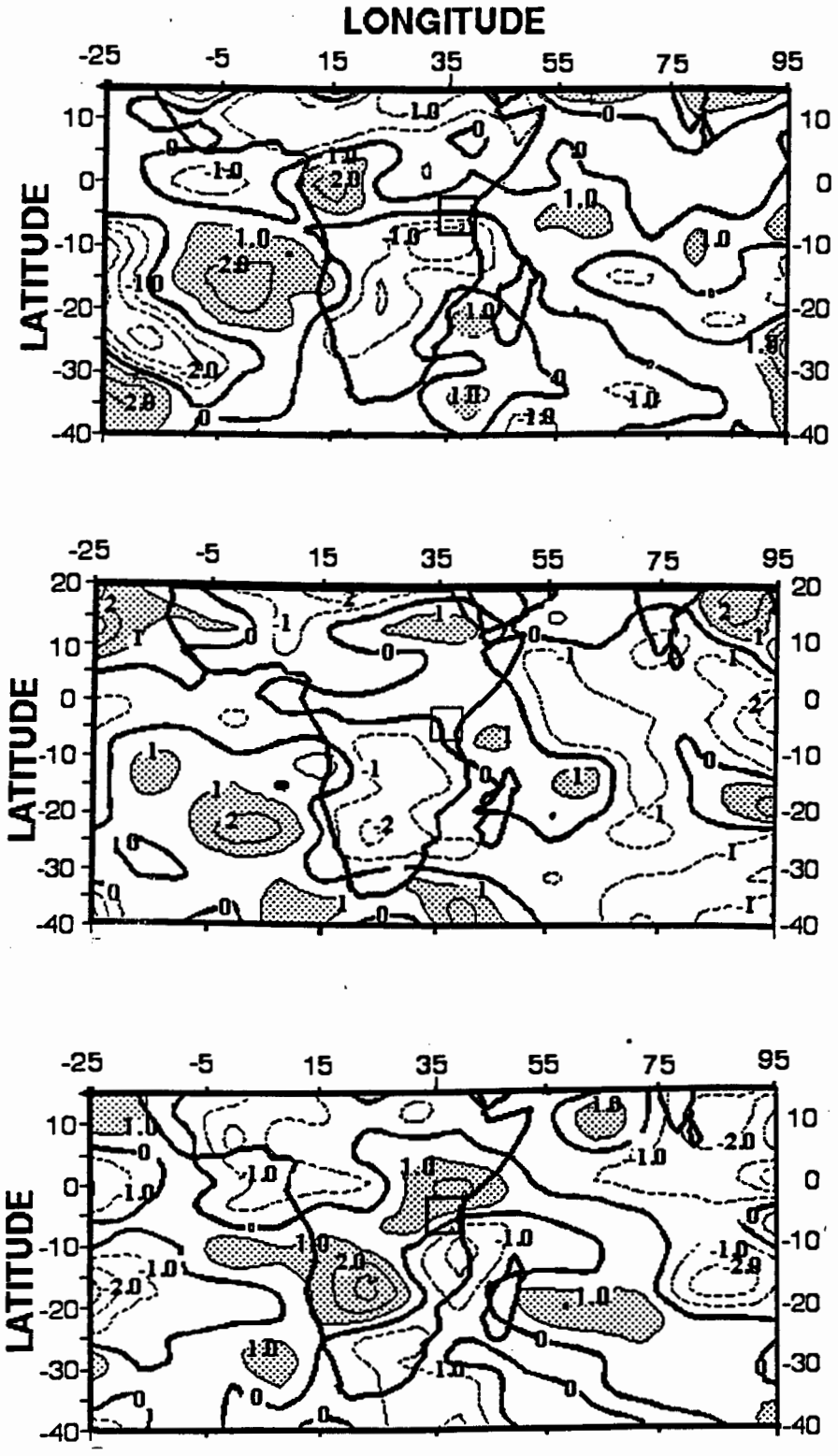

Figure 6.6(a): Divergence field anomalies at 200 hPa for Vuli wet spell
Contour interval is $1 \times 10^{-5}\ s^{-1}$

$\geq 1 \times 10^{-5}\ s^{-1}$

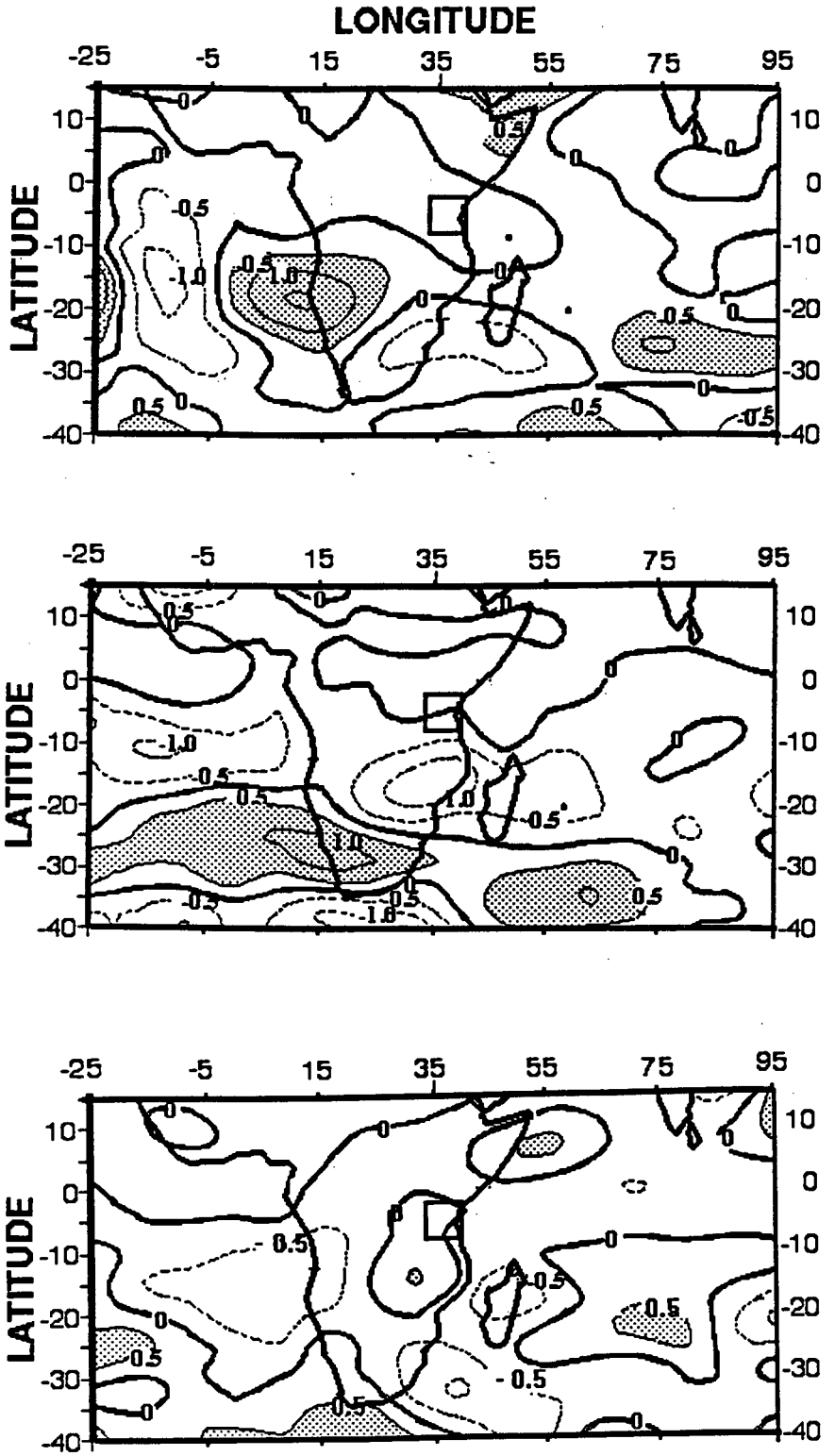

Figure 6.6(b): Vorticity field anomalies at 200 hPa for Vuli wet spell
Contour interval is 0.5×10^{-5} s^{-1}

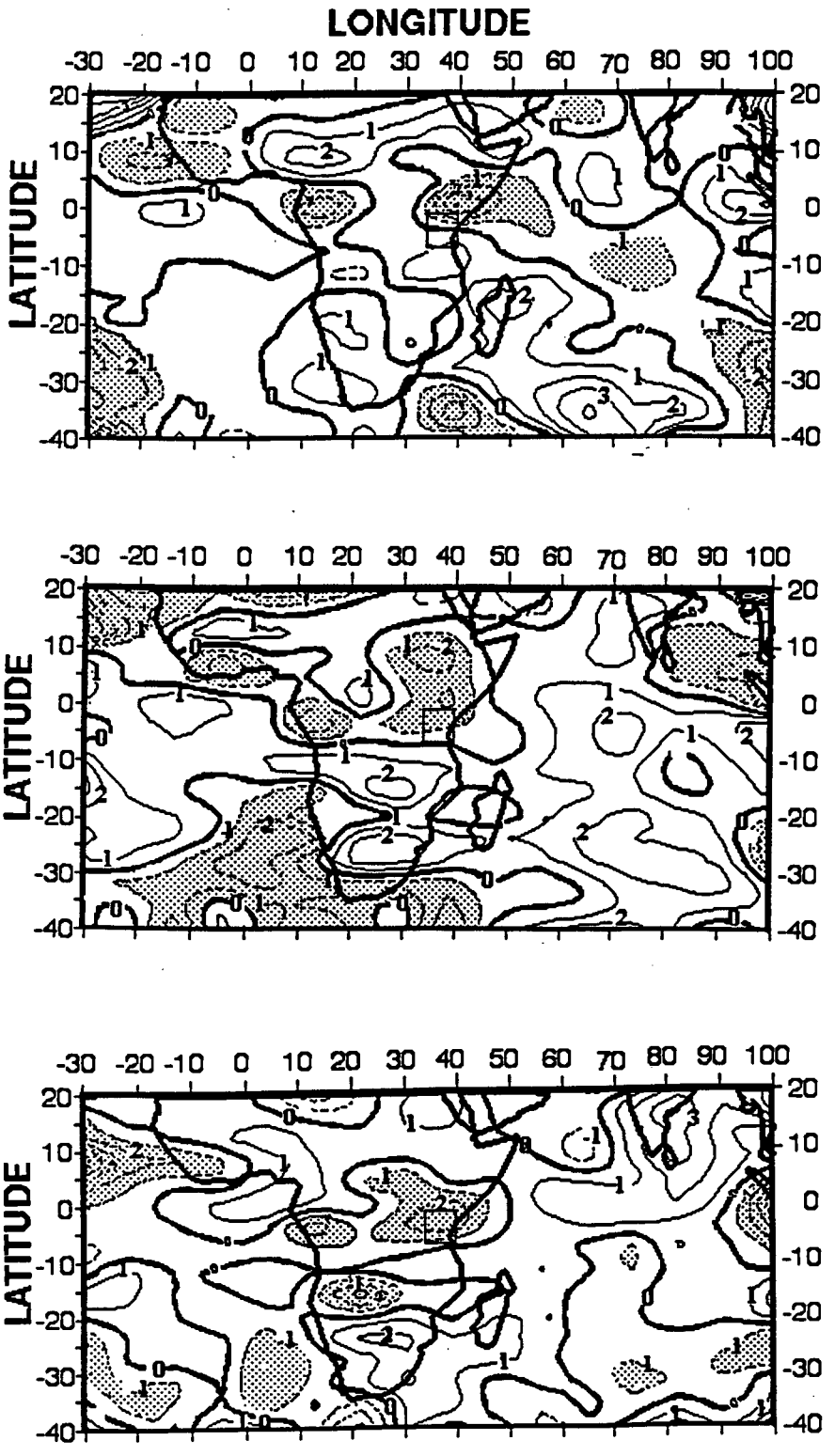

Figure 6.7: 500 hPa Vertical motion anomalies for Vuli wet spell
Contour interval is 2×10^{-4} Pa s^{-1}

$\square \leq 1 \times 10^{-4}$ Pa s^{-1}

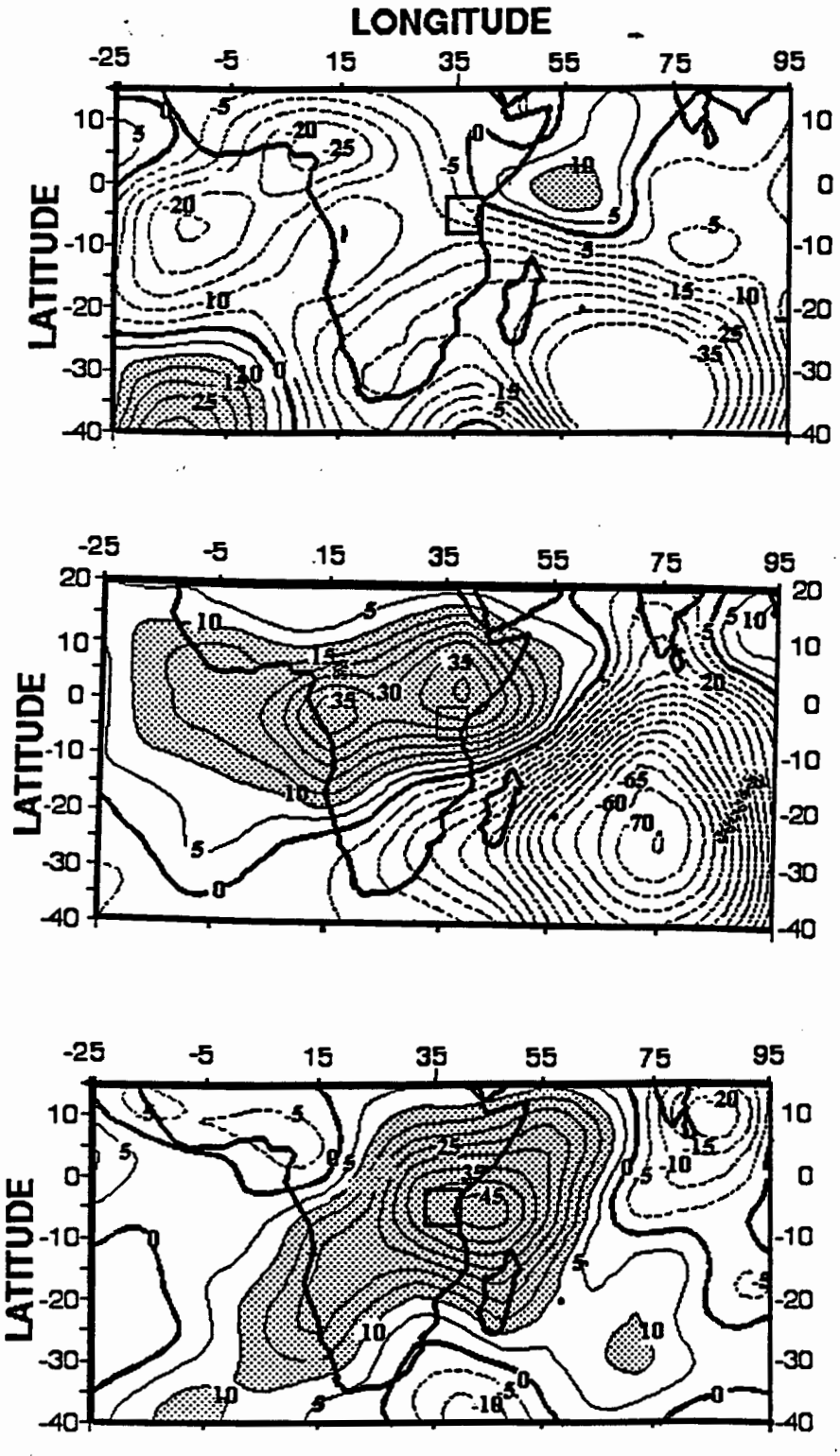

Figure 6.8(a): Velocity potential of WVF anomalies integrated from surface to 500 hPa for Vuli wet spell
Contour interval is 5×10^6 kg s^{-1}

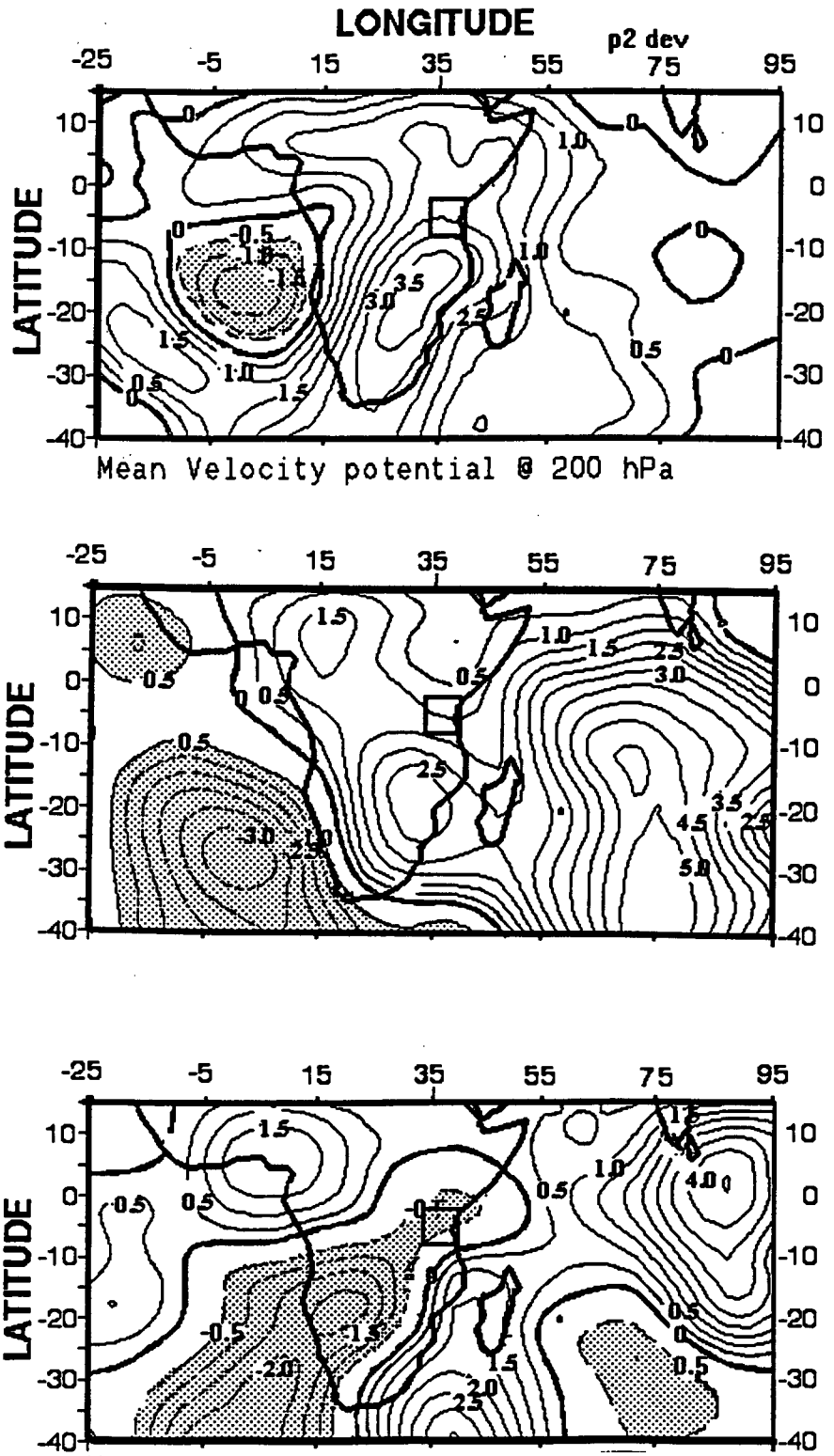

Figure 6.8(b): Velocity potential field anomalies at 200 hPa for Vuli wet spell
Contour interval is 0.5×10^6 m^2 s^{-1}

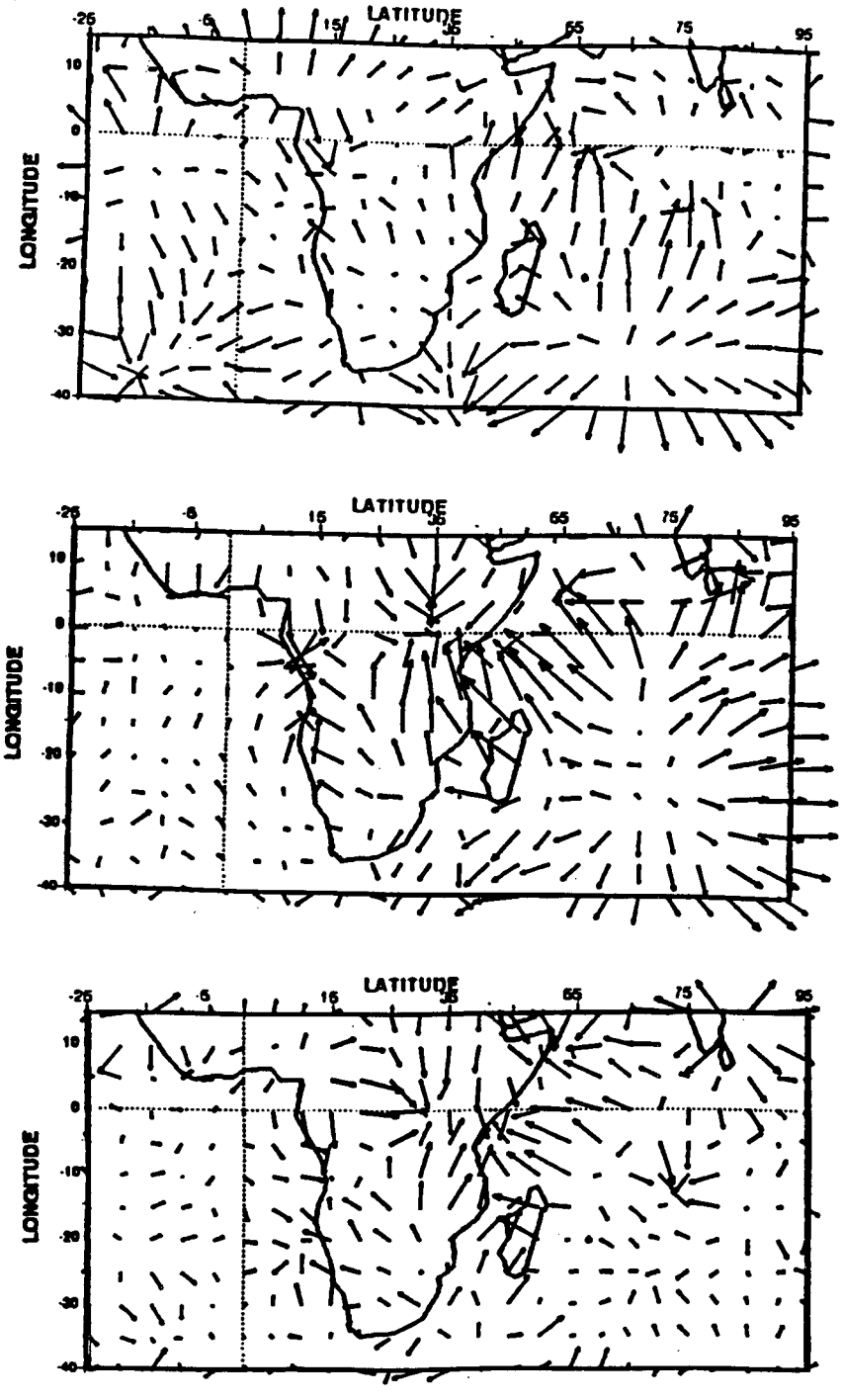

Figure 6.9 (a): Divergent water vapour flux anomalies:
vector is equivalent to 20×10^6 kg m^{-1} s^{-1}

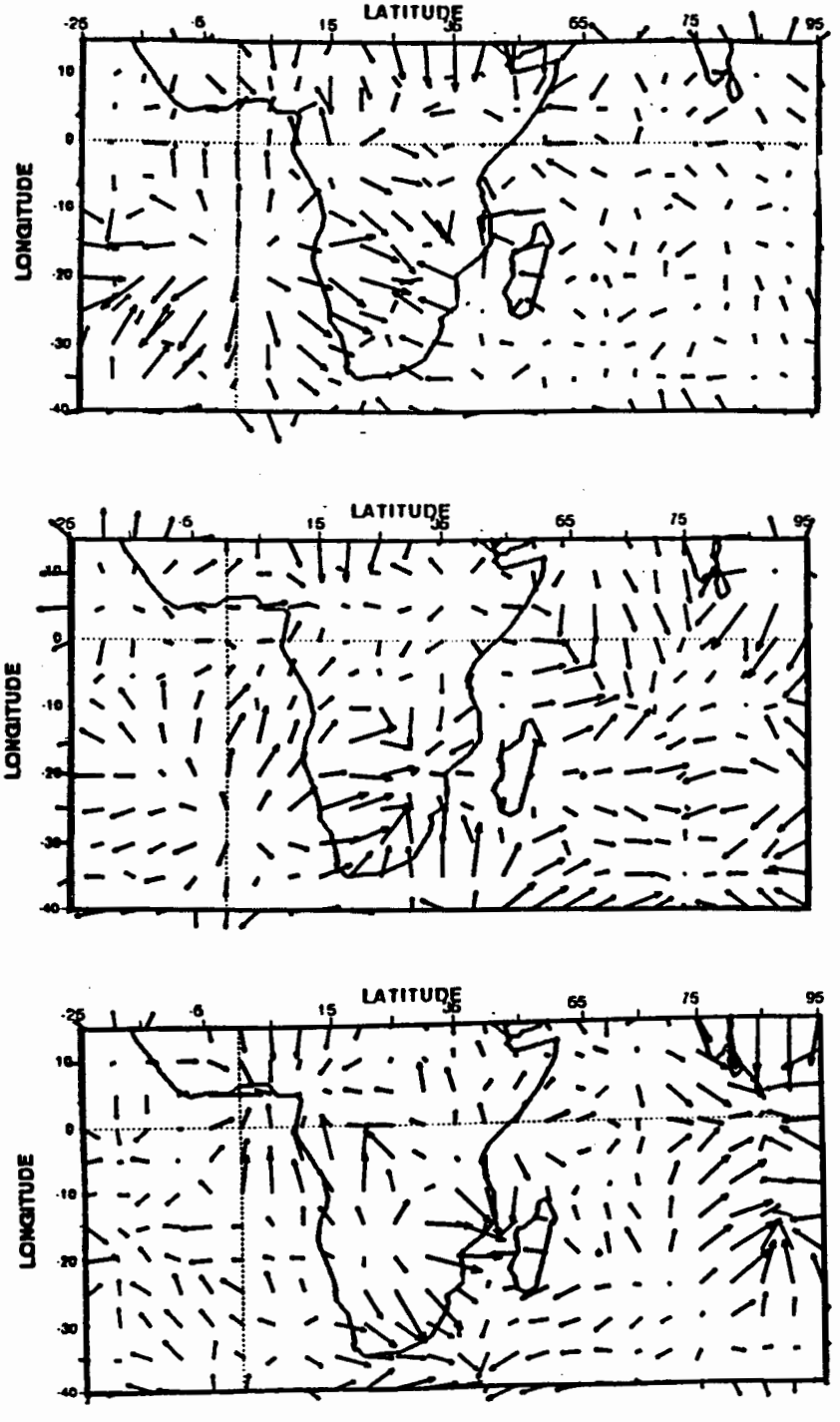

Figure 6.9 (b): Divergent wind anomalies:
vector is equivalent to 2.0 m s $^{-1}$

Chapter 7: Intra-Seasonal Oscillations: Vuli dry spells:

7.1 Introduction

Vuli season in Northern Tanzania is a rainy season characterized by longer alternating dry spells in comparison to Masika season. However, there are times when accumulated rainfall during Vuli season fall below the expected average and sometimes dry spells are longer than expected or even more frequent. Intra-seasonal analysis can be used to understand the above events. In this study the focus is on the 1987 drought over northern Tanzania. ECMWF meteorological parameters are analyzed to understand the course of drought and determine the corresponding parameters for predictive purposes.

7.2 Methodology:

Pentad area-averaged rainfall (Figure 2.3b) was inspected and the 1987 season was found to be the driest of all 6 years with overlapping ECMWF data. Seven of the driest pentads were selected to form pentad composites for analysis of the surrounding weather patterns using ECMWF data in the period 1986-1991. Pentad anomalies were computed as before in respect of the OND mean for all years. Hence, the composites are based on 7 pentads (35 days) minus the seasonal mean; (90 days x 6 yr. or 540 days). The 7 extended dry pentads for 1987 are pentads 5, 6, 10, 11, 13, 15 and 16 (see figure 2.3b). Results are contrasted with the wet spell anomalies of chapter 6.

7. 3 Results of ECMWF pentad analysis

7.3.1 Geopotential Height:

Geopotential heights at 850 hPa are presented in figure 7.1, the areas usually occupied by quasi-stationary anticyclones in the southern hemisphere reveal negative geopotential anomalies. The St. Helena high in the South Atlantic experiences a value 15 gpm below the mean, while the Mascarene anticyclone is 5 gpm below normal. Positive anomalies prevail in the northern hemisphere and extend to central Africa and Angola. The 200 hPa analysis (figure 7.2) shows a strong anticyclone in the Mozambique Channel, with a central value of 84 gpm greater than the 1986-1991 mean. Equatorial regions reveal weak positive anomalies. The configuration revealed in this analysis leads to drought over northern Tanzania. The subtropical highs are weaker and the upper trough over Madagascar is suppressed.

7.3.2 Precipitable Water:

The Sahel region is dry with a central value of 6 mm below the mean (figure 7.3). This extends eastward to cover northern Tanzania. Another area of dry atmosphere relative to the mean is the southwest Atlantic which extends into the Indian Ocean south of 40° latitude. Most of equatorial and southern Africa are relatively moist with a maximum value in the Mozambique Channel extending slightly westward inland.

7.3.3 Water vapor flux and Horizontal wind at 200 hPa:

Figures 7.4 and 7.5 represent vector anomalies of water vapor flux and horizontal wind at 200 hPa. Strong northeasterly flow emanating from the Arabian Sea diverges on reaching the equator while in the south, an anticyclone exists in the Mozambique Channel. In the western Atlantic Ocean an anticyclonic anomaly is revealed. The 200 hPa wind vectors shows a cyclonic gyre that overlies the whole of tropical Africa with a feeding of westerlies across the Sahara desert.

7.3.4 Divergence and Vorticity: 850 and 200 hPa

Figure 7.6 displays the low level divergence anomaly fields for the composite Vuli dry spell, whilst figure 7.8 depicts the vorticity. Low-level divergence is noted over the East African coast and hinterland, while further inland a weak convergence is evident. Strong divergence occurs over equatorial west Africa. The vorticity field reveals areas of anticyclonic vorticity in the equatorial western Indian Ocean and Eastern Atlantic Ocean. A low level cyclonic vorticity anomaly (-0.8×10^{-6} s^{-1}) is located in the southwest Atlantic Ocean. Important features are the divergence cell over Gabon and a +/- pair over the western Indian Ocean which is in response to equatorial westerly anomalies

Upper-level convergence, is noted over the study area (northern Tanzania) and extends zonaly into the Indian Ocean as illustrated in figure 7.7 The west African interior obtains convergence (-4×10^{-6} s^{-1}), whilst the eastern Atlantic

Ocean shows widespread upper level divergence. Upper level vorticity fields in figure 7.9 are dominated by an anticyclone cell extending from the south east Atlantic Ocean to the south west Indian Ocean.

The divergence anomaly fields for lower and upper levels reveal coupling between upper level convergence and lower level divergence over East Africa which act to suppress convection. The vorticity analysis illustrate a lower (upper) anticyclonic (cyclonic) pattern in the Vuli dry spell.

7.3.5 Vertical motion anomalies at 500 hPa

Vertical motion anomalies are illustrated in figure 7.10 where positive values represent sinking motion and negative values represent ascent. The study area (northern Tanzania) obtains the expected sinking motion that extends northward to the Sudan. Strong sinking motion is also revealed over Equatorial West Africa, Central Africa and Madagascar. South Africa and East Atlantic Ocean depict ascending motion anomalies during Vuli dry spells. The western equatorial Indian Ocean show weak sinking motion, however, ascending motions are prevalent over the Indian sub-continent. It can be noted from this and the previous sub-section that widespread upper level convergence and mid-tropospheric sinking motion overlap over East Africa and the Congo basin. However, enhanced low-level divergence is of a more localized nature.

7.3.6 Velocity Potential anomalies; (Divergent WVF and 200 hPa Velocity potential):

The importance of using divergent WVF in this thesis has been highlighted in chapter 6. In figure 7.11 large scale divergent anomalies for WVF cover the western Indian Ocean and extend westward to join another intense cell over the west African coast and interior. The central east Atlantic Ocean and southeastern Africa reveal a weak low level convergence with NW-SE orientation. However a deep convergent center (55×10^9 kg s^{-1}) is indicated in the southwest Indian Ocean at 85° E, 25° S. At 200 hPa figure 7.12, an important feature is the upper level circulation convergence over central Africa and a strong divergence (-5.0×10^7 m^2 s^{-1}) in the east Indian Ocean (87° E, 15° S). A low level convergent cell in the Atlantic Ocean and southeastern Africa is supported by a weak divergence anomaly aloft, though displaced southwestward. From these velocity potential field analysis, it is shown that during prolonged drought in northern Tanzania enhanced low-level convergence shifts to Southern Africa. The low level convergence anomaly over the Indian Ocean is enhanced by upper level divergent velocity potential, with a SW-NE alignment with height.

7.3.7 Divergent WVF / Horizontal wind at 200 hPa:

Figure 7.13 shows the vectors of vertically integrated divergent water vapor flux (WVF) anomalies from the surface to 500 hPa. The most impressive

features are the line of convergence along 80°E, south of equator and divergence off the Somali coast that extends along the equator towards the eastern Indian Ocean. A divergent flow penetrates inland from on the western Indian Ocean. It proceed to converge along 32°E with westerlies south of equator.

Figure 7.14 illustrate the divergent winds at 200 hPa. Wind vectors are depicted in the opposite sense to that of divergent WVF though with a slight easterly displaced. Upper-level convergence exists over Tanzania which enhance local low-level divergence over northern Tanzania.

7.4 Discussion and summary

In this study, the year 1987 was found to be a relatively drier year. A number of features that led to the dryness have been observed, the following of which are most conspicuous at the intra-seasonal scale:

- Water vapor flux anomalies indicate low-level moisture divergence over northern Tanzania coupled with upper-level incursion of dry (low PW) Saharan air which is depicted by 200 hPa horizontal wind patterns. Having dryer air aloft results into any moisture available to evaporate and hinder deep cloud formation even in the presence of low-level uplifting.

- It is apparent though, from the vertical motion anomalies that subsidence exists over the study area. This is supported by upper-level cyclonic anomalies revealed on 200 hPa wind and vorticity.
- Geopotential heights in the lower levels rise in the vicinity of the study area and block moisture advection. This is revealed by precipitable water anomaly patterns which show an area of moisture deficit that extends from the Azores to Northern Tanzania.

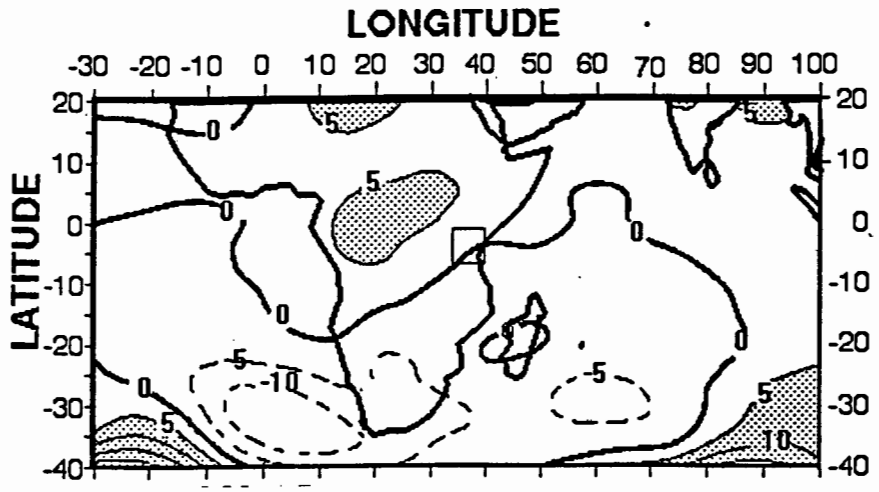

Figure 7.1: Geopotential height anomalies at 850 hPa for Vuli dry spells
Contour intervals are 5 gpm.

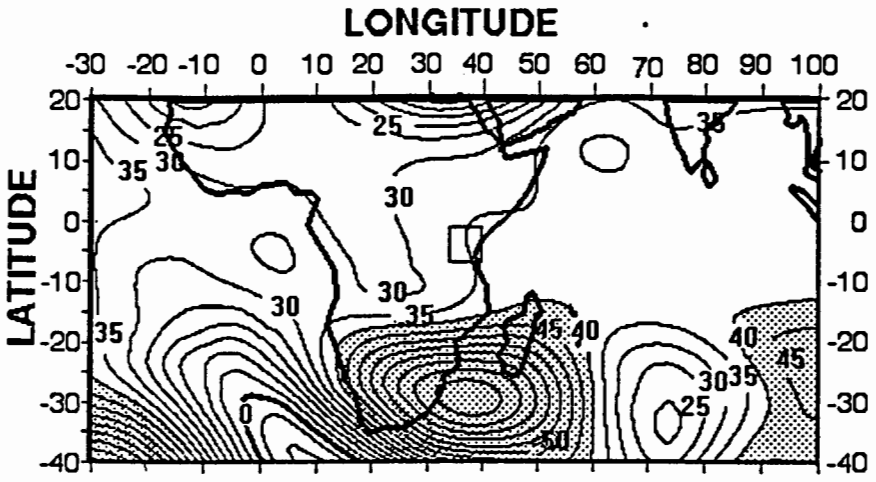

Figure 7.2: Geopotential height anomalies at 200 hPa for Vuli dry spells
Contour intervals are 5 gpm.

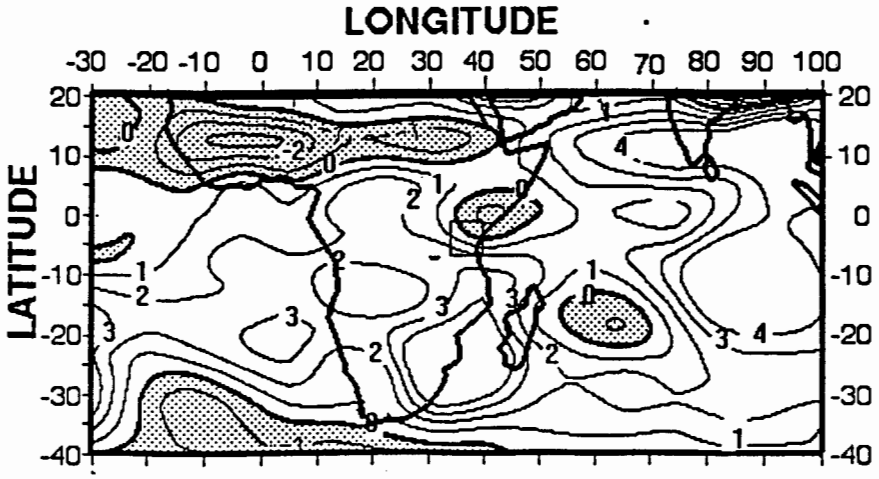

Figure 7.3: Precipitable water anomalies between surface and 300 hPa for Vuli dry spells
Contour intervals are 1 gpm.

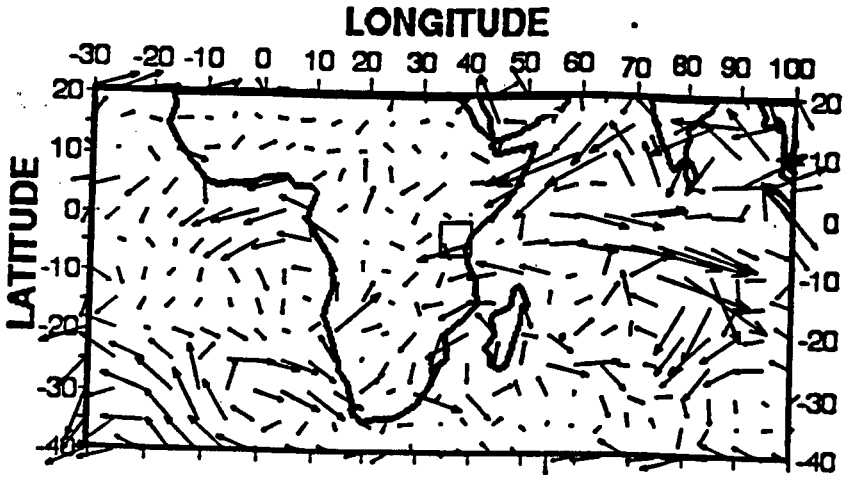

Figure 7.4: Vertically integrated water vapour flux anomalies for Vuli dry spells
⟶ vector is equivalent to 50 kg m^{-1} s^{-1}

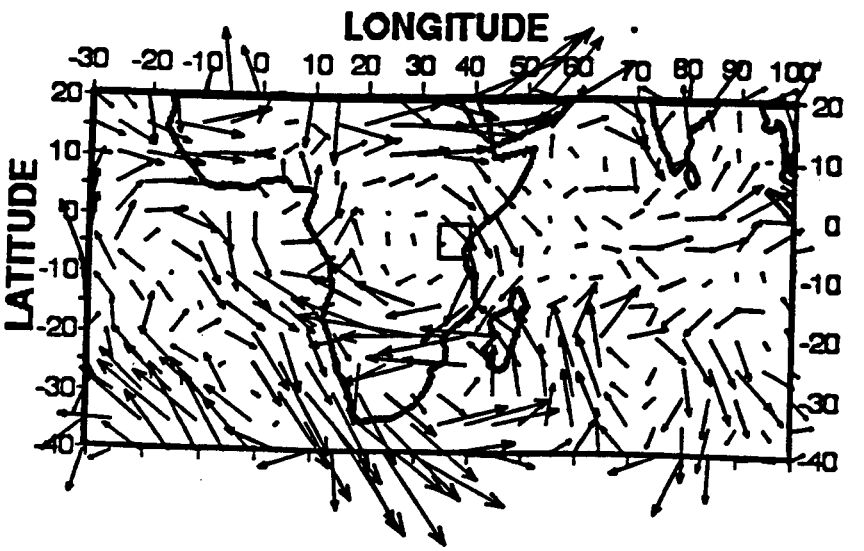

Figure 7.5: Horizontal wind vector anomalies at 200 hPa for Vuli dry spells
⟶ vector is equivalent to 5 m s^{-1}

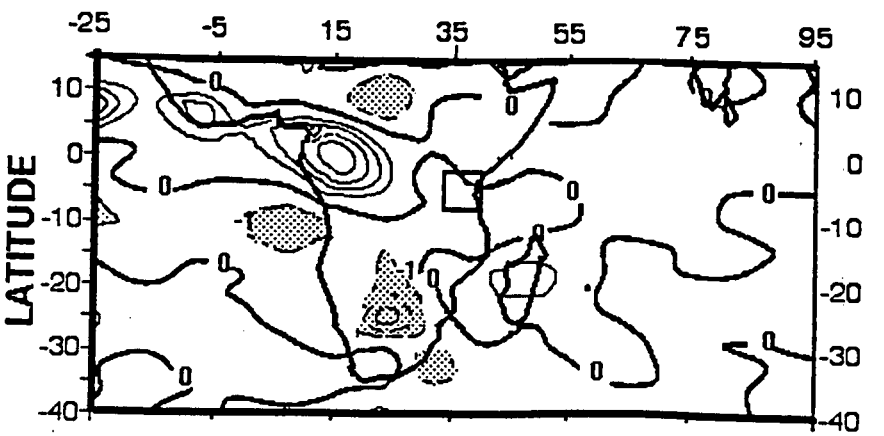

Figure 7.6: Divergence field anomalies at 850 hPa for Vuli dry spells
Contour interval is 1×10^{-5} s^{-1}

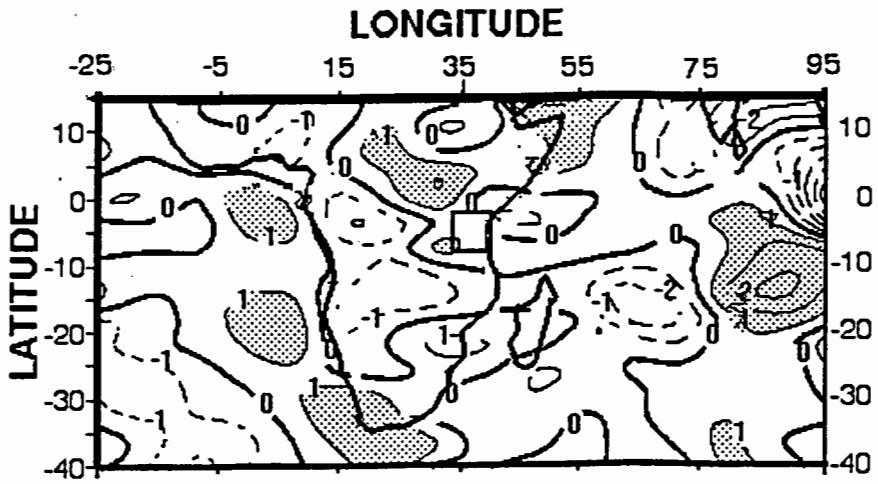

Figure 7.7: Divergence field anomalies at 200 hPa for Vuli dry spells
Contour interval is 1×10^{-5} s^{-1}

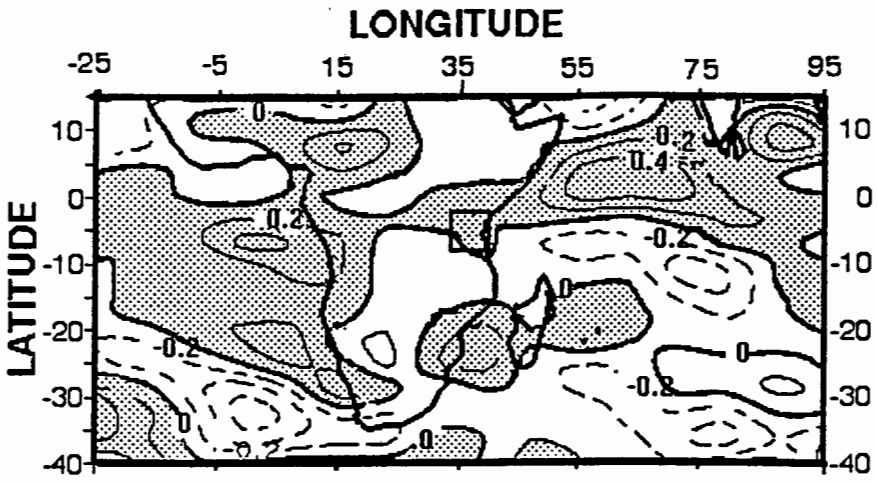

Figure 7.8: Vorticity field anomalies at 850 hPa for Vuli dry spells
Contour interval is 0.2×10^{-5} s^{-1}

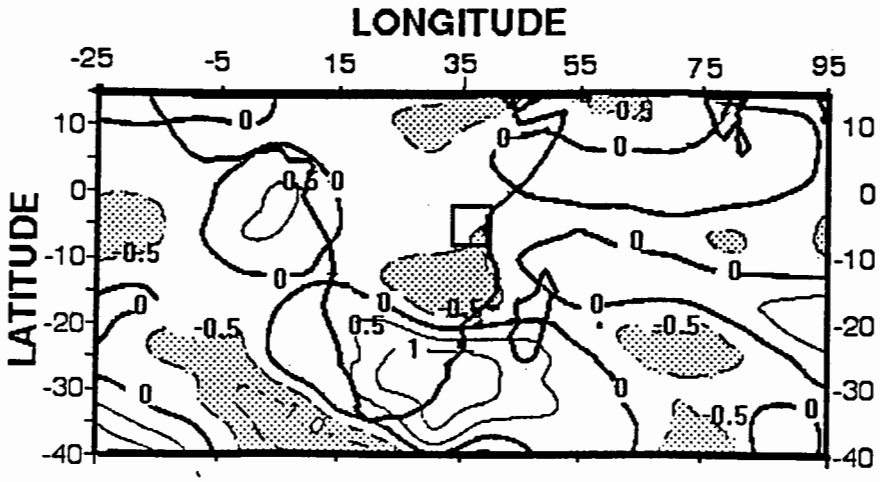

Figure 7.9: Vorticity field anomalies at 200 hPa for Vuli dry spells
Contour interval is 0.5×10^{-5} s^{-1}

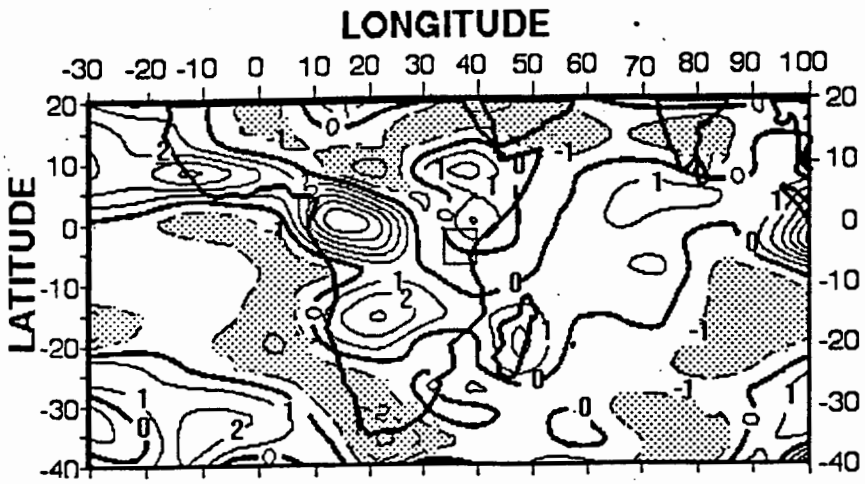

Figure 7.10: 500 hPa Vertical motion anomalies for Vuli dry spells
Contour interval is 1×10^{-4} Pa s^{-1}

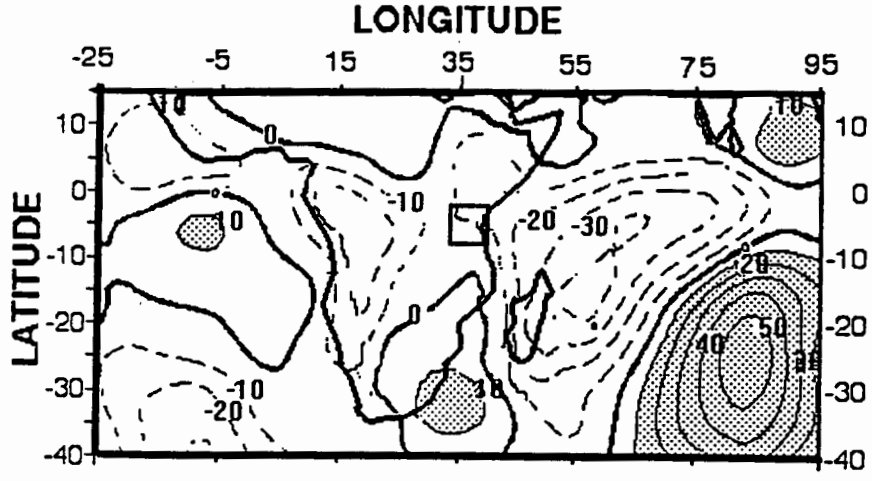

Figure 7.11: Velocity potential of WVF anomalies for Vuli dry spells integrated from surface to 500 hPa
Contour interval is 5×10^{6} kg s^{-1}

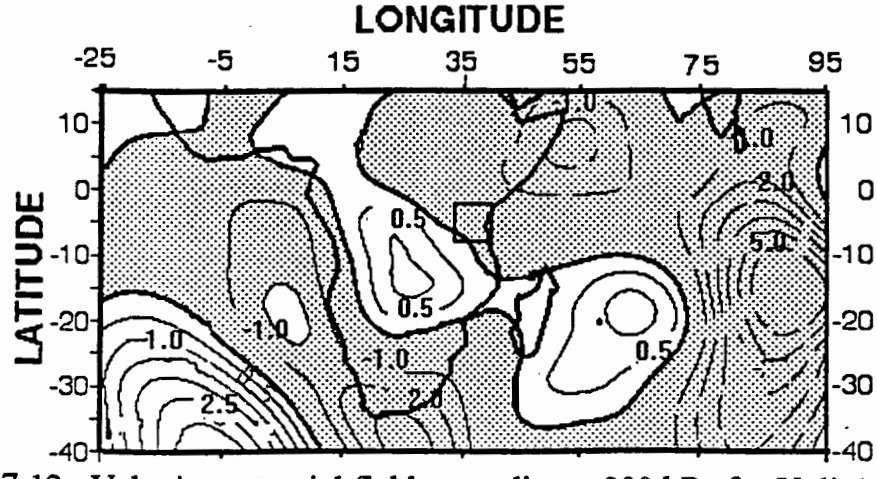

Figure 7.12: Velocity potential field anomalies at 200 hPa for Vuli dry spells
Contour interval is 0.5×10^{6} m^2 s^{-1}

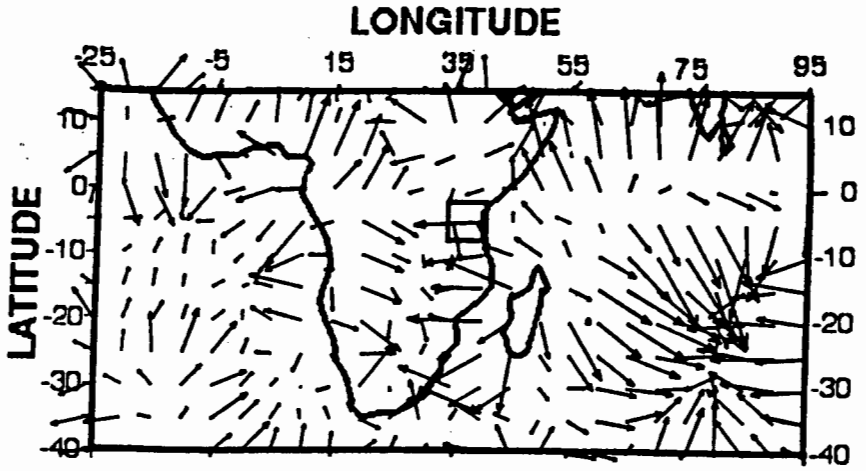

Figure 7.13: Divergent water vapour flux anomalies for Vuli dry spells
⟶ vector is equivalent to 15×10^6 kg m^{-1} s^{-1}

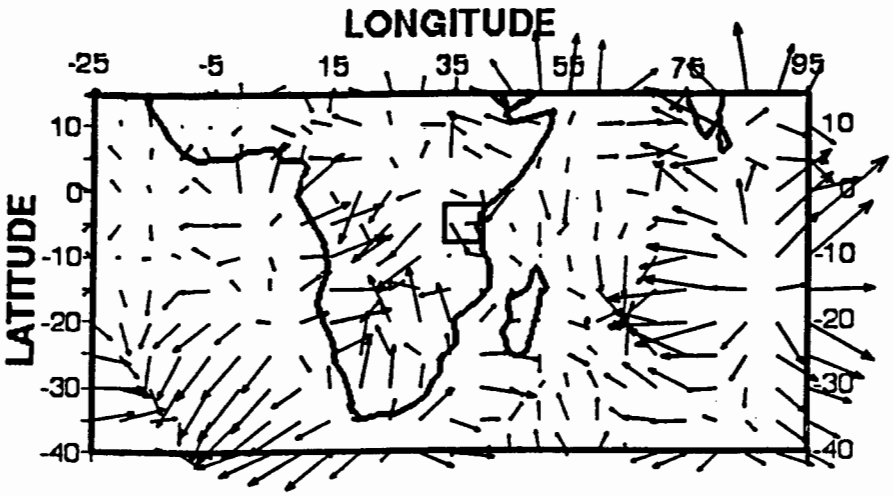

Figure 7.14: Divergent wind anomalies for Vuli dry spells
⟶ vector is equivalent to 2.0 m s^{-1}

Chapter 8: Daily analysis of an extreme flood case (Dec 31 1989)

Introduction:

The extreme flood over the city of Dar es Salaam, Tanzania that occurred on 31 December 1989 is the basis for a case study presented in this chapter. The study was provoked by the incidence of a sudden short-lived storm, coupled with strong winds, which had devastating effects resulting in loss of lives and property.

The chapter aims to analyse the dynamics and development of the meteorological patterns that prevailed for a period two days before to one day after the flood. The discussion is based upon ECMWF data and satellite images for the corresponding days.

Daily 12 UT ECMWF data for 29, 30, and 31 December 1989 and 1 January 1990 are analysed in the domain 10° N-20° S, 20-60° E. The relevant observed and derived parameters are displayed in figures 8.1 to figure 8.10.

Satellite images (fig. 8.11-8.14) show that the precursor of the flood event which developed on 31 December 1989, was a persistent cyclone in the Indian Ocean and a cloud band that covered most of Equatorial Africa. Tropical storms forming over southwestern Indian Ocean tends to deflect the southeasterlies and northeasterlies towards their position, thus reducing moisture influx and hence precipitation significantly over land. These characterlistics are evident when storms are far from the coast. When they are closer to the coast they tend to enhance precipitation due to advection of masses over land (Nyenzi, 1988). The tropical

cyclone ALIBERA was reported to dwell in the western Indian Ocean from 16 December 1989 to 7 January 1990 (Saison Cyclonique, 1990). On 31 December 1989 she was reported at 51°E, 18°S.

8.1 Daily ECMWF data analysis:

8.1.1 Geopotential Height:

Geopotential heights at 850 hPa on 29 December in figure 8.1, reveal a low pressure centre with a minimum below 1480 gpm northeast of Madagascar; the position of tropical cyclone ALIBERA.

By 30 December, an indication of pressure falling toward Dar es Salaam was evident from the south. On 31 December, ALIBERA progressed westward in full contact with northern Madagascar resulting in the merging of low pressure areas over Dar es Salaam in sympathy.

As ALIBERA progressed southward on 01 January 1990, pressures rose over Dar es Salaam and elsewhere except in the southwest (25°E, 15°S).

- There is a certain spot where a tropical cyclone should be positioned in the Indian Ocean so that a "feeder band" to north west, will have effect on the weather over Dar es Salaam.

Figure 8.2 presents geopotential height at 200 hPa, higher pressures are shown to increase toward Dar es Salaam from the southwest by 29 December. However,

eastward progression and pressure erosion with time are evident. These lead to higher pressures remaining over central Madagascar on 01 January, in conformity with the position of the cyclone revealed in figure 8.1.

8.1.2 Precipitable water (PW):

From what has been discussed in the previous chapters, the month of December is expected to obtain a high PW since it is part of the Vuli rainy season. In this case study, figure 8.3 shows three distinctive areas of high PW throughout the flood. The maximum occurs 25°E, 15°S, and other areas reveal moisture increase with time at its expense.

8.1.3 Vertical Motion at 500 hPa:

Centres of mid-tropospheric vertical motion are shown in figure 8.4. Strong uplift is evident at over 8° N, 35° E which moves southeastward with time. On 30 and 31 December, strong uplifting centre was maintained over Dar es Salaam, while ALIBERA was characterised by strong upward motion over Madagascar. Intense subsidence (positive values) remained in the Mozambique Channel throughout the sequence and showed intensification with time.

On 1 January, a northward shift of negative values was evident over Dar es salaam, as subsidence in the Mozambique Channel pushed northward. North Madagascar and the area around 30°E, 15°S maintained strong uplifting.

8.1.4 Water vapour flux and Horizontal wind at 200 hPa.

Water vapour flux integrated from the surface up to 500 hPa on 29 December in figure 8.5 reveals a moist inflows from northeast and southwest. The southwest flow was enhanced by a local anticyclone that developed along 30°E south of the equator. On 30 and 31 December northeasterlies and southwesterlies intensified and Dar es salaam city became the centre of confluence of these two flows. An additional contribution to the moisture availability over Dar es salaam was lower level outflow from the tropical cyclone which was swept toward Dar es salaam by southerlies in the Mozambique Channel.

- The interaction of the TC with the monsoon and local flows made it possible for moisture to converge over Dar es Salaam.

On 1 January 1990, Dar es salaam was "relieved" of moisture advection by local anticyclonic flow. Monsoon convergence shifted northward to the equator and ALIBERA progressed slightly southward.

Horizontal winds at 200 hPa are illustrated in figure 8.6. On 29 December the anticyclonic flow observed in the lower level is overlain by cyclonic flow with its eastern flank sweeping over Dar es salaam. South-easterly flow remained the dominant feature throughout the evolution. On 1 January 1990, south-easterly flow from the Indian Ocean was joined by anticyclonic flow off the Somali coast. This effectively evacuated mass and made convective overturning efficient. The main link is to the northern Hadley cell.

effectively evacuated mass and made convective overturning efficient. The main link is to the northern hadley cell.

8.1.5 Divergence and Vorticity:

The 850 hPa level divergence and vorticity fields are represented in figures 8.7 and 8.8 respectively. In figure 8.7 the negative values depict convergent areas while the cyclonic vorticity fields are represented by negative values in figure 8.8. The dominant convergent area on 29 December was the area east of Madagascar. On propagating westward with time, it diminished in size due to the frictional effect from land the surface. From 31 December to 01 January, a southerly progression was maintained. Dar es Salaam surrounding areas were under strong convergence only on 30 December. Divergence was notable off the Somali coast. Otherwise weak convergence prevailed.

Maximum cyclonic vorticity is revealed northeast of Madagascar at the position of ALIBERA in figure 8.8. A weaker intensity over the southern coast of Tanzania and over Zambia (25°E, 15°S) persisted and intensified throughout the sequence. An impotant feature is the North-West axis of cyclonic vorticity extending from the tropical cyclone. The upper-level divergence field (figure 8.9) and vorticity field (figure 8.10), illustrate divergence over northwest Madagascar and a northeast-southwest band of divergence extending west of Dar es Salaam on 29 December.

The upper-level patterns are opposed by their lower-level counterparts and suggest vigorous convective overturning.

8.2 Discussion and summary

The main result of this brief study is that rapid development and propagation has been identified. Satellite images identify the position and a of the tropical cyclone and spiral band fed by the northeast Monsoon.

Other important observations to pay attention to are;

- A fall of low-level pressure at the station prior to the flood.
- Excessive low level moisture and moisture advection from high PW centres toward Dar es Salaam prior and during the floods.
- Development of strong upward motion is another key element in determining the intensity of the flood.
- Finally a local cyclonic (WVF) circulation cell concentrated convection over Dar es Salaam.

It is apparent from the above that for the tropical cyclone in the Indian Ocean to produce copious rainfall over Dar es Salaam and the hinterland, a spiral band has to be positioned to its northwest. The fact that the life span of ALIBERA in the Indian Ocean was from 16 December 1989 to 7 January 1990, while its notable effect over Dar es Salaam was recorded on 31 December 1989 illustrates this argument. The analysis of this flood event will help in forecasting similar events.

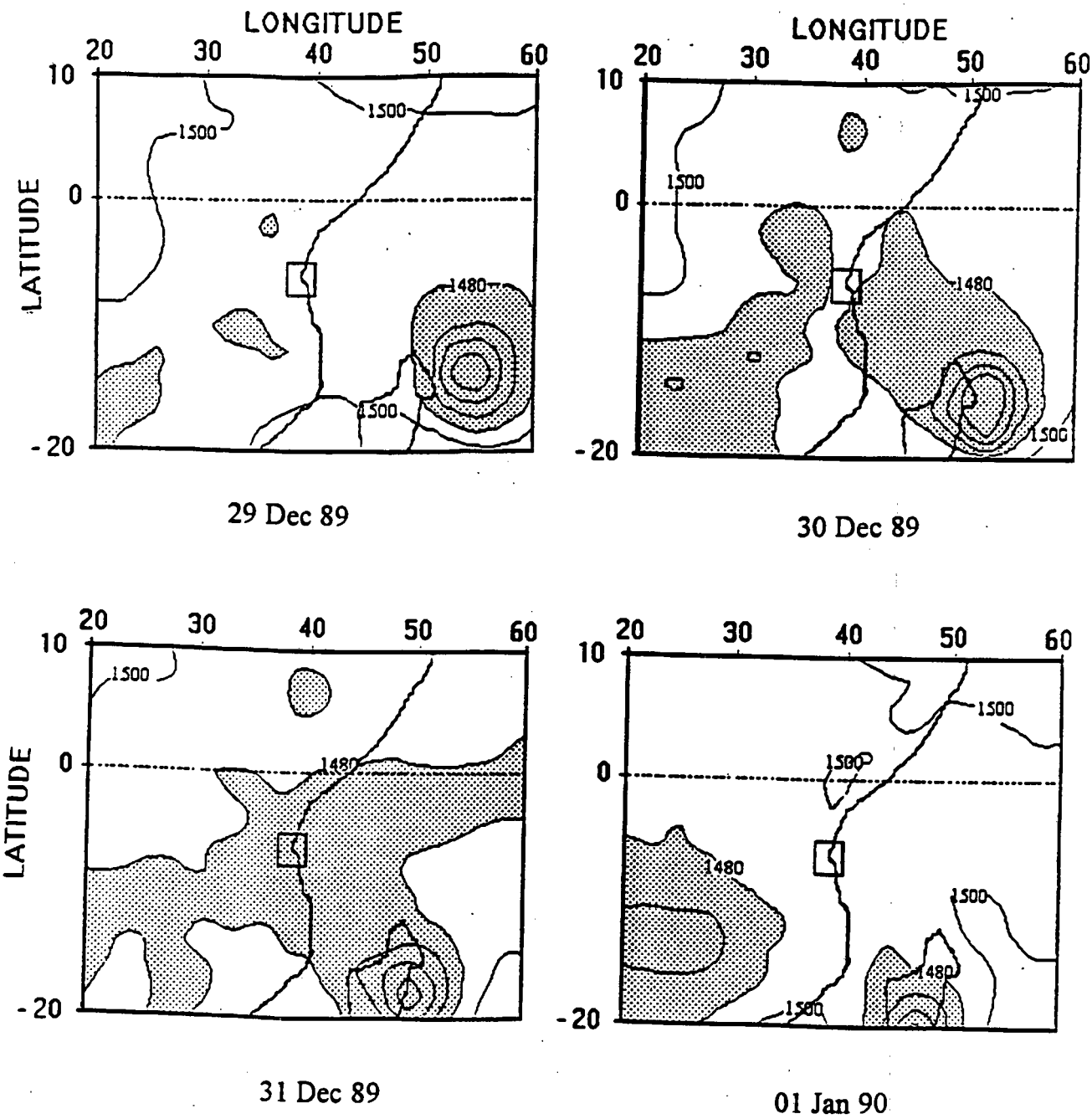

Figure 8.1: Geopotential height at 850 hPa for extreme flood case
Contour intervals are 20 gpm.

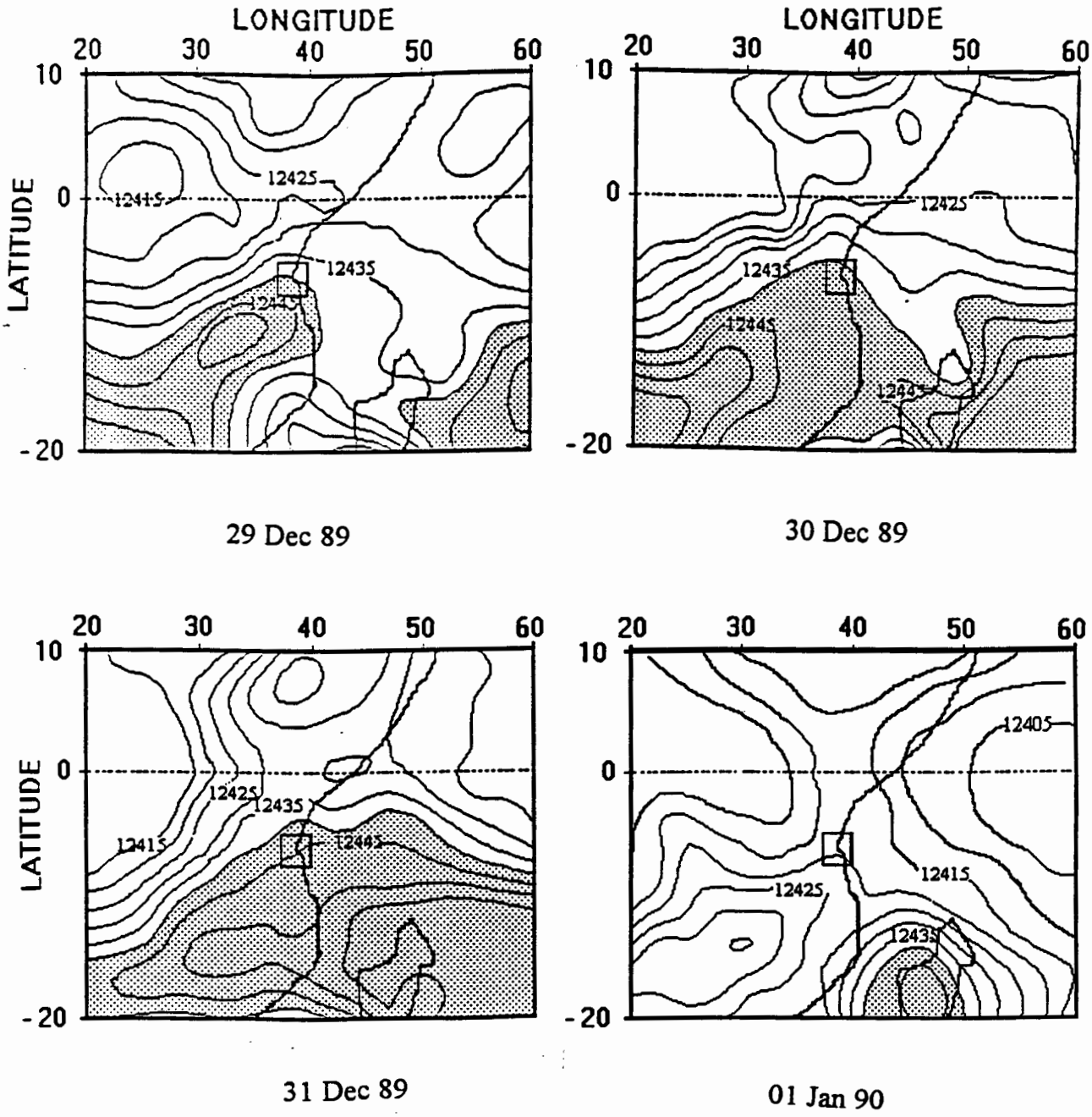

Figure 8.2: Geopotential height at 200 hPa for extreme flood case
Contour intervals are 5 gpm.

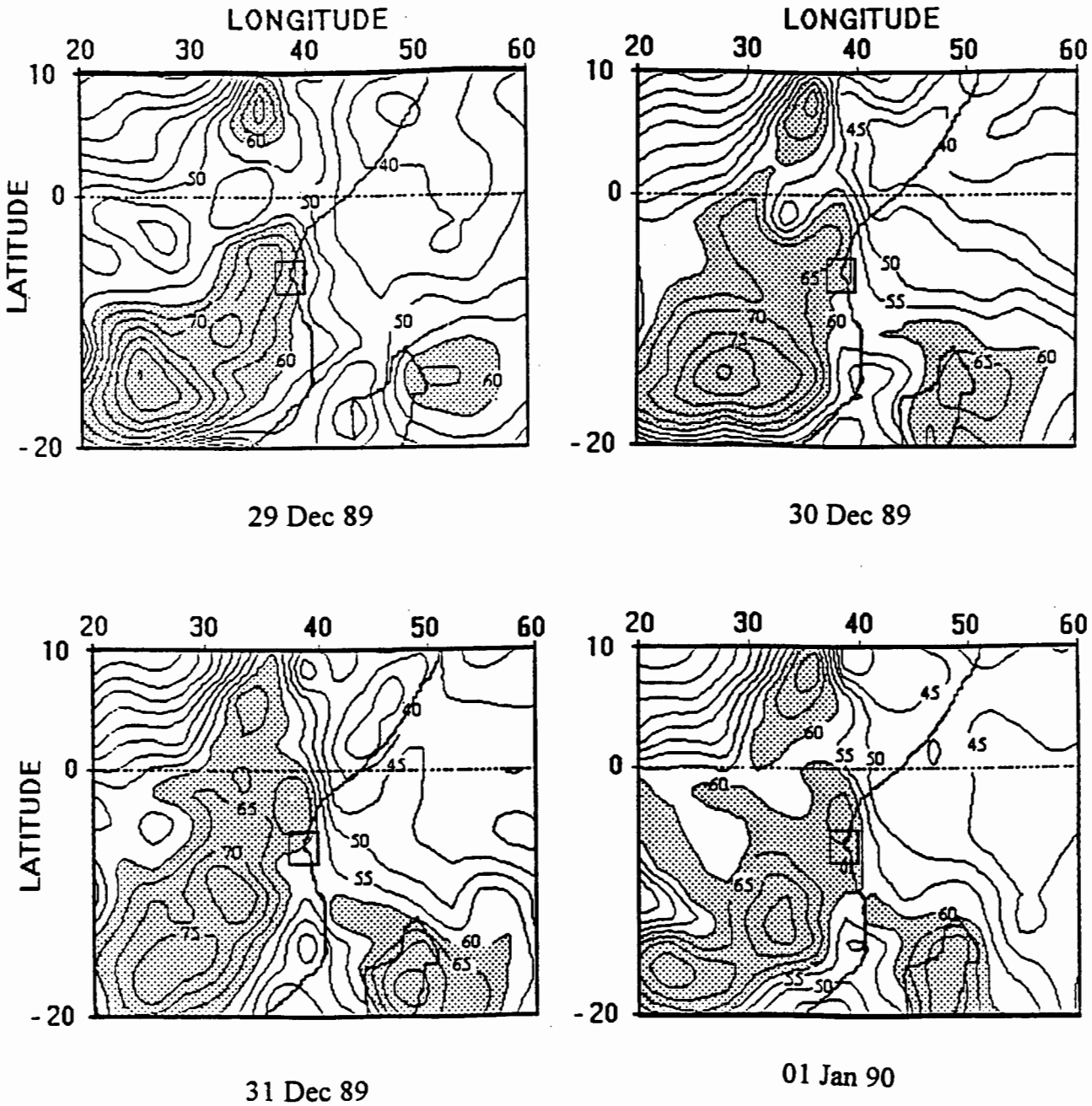

Figure 8.3: Precipitable water between surface and 300 hPa for extreme flood case
Contour intervals are 5 mm.

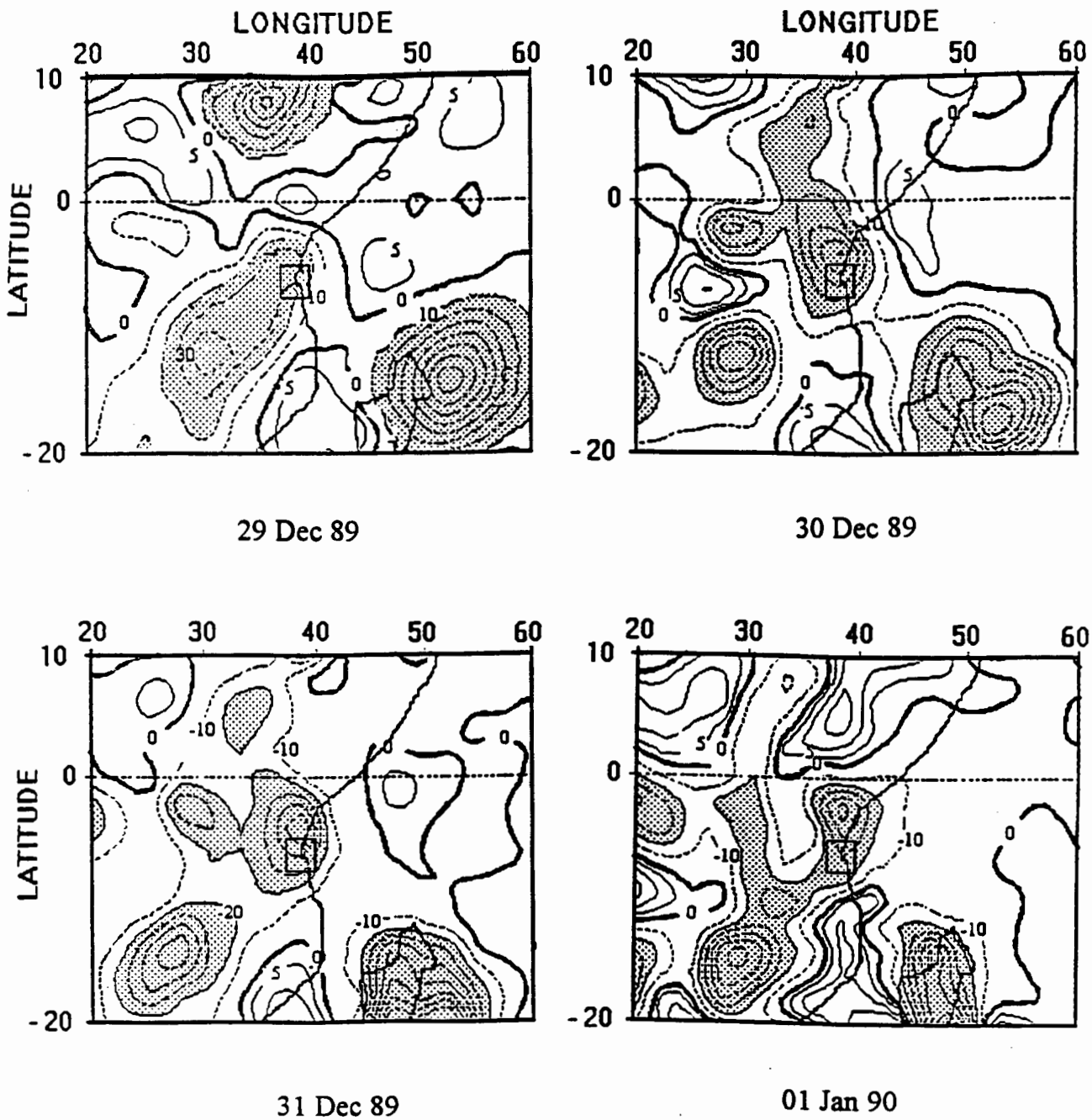

Figure 8.4: Vertical motion at 500 hPa for extreme flood case
positive contour intervals are 5×10^{-4} Pa s^{-1} .
negative contour intervals 10×10^{-4} Pa s^{-1} .

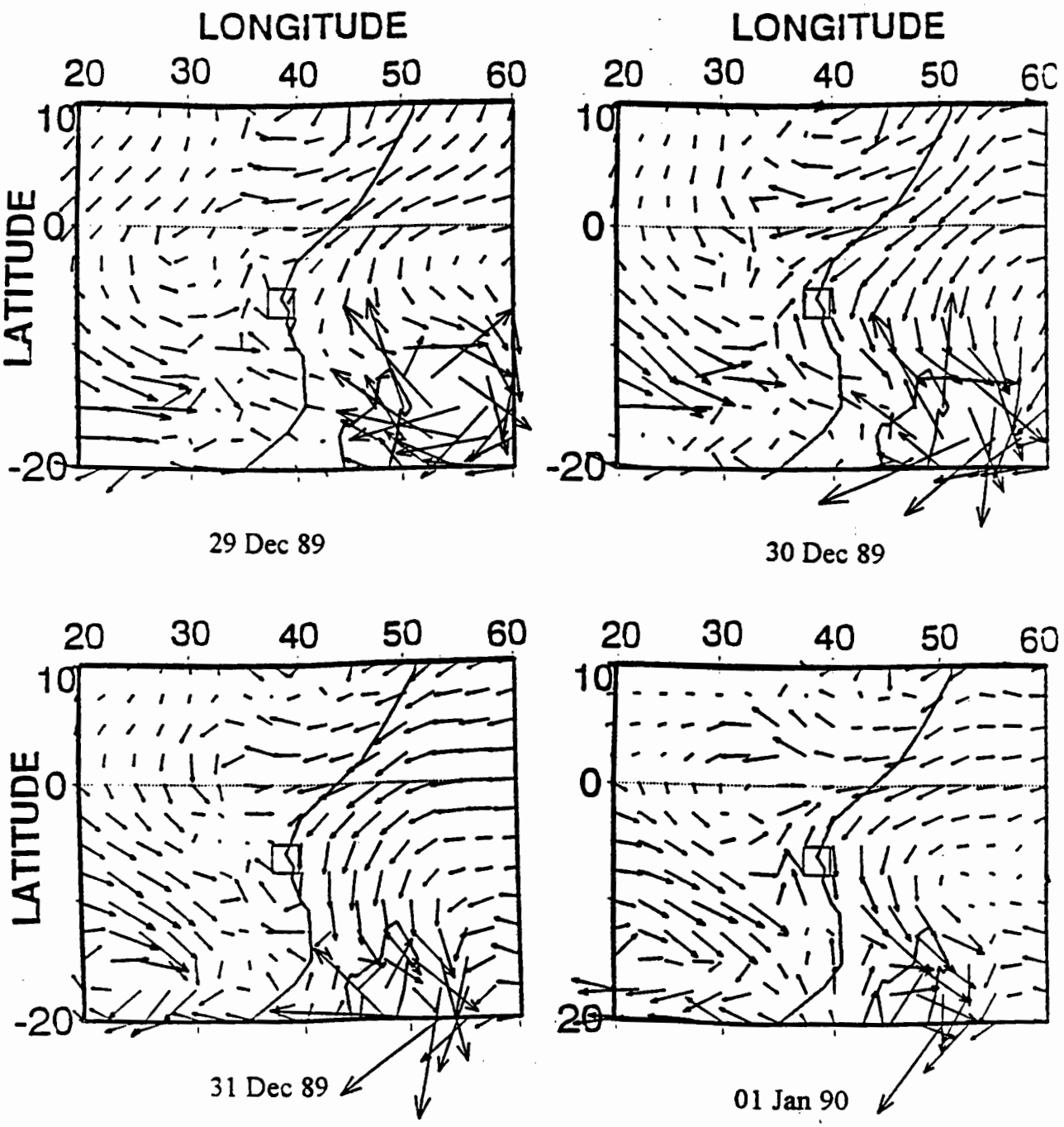

Figure 8.5: Water vapour flux integrated from the surface up to 500 hPa for extreme flood case

— vector is equivalent to 15×10^6 kg m^{-1} s^{-1}

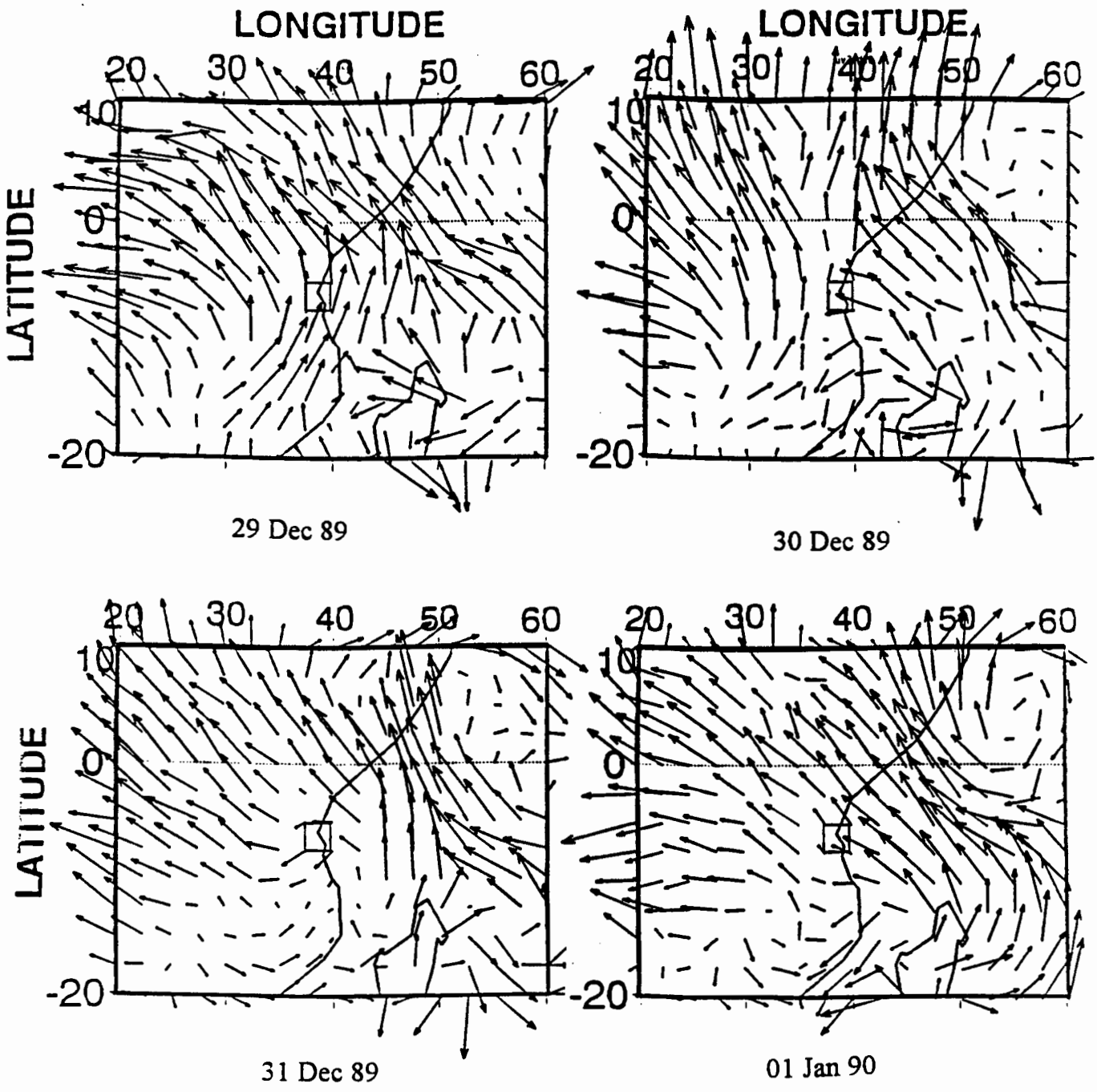

Figure 8.6: Horizontal wind at 200 hPa level for extreme flood case
vector is equivalent to 10 m s^{-1}

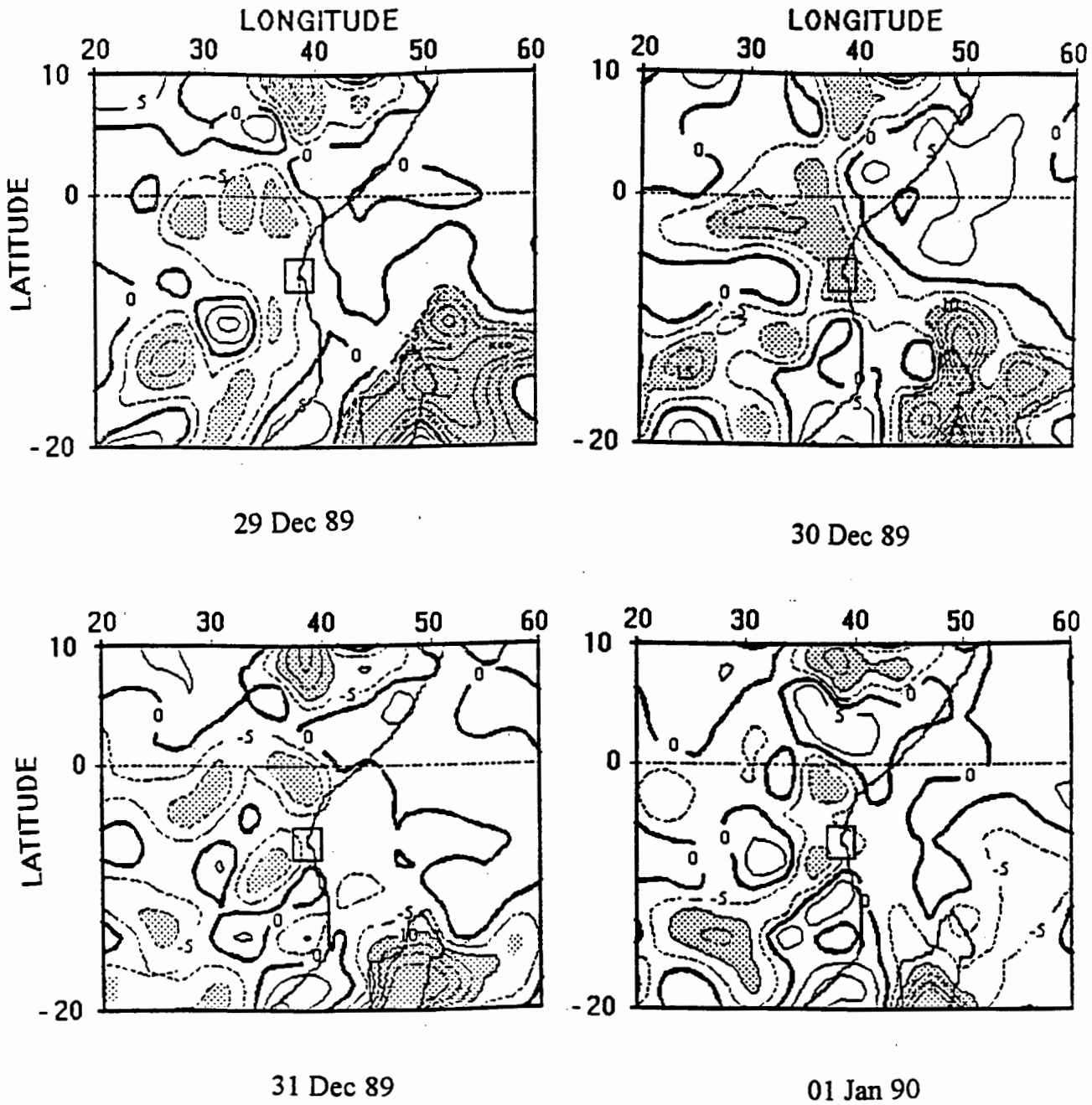

Figure 8.7: Divergence at 850 hPa for extreme flood case
Contour interval is 5×10^{-5} s^{-1}

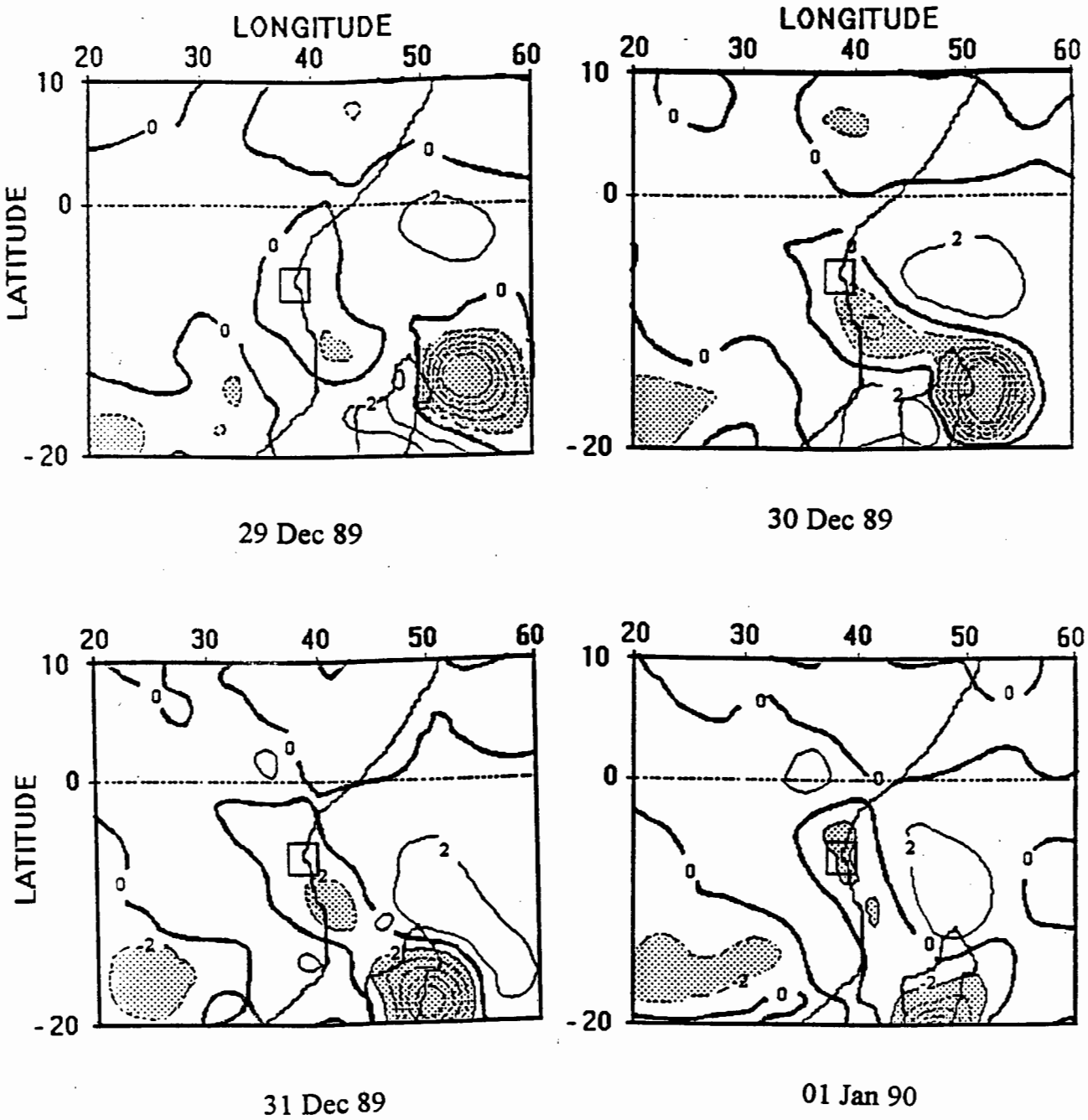

Figure 8.8: Vorticity at 850 hPa for extreme flood case
Contour interval is 2×10^{-5} s^{-1}

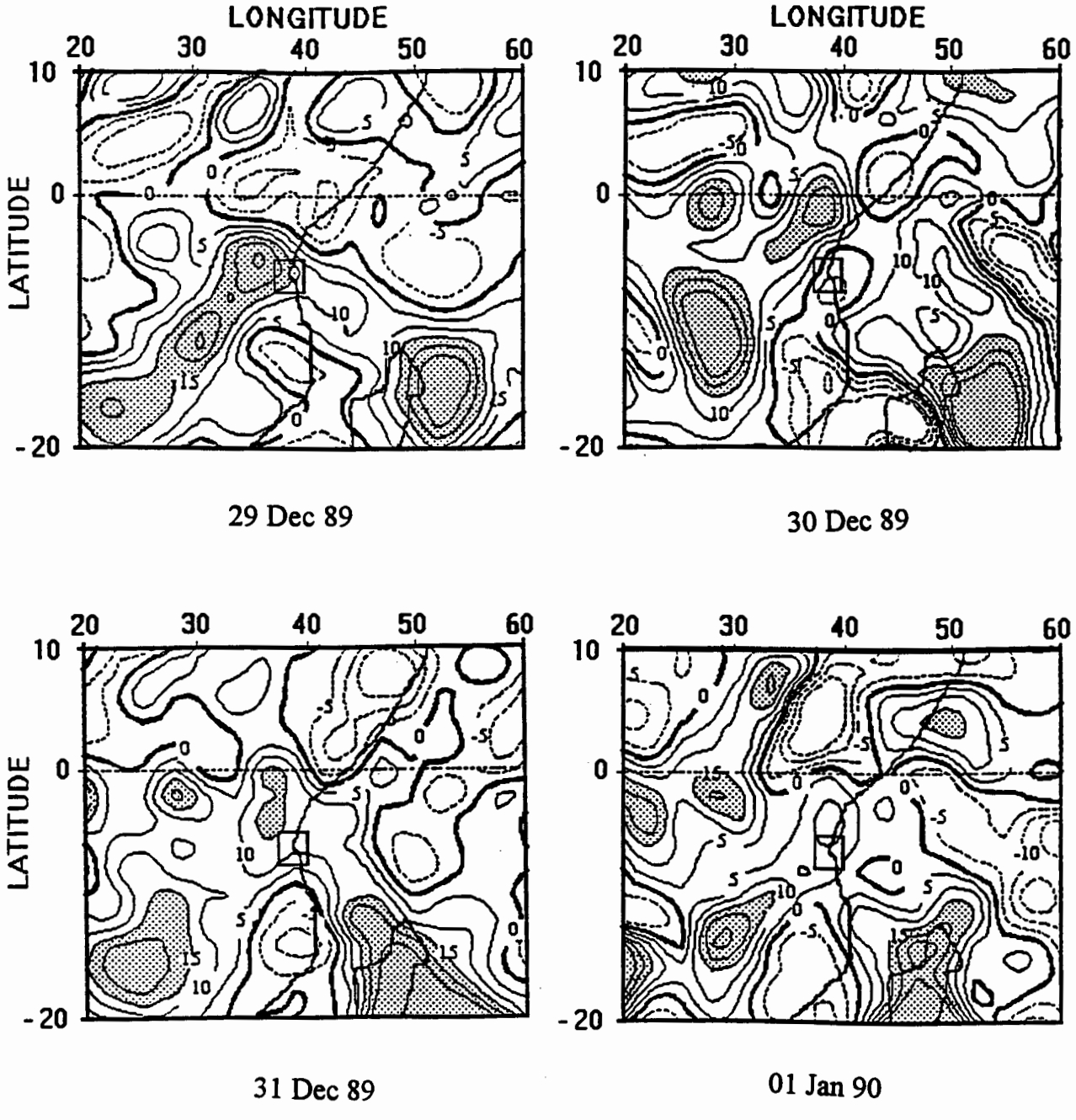

Figure 8.9: Divergence at 200 hPa for extreme flood case
Contour interval is 5×10^{-5} s^{-1}

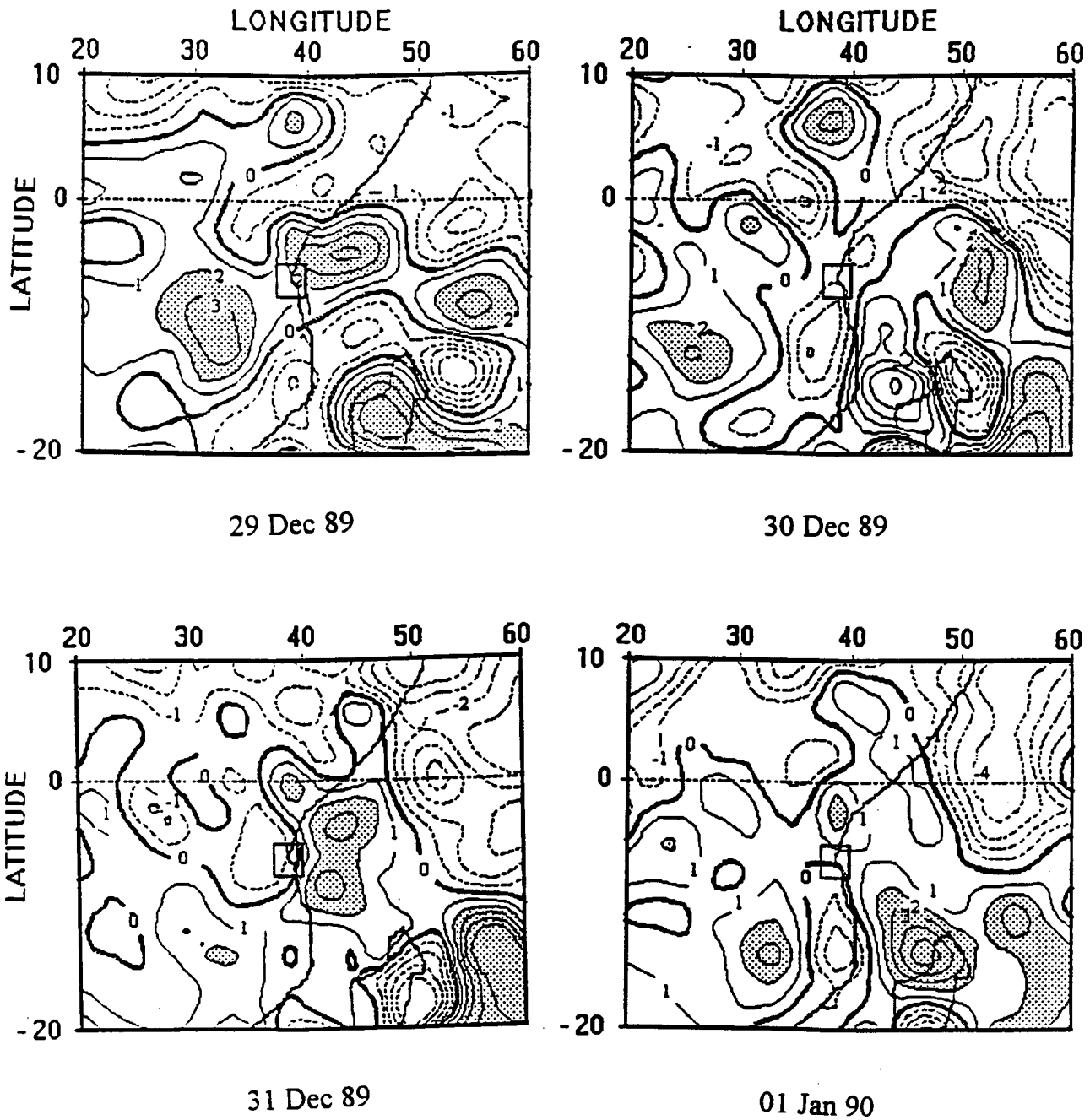

Figure 8.10: Vorticity at 200 hPa for extreme flood case
Contour interval is 1×10^{-5} s^{-1}

Figure 8.11

29 Dec 89

Figure 8.12

30 Dec 89

8.11-8.14 Satellite imagery of Tropical Cyclone "ALIBERA" during extreme flood case

Figure 8.13

31 Dec 89

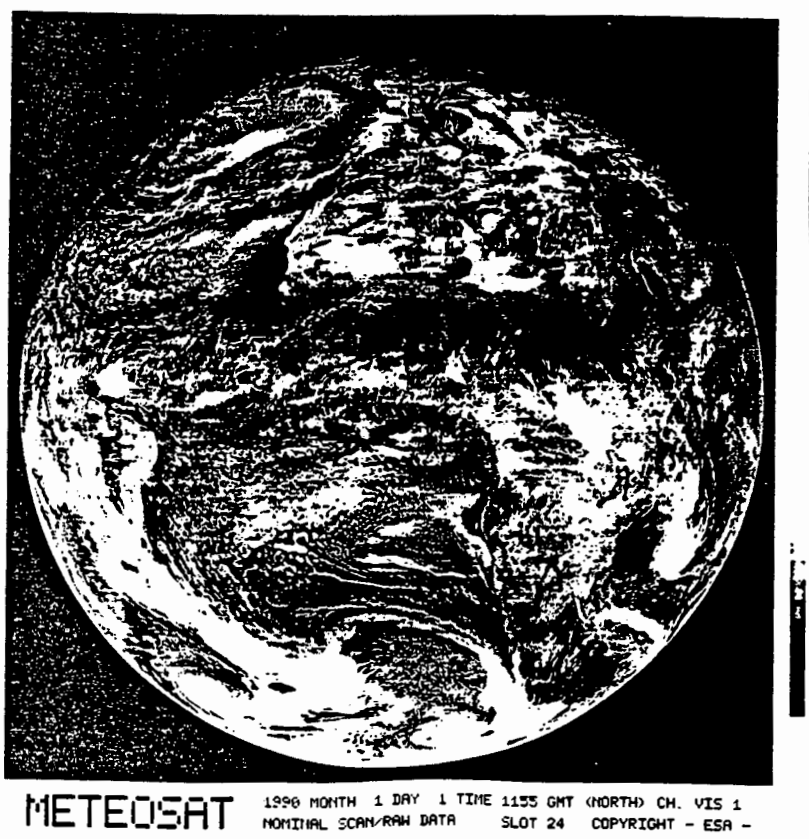

Figure 8.14

01 Jan 90

8.11-8.14 Satellite imagery of Tropical Cyclone "ALIBERA" during extreme flood case

Chapter 9: Discussion and conclusions

Economic development in Tanzania depends largely on the climate-driven agricultural sector. However, this sector is hampered by rainfall variability and lack of forecasting knowledge. This thesis is intended to highlight the background climate and weather patterns in the rainy inter-annual, intra-seasonal and event scales. Much emphasis has been put on the Vuli (October-December) rainfall season, the season affecting northern sector of Tanzania. The hypotheses given in chapter 1 will be discussed in this chapter and then associated with the results obtained.

9.1 Discussion

9.1.1 Rainfall Variability

Northern Tanzania's rainfall distribution is bimodal, one mode centered on April and the other on November, known as Masika and Vuli respectively. Seasonal distribution is variable from the coast to Lake Victoria. Coastal stations have heavier rainfall due to being first exposed to the moisture regime advecting from the ocean coupled with a sea-breeze. Stations over the eastern highlands receive less rain due to moisture depletion. However Lake Victoria basin show good rain due to the lake-breeze and extra moisture supply from the Congo.

Inter-annual periodicities in seasonal rainfall show a cyclic of 2.3 and 5 years for Vuli season attributed to the QBO and SO. Masika season spectral amplitude

peaks around 3.8 years cycle. The following observation was found out in this study:

- Strong negative correlation exists between SO and November rainfall only for coastal and northeastern highland stations.
- Cycles at the SO frequency are weaker during Vuli when Lake Victoria basin was considered.
- However it is possible to predict over 20% variance of Vuli rains using SO correlation in northern Tanzania as early as two months prior to their occurrence.

9.1.2 Seasonal composites and precursors

This part of the thesis (chapter 4) investigated characteristics of wet and dry seasons. Using anomaly fields at various lags, the structure and magnitude of SST, OLR and upper and lower winds was outlined for predictive purposes. Prior to the onset of wet Vuli season, cooler water emanates from Australia spreading to 90° E, 15° S, and positive SST anomalies along the Brazil coast is observed throughout. Warm SSTs, consistent with an El Nino, affect the western Indian Ocean. Operationally, it is possible to predict wet Vuli season as early as two months in advance using East Africa coast SSTs since positive anomalies there are established 2 months before the season. Convection over Tanzania is controlled by an opposing center of action in the eastern Indian Ocean with subsidence indicated

by positive OLR anomalies. Nyenzi (1988) found surface winds in this area to be below normal during wet Vuli years. Strong uplift develops in the western Indian Ocean closer to East Africa in sympathy. These two action centers constitute the two arms of a Walker cell, where the ascending and the descending arms are over western and Eastern Indian Ocean respectively.

Observations that anticipate a dry Vuli season are; persistent of below normal SST throughout the entire period of evolution, notably two months before the Vuli season when tropical SST decrease in the western Indian Ocean.

Wet Masika (MAM) OLR patterns, shows a northwest-southeast tilted convective region over Tanzania, whilst wind vectors reveals confluent (diffluent) low (upper) level flow. Cyclonic 200 hPa wind gyres in the southwest Atlantic and south Indian Ocean at -4 months are useful predictors.

Dry Masika (MAM) circulation patterns are nearly opposite to the wet with anticyclonic gyres in the southwest Atlantic and south Indian Ocean and tropical easterly flow during drought. A brief outline of seasonal predictors is given in table 9.1.

Table 9.1: Significant predictors from seasonal analysis;

Season	Masika (MAM)	Vuli (OND)
Wet	**SST**: Warm pool from Somali to Tanzania coast. **OLR**: Enhanced negative anomalies over East Africa throughout. **Wind**: Cyclonic 200 hPa wind gyres in the southwest Atlantic and south Indian Ocean.	**SST**: Positive SSTs - along eastern African coast starting 2 months before. **OLR**: uplifting in northwestern Indian Ocean (negative OLR) starting six month before. **Winds**: Upper level cyclonic flow southwest Indian Ocean and enhanced anticyclonic overland.
Dry	**SST**: below normal SSTs along East African coast. **OLR**: Uplifting in the central Indian Ocean while subsidence (positive) anomalies over the African continent.	**SST**: below normal tropical SSTs throughout. **OLR**: near normal to positive OLR values (Subsidence) **Winds**: Walker cell anomaly in the central Indian Ocean (weak winds though).

9.1.3 Vuli mean circulation and composite (pentads) analysis.

Chapter 5 was dedicated to study the mean characteristics of selected long-term meteorological fields for Vuli season and evolution of the wet pentads from onset to maturity. The 1986-1991 mean revealed that southeasterly flow plays a bigger roll in furnishing northern Tanzania with moisture. These winds converge over that area mainly due to uplift by north-south mountain ranges. The influence of northerly monsoon flow over the area was less obvious and more confined north of the equator. The composite mean pentad evolution revealed high precipitable water content in comparison with the seasonal mean since they were composed of peak rain days.

9.1.4 Contrast between wet spells and a dry seasonal composite.

In chapter 6, evolution of Vuli wet spells from formation stage, development and maturity stage were investigated. While in chapter 7 composites of extremely dry pentads for Vuli season 1987 were considered. Comparing the results obtained from the two chapters, there are many opposing features in meteorological fields at formation stage. Water vapour flux for dry anomalies show disorganized flow west of Madagascar while on the formation stage the wet spell there existed an anticyclonic flow in the Southwest Indian Ocean. During dry Vuli periods, northeasterlies fail to reach northern Tanzania due to divergence upstream over the Kenyan coast. It is important to note that upper-level Saharan air that circulates

over Tanzania is responsible for drying the ambient atmosphere. The characteristics of the meteorological fields for these extreme climatic phases will be useful in forecasting the onset of wet and dry spells. Table 9.2 give a brief outline of useful predictors for wet and dry spells.

Table 9.2: Significant predictors from pentads analysis;

Wet Vuli Spells	Dry Vuli
• **Water Vapour flux**: Strong Southeasterlies enhanced by low level pressure rise in southwest Indian Ocean ten days prior. • **200 hPa Winds**: moist westerlies (Atlantic Ocean origin) • **Vorticity**: low level cyclonic vorticity • **Vertical Motion**: uplifting (negative anomalies)	• **Water vapour flux** : disorganised over East Africa but converging in the central Indian Ocean. • **200 hPa Winds:** dry northwesterlies (Sahara origin) • **Vorticity:** low level anticyclonic vorticity. • **Vertical Motion**: Subsidence (positive anomalies)

9.2 Conclusions

- For predictive purpose, water vapor flux anomalies, vertical motion and low-level pressure patterns are able to show distinctive differences between the dry and wet periods.
- Using ECMWF data and the analysis method in this thesis, a 10-15 day evolution pattern can be adopted for use in medium-range forecasting which is ideal for farming and planing management.

- SST and OLR anomalies in the western Indian ocean are ideal for prediction purposes. Positive SST anomalies relate to negative OLR which extends over northern Tanzania. The opposite is true in "cold pool" events.

Future work of this type should try to investigate why the northeasterly and southeasterlies do not converge sufficiently to drive the convective process. As a starting point, Kinuthia and Asnani (1982) found a low level jet over Kenyan coast causing part of northeasterlies to recurve. Similar characteristics are observed over northern Tanzania where the southeasterly is recurved westward. The findings from this and other previous works, will be ideal to operational weather forecasting over northern Tanzania area and its surrounding.

In Chapter 8 extreme flood event which occurred on 31 December 1989 over Dar es Salaam was investigated, revealing that excessive moisture was advected toward Dar es Salaam. The tropical cyclone ALIBERA was the driving force of moisture from northeastern. However satellite pictures show a deep convective activity overland (Zambia) another source of moisture that converged over Dar es Salaam. While this thesis has improved our understanding of intra-seasonal convective forcing in the Vuli (OND) season; similar work could be done for the Masika (MAM) season.

References

Alusa, A. L and Mushi, M. T., 1974: A study of the onset, duration and cessation of the rains in East Africa. *International Tropical Meteorological Meeting*, Nairobi, Kenya, 133-140.

Alusa, A. L and Gwange, P.M., 1978: The occurance of dry spells during the East Africa long rains. *Research report No.5/78,* E.A Institute for Meteorology. P. 1-18.

Anyamba, E.K., 1992:Some properties of a 20-30 day oscillation in tropical convection. *J. Afr. Met. Soc.* 1, 1-19.

Asnani, G.C., 1993: *Tropical Meteorology*. Noble Printers, Pune-India, 1202pp.

Bengtsson, L. and Shukla, J., 1988: Integration of space and in situ observations to study global climate change, B*ulletin of American Meteorological Society*, Vol. 69, 1130-1143

Bluestein, H.B. 1992: *Synoptic-Dynamic Meteorology in Midlatitudes* Vol.1, 82-152

Cadet, D.L., 1985: The Southern Oscillation over the Indian Ocean, *Journal of Climatology*, Vol. 5, 189-212

Chen, T-C., Tzeng, R-Y., 1990: Global scale Intra-seasonal and annual variation of divergent water vapour flux. *Meteorol.Atmos. Phys.*, 133-151

Freedman D., Pisani R., Purves R., 1978: *Statistics*. Published by George J. Mcleod Limited, Toronto Canada., pp 409-415.

Hastenrath S., Nicklis A. and Greischar L., 1993: Atmospheric-hydrospheric mechanisms of climate anomalies in the western equatorial Indian Ocean, Journal of Geographical Research, 98(C11) 20219-20235

Hoskins, B.J., Hsu, H.H., James, I.N., Masutani, M., Sardeshmukh P.D., White, G.H., 1989: Diagnostics of the global atmospheric circulation based on ECMWF analysis 1979-1989, WMO/TD-No 326

Jury M.R and Levey K. 1993: The Climatology and characteristics of Drought in the Eastern Cape of South Africa, *International Journal of Climatology*, Vol. 13, 629-641

Jury M.R and McQueen C. 1993: Correlation atlas of climatic determinants for Tanzania.

Kapala A., Born K. and Flohn H., 1994: Monsoon anomaly or an El nino event at the Equatorial Indian Ocean? Catastrophic rains 1961/62 in East Africa and their teleconections, WMO/TD-No 619., 119-126

Klinker E., 1991: *Aspects of Large Scale Modelling, Energy and Water Cycles in the Climate System*, NATO ASI Series., 43-67

Kavishe, M.M., 1993: Climate change and global warming. Paper presented at a seminar organised by Tanzania Meteorological Society DSM. 29 October 1993. (Unpublished).

Kinuthia J. H and Asnani G. C., 1979: Diurnal variation of precipitation in East Africa. *Research report No.5/78* E. A. Institute for Meteorology.

Kinuthia J. H and Asnani G. C., 1982: A newly found jet in Northern Kenya (Turkana Channel). *Mon. Wea. Rev.*, 110, 1722-1728.

Levey, K.M., 1993: Intra-seasonal oscillations of convection over southern Africa. *Msc. Thesis*, University of Cape Town.

Lindesay J.A., 1988: The Southern Oscillation and Atmospheric circulation changes over Southern Africa, *PhD. Thesis* University of the Witwatersrand

Makarau, A., 1994: Intra-seasonal oscillatory modes of the southern Africa summer circulation., *PhD. Thesis*, University of Cape Town, Cape Town, South Africa.

Mason, S.J., 1992: Sea surface temperatures and South African rainfall variability. *PhD Thesis*, University of the Witwatersrand

Matarira, C.H., Jury, M.R., 1992: Contrasting Meteorological structure of Intra-seasonal wet and dry spells in Zimbabwe. *International Journal of Climatology*, Vol. 12, 165-176

McCreary, J.P. , Jr, 1994: A numerical investigation of the annual-mean heat input through the surface of the Indian Ocean.,*WMO/TD-No* 619.,505-644

Mhita, M. S. And Nassib I. R., 1987: The onset and end of rain in Tanzania *Proc. 1st Tech. Conference*. Meteor. Res. Eastern and Southern Africa, Nairobi, pg 101-115.

Mhita M.S., Venäläinen A., 1992: The Variability of Rainfall in Tanzania., FINNIDA/SATCC/WMO-Meteorology project Helsinki. Finnish Met. Institute.

Murakami, T., 1988: Intraseasonal atmospheric teleconection patterns during the northern hemisphere winter, *Journal of Climate*, Vol.1, 117-131.

Nassor, A., 1994: Monsoon surges, tropical cyclones and extreme rainfall events in NW Madagascar, *Msc. Thesis,* University of Cape Town.

Nicholson and Nyenzi, B.S., 1990: Temporal and Spatial Variability of SSTs in the Tropical Atlantic and Indian Oceans, *Meteorol Atmosp Physics,* Vol. 42, 1-17.

Nicholson S.N., 1986: Rainfall variability in southern and equatorial Africa: Its relation to Atlantic sea surface temperatures and the southern oscillation. *American Meteorological Society*, 472-.475

Nigam S. and Shen, H., 1993: Structure of Oceanic and Atmospheric Low-frequency Variability over the Tropical Pacific and Indian Oceans. Part I: COADS Oservations, American Meteorological Society, 657-676.

Njau, L., 1987: Seasonal Variability of Kenya rainfall and its teleconnection. *Proc. First Technical conference* on Met Research in Eastern and Southern Africa. Nairobi Kenya , 6-9 January 1987, 160-165.

Nyenzi, B.S, 1984: Equatorialy zonally moving disturbances which contributed to the East African long rains March to May 1979., *Msc. Thesis* Florida State University 73pp.

Nyenzi, B.S, 1988: Mechanisms of East African Rainfall variability., *PhD. Thesis*, Florida State University 184pp.

Ogallo, L. J., 1986: Relationship between seasonal rainfall in East Africa and Southern Oscillation, *Second international conference on Southern Hemisphere Meteorology.* American Meteorological Society, 468-471.

Ogallo, L. J., 1987: Teleconnections between rainfall in East Africa and global parameters, *Proc. First Technical conference* on Met Research in Eastern and Southern Africa. Nairobi Kenya , 6-9 January 1987, Pg. 71-75.

Ogallo, L. J. and Suleiman, K. A., 1987: Rainfall characteristic in East Africa during the El-nino year. *Proc. First Technical conference* on Met Research in Eastern and Southern Africa. Nairobi Kenya , 6-9 January 1987, 76-80.

Ogallo, L. J., 1988: Relationship between seasonal rainfall in East Africa and Southern Oscillation, *Journal of Climatology*, Vol. 8, 31-43.

Ogallo, L. J., 1989: The spatial and temporal patterns of the East African seasonal rainfall derived from principle component analysis,
Royal Meteorological Society, 145-167.

Ogallo, L. J. 1994: Interannual variability of the East African monsoon wind systems and their impact on East African Climate, WMO/TD-No 619., 99-104.

Ogallo L. J., Okoola R.E. and Wanjohi D.N. , 1993: Characteristics of Quasi-Biennial Oscillation over Kenya and their predicterbility potential for the seasonal rainfall. Submitted to J. Afr. Meteorol. Soc., Nairobi

Park, C. and Schubert, S.D., 1993: Remotely forced intraseasonal oscillations over the tropical Atlantic, *Journal of Atmospheric Science*, Vol. 1, 89-103.

Parker, B. A., 1994: Composite structure of tropical cyclones in the SW Indian Ocean, *Msc thesis*, University of Cape Town, South Africa.

Rocha A., 1992: The Influence of global SSTs on the Southern African summer climate, *PhD thesis*, University of Melbourne, Australia. 249pp.

Rui, H. and B. Wang, 1990: Development characteristics and dynamic structure of tropical intraseasonal convection anomalies. J. Atmos. Sci., 47, 357-379.

Direction de la Meteorologie service regional de la Reunion., 1990: *Saison cyclonique* 83pp.

Sardeshmukh P.D. and Hoskins B.J., 1988: The generation of global rotational flow by steady idealized tropical divergence. *Journal of Atmospheric Science*, Vol. 45, No. 7 1228-125.1

Zhu, B., and Wang, 1993: The 30-60 day convective seesaw between the tropical Indian and Western Pacific Oceans. *J. Atmos. Sci.*, 50, 184-199.

Appendix 1:

Statistical significance test:

A statistical test was performed on the SST predictor zone in the South-West Indian Ocean prior the onset of a rainy season. Using wet -dry data, zones with highest signals were identified. The most significant signal was detected at two months prior the season (figure Appx 1).

A *t-test* was performed on this zone; (0-10°S, 40°E-60°E). The statistical formula is:

$$t = \frac{\text{observed} - \text{expected}}{\text{SE}}$$

The observed is the composite mean for the wet or dry years selected, while the expected is the long term mean. The period is 4 and 15 years respectively in this case. SE = standard error.

A more detailed description of this method is given by David Freedman et.al., (pp 409-415).

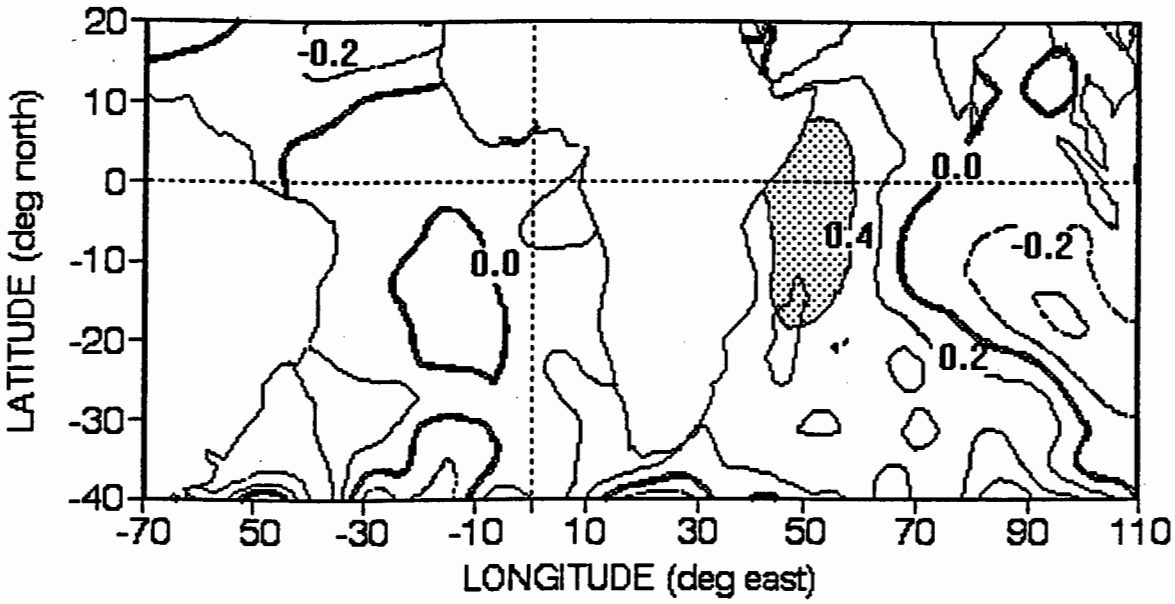

Figure Appx1: SST wet minus dry field (deg C). Shaded area is > 0.4 C. The significance test is performed within this western Indian Ocean area.

For an area of the western equatorial Indian Ocean (0-10°S, 40°-60°E), the wet composite mean, dry composite mean and long term mean are 26.44°C, 25.98°C and 26.25°C respectively. The standard error is 0.077. The *t-test* applied to this small sample yields 2.45 and -3.49 for wet and dry respectively, both significant at the 95% confidence limit. However SST signals are small, and therefore for operational purposes it is suggested that OLR and wind should be considered.

Acknowledgements

I wish to thank my supervisor, Dr. Mark R. Jury of the Oceanography Department, University of Cape Town for his tireless support, guidance and suggestions throughout this study. Special thanks are extended to all staff in the Oceanography Department, particularly Professor G. Brundrit for constant encouragement. I am grateful to members of the Climate and Weather Research Lab. for their helpful technical discussions and suggestions during the course of this research.

My thanks goes to the Tanzania Meteorology Department, and staff and Foundation for Research Development (FRD) for giving me the opportunity to further my education at University of Cape Town.

I wish to thank my wife Nyakato Leila, my children, Kemilembe, Mwombeki, Mukahumbya and Tabaro for their constant encouragement and accepting living in separation during the whole period of this study.

Lastly thanks are conveyed to F. Kilele for utilising her computer and useful discussions at different stages of my research.